Multiscale modelling, analysis and simulation of a Cahn–Larché system with phase separation on the microscale

Dissertation

zur Erlangung des akademischen Grades

Dr. rer. nat.

eingereicht an der
Mathematisch-Naturwissenschaftlich-Technischen Fakultät
der Universität Augsburg

von

Lisa Reischmann

Augsburg, Oktober 2019

Erstgutachter: Prof. Dr. Malte A. Peter
Zweitgutachter: Prof. Dr. Dirk Blömker

Tag der mündlichen Prüfung: 13. Dezember 2019

Abstract

We consider the process of phase separation of a binary system under the influence of mechanical stress and we derive a mathematical multiscale model, which describes an evolving microstructure taking into account the elastic properties of the involved materials. Motivated by phase-separation processes observed in lipid monolayers in film-balance experiments, the starting point of the model is the Cahn–Hilliard equation coupled with the equations of linear elasticity, the so-called Cahn–Larché system. Owing to the fact that the mechanical deformation takes place on a macrosopic scale whereas the phase separation happens on a microscopic level, a multiscale approach is imperative. We assume the pattern of the evolving microstructure to have an intrinsic length scale associated with it, which, after non-dimensionalisation, leads to a scaled model involving a small parameter $\epsilon > 0$, which is suitable for periodic-homogenisation techniques. Furthermore, we present a linearised Cahn–Larché system. For the associated ϵ-dependent problem, we proof the existence and uniqueness of a weak solution by a Galerkin approach, for every $\epsilon > 0$. As discretisation in space leads to a linear differential–algebraic system of equations, we apply solution theory for such equations in a weak setting. A-priori estimates enable us to homogenise the linear system rigorously using the concept of two-scale convergence. The full nonlinear problem is formally homogenised using the method of two-scale asymptotic expansion. Both systems leads to models of distributed-microstructure type in the limit. Properties of the limit models are discussed. Finally, numerical simulations based on a finite-element approach are considered to showcase the model behaviour of the nonlinear distributed-microstructure model.

Acknowledgements

There are many people – family, friends and colleagues – who have supported me during my PhD studies and to whom I am deeply grateful. I think and hope that they all know how grateful I am to each one of them and how much I appreciate their support. Therefore, and because it is my way to keep such things rather short, I will refrain from listing every single one of them here now. However, there are four people who definitely need to be mentioned here.

First of all, I would like to thank my PhD supervisor Prof. Dr. Malte Peter, for making my doctorate possible in the first place and for his support of this research and of my dissertation, but most of all for the many opportunities to broaden my horizon and for everything I learned from him.

My special thanks also go to my colleague and dear friend Ursula Weiß for her support and friendship, the numerous rays of hope and the many colours in everyday life, the "Pinacolada" moments and "Helsinki" trips that will always remain in my memory and for much more. Many thanks also to little Florian, who always makes one smile, for all the entertaining breaks and of course for always making me smile.

And last but not least, special thanks to Dr. Yuri Iliash, for always solving my computer problems and especially for defending the cluster for me in the final phase of my doctorate.

Contents

1 Overview

Motivated by phase-separation processes observed in lipid monolayers in film-balance experiments, we investigate the following scaled Cahn–Larché system, which describes a phase-separation process on the microscale, taking into account influences of mechanical processes which happens on the macroscale:

$$\begin{aligned} \partial_t c_\epsilon &= \epsilon^2 \Delta\Big(f'(c_\epsilon) - \epsilon^2 \lambda \Delta c_\epsilon - e'(c_\epsilon) \operatorname{tr} \mathcal{S}_\epsilon + (\mathcal{E}(u_\epsilon) - e(c_\epsilon)\mathbb{1}) : \mathcal{A}'(c_\epsilon)(\mathcal{E}(u_\epsilon) - e(c_\epsilon)\mathbb{1}) \Big), \\ 0 &= \nabla \cdot \Big(\mathcal{A}(c_\epsilon)\big(\mathcal{E}(u_\epsilon) - e(c_\epsilon)\mathbb{1}\big) \Big). \end{aligned} \tag{1.0.1}$$

This system is introduced in detail in chapter 2. It is scaled by exponents of ϵ, a small positive parameter, which ensures that the very differing length scales associated to mechanics and diffusion are taken into account in the model. This is necessary in the course of homogenisation in order to obtain a reasonable limit system that describes the considered processes correctly and adjusts them to each other. As we see in § 2.4, such a scaling results in a natural way in the process of a non-dimensionalisation.

This thesis is organised as follows. As they are motivating this study, in chapter 2, we first describe the above mentioned film-balance experiments and the physical context and give some background information. In order to describe these processes mathematically, in § 2.2 we first introduce the Cahn–Hilliard model and afterwards, the Cahn–Larché system, which is the resulting system of equations when coupling the Cahn–Hilliard equation with the equations of linear elasticity. Then, we perform a non-dimensionalisation, which leads to the scaled Cahn–Larché system (1.0.1). We end the first section by deriving a linearisation of (1.0.1).

In chapter 3, we give a short introduction to the idea of periodic homogenisation and we introduce two concepts which we work with in this thesis. First, in § 3.1 we introduce the heuristic method of asymptotic expansion, which allows one to homogenise an equation formally. After, in § 3.2 we turn to the concept of two-scale convergence in L^p-spaces, a special type of convergence which takes rapidly periodic oscillations into account. Since this concept has a very wide range of application and numerous results exist in its context, we restrict to those we need in the following sections of this thesis. In addition, we present a result about the convergence of sequences of second-order derivatives scaled by ϵ^2 as well as a generalisation of a well-known result which enables to pass to the limit of products of several certain sequences.

Using the method presented in § 3.1, in chapter 4 we formally derive a model, which turns out to be of a so-called distributed-microstructure type. In preparation for this, we first introduce special periodic auxiliary problems for periodic homogenisation in mechanics in § 4.1, known as cell problems. Afterwards, in § 4.2 we first formally homogenise the nonlinear system (1.0.1) and clarify the notion of a distributed-microstructure model in this context and, in the same way, we derive the formally homogenised system of the linear system introduced in § 2.5. The resulting limit systems are given by (4.2.22), (4.2.23) and (4.2.35), (4.2.36).

Chapter 5 is devoted to the rigorous analysis of the linearised scaled Cahn–Larché system. Since we want to work in a weak setting, we first specify the framework for this and state the weak formulation of the linear system. In § 5.2, an a-priori estimate is given and proven, which shows that the solutions of the system are uniformly bounded with respect to ϵ. Then, in § 5.3, we proof the existence and the uniqueness of a weak solution of the considered linear system for every ϵ by a Galerkin approach. Since the resulting semidiscrete system represents a linear differential–algebraic system of equations, we present the required solution theory of linear differential–algebraic equations in a weak setting in § 5.3.

In chapter 6, we homogenise the linear Cahn–Larché system in a mathematically rigorous way using the concept of two-scale convergence. Afterwards, we discuss the homogenised system and its properties. As it turns out, it is the same as the formally homogenised system from § 2.5 and, further, linearisation commutes with homogenisation.

Numerical simulations of the formally homogenised nonlinear Cahn–Larché system are presented in chapter 7. These are based on a micro–macro finite element approach of the corresponding system of equations. We showcase the behaviour of the distributed-microstructure model by considering simulations of binodal and spinodal phase separation with isotropic or anisotropic elasticity with cubic symmetry.

Finally, in chapter 8, we summarise our results and give an outlook on further interesting aspects and questions that arise in this context, but go beyond the scope of this thesis.

At this stage, we make a few remarks about the notation. We use standard notation concerning function spaces: For $p \in [1, \infty)$, we denote by $L^p(\Omega)$ the space of p-integrable functions and by $L^\infty(\Omega)$ the space of essentially bounded functions. We write $W^{k,p}(\Omega)$ for the Sobolev space containing p-integrable functions with p-integrable weak derivatives up to order k, and we write $H^k(\Omega) \coloneqq W^{k,2}(\Omega)$ in the special case $p = 2$. For the time-dependent functions, we make use of the well-known Bochner spaces $L^2((0,T), X)$, where X denotes a Banach space. Further, for two matrices $A = (a_{ij})_{1\leq i,j\leq N}, B = (b_{ij})_{1\leq i,j\leq N} \in \mathbb{R}^{N\times N}$ we denote the Frobenius product by $A : B = \sum_{i,j=1}^{N} a_{ij}b_{ij}$. We use the symbol # as subscript of a function space to identify periodic boundary conditions. And finally and for the sake of simplicity, we denote many constants that occur in estimates by $C, \tilde{C}, C_1$, which can vary in each step.

2 Phase separation in an elastic medium

As this thesis is motivated by phase-separation processes observed in lipid monolayers in film-balance experiments, we first turn to these to explain the considered processes and to clarify the physical background. After, we introduce a mathematical model, the Cahn–Hilliard model, which has already been successfully adapted to study phase-separation processes in lipid bilayers, see [BFL$^+$13] and [Fra14]. However, since the Cahn–Hilliard model does not take all relevant mechanisms of the considered physical processes into account, we then focus on the Cahn–Larché system, which is obtained by coupling the Cahn–Hilliard equation with those of linear elasticity. In the course of a non-dimensionalisation, we will then fathom the already introduced scaling of the Cahn–Larché system (1.0.1) in detail and derive a linearised system at the end of this chapter.

2.1 Phase separation in lipid monolayers

We consider the process of phase separation in lipid monolayers, which can be observed in film-balance experiments, where phospholipid monolayers are compressed. Such monolayers are of common interest and were often used for experiments since phosphatidylcholines (PC) are the main phospholipids found in mammalian cell membranes. The lipid Dipalmitoylphosphatidylcholine (DPPC) is particularly common in this context (see e.g. [Bur11], [KV96], [MV97], [NBRK91]), but many other phosphatidylcholines and, more generally, other phospholipids are used, such as DMPC, DMPG, DMPE, DOPC, DLPC (see e.g. [Ste05], [MM87] [Möh95], [KL00]). Biomembranes actually have the structure of a bilayer, but a monolayer, which provides a simplified model of such a membrane, has the advantage of simplified production. In addition, a monolayer has the advantage that the molecular density can be determined by varying the area per molecule on a Langmuir film balance [MV97]. For what follows we refer to [Ste05], [Bur11] and [Lei08].

Figure 2.1 shows a simple schematic representation of the structure of a lipid molecule. It consist of a hydrophilic head group and two hydrophobic tails made up of hydrocarbon chains. Due to these amphiphilic properties, lipid molecules align themselves accordingly when coming into contact with water. This property enables the production of monolayers as well as other structures such as bilayers or giant unilamellar vesicles (GUVs).

Figure 2.1: Schematic drawing of the structure of a lipid molecule with hydrophilic head (red coloured) and hydrophobic tail (black coloured).

The schematic setup of a film balance used in experiments motivating this study is shown in figure 2.2. A film balance is essentially a kind of water trough, equipped with a controllable teflon barrier, a fluorescence microscope and a so-called Wilhelmy plate. The total area of the lipid monolayer and consequently the density of the molecules can be controlled by moving the barrier.

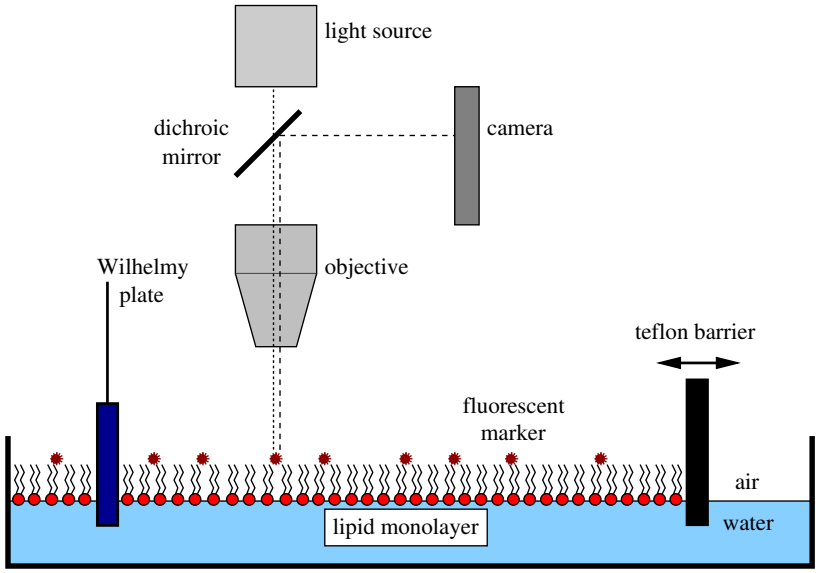

Figure 2.2: Schematic setup of a film-balance experiment.

Lipid monolayers are produced by spreading a lipid mixture using the so-called Langmuir-Blodgett technique. A certain amount of lipid molecules dissolved in a solvent, for instance chloroform, are dripped onto water. After a short time, the solvent evaporates while the lipid molecules remain, which then align themselves with their hydrophilic head groups in the direction of the water due to their amphiphilic properties. The inclusion of dye-labelled lipid molecules enables optical characterisation, which can be detected with the fluorescence microscope. By sliding the teflon barrier, the area available to the lipid molecules can then be reduced until a lipid monolayer is formed. By moving the barrier, the monolayer can be further compressed. This process leads to a lateral pressure in the monolayer, which is related

to the force which is needed to compress the monolayer and which can be measured with the Wilhelmy plate.

Lipids show different states or phases depending on certain factors. Figure 2.3 gives a schematic representation of the alignment of the lipid molecules in the different phases. Assuming constant temperature, the monolayer becomes denser and more rigid as the area available for the lipid monolayer is reduced, which corresponds to increasing the lateral pressure.

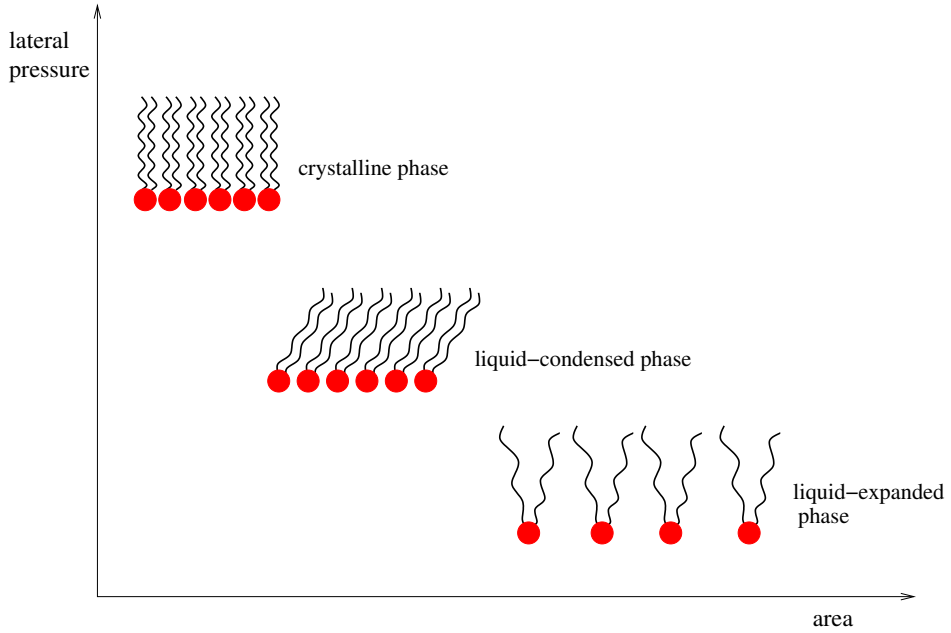

Figure 2.3: Representation of the alignment of the phospholipid molecules in different phases depending on the area available to the molecules or the lateral pressure.

In the crystalline phase, the chains are strictly ordered and the molecules are tightly packed to each other. In the liquid-expanded (LE) phase, the molecules are disordered and the chains partly are of convoluted structure. In between, the liquid-condensed (LC) phase can be observed. The molecules are packed and ordered close to each other, but less strictly than in the crystalline phase.

After spreading the lipid mixture on the film balance, the lipid molecules initially have plenty of space and are in a state known as the gas-analogue phase. If the space available to the molecules is then reduced, a phase transition occurs in which parts of the monolayer are transferred into the LE phase until, with further compression, the entire monolayer is present in the LE phase. Further compression results in a further phase transition into the LC phase. This part is now the focus of this work: In experiments, the formation of two-phase regions

can be observed in which regions in the LC phase are dispersed in the less ordered LE phase. The addition of a fluorescent dye enables the visualisation of the two co-existing phases and hence the observation of an evolving microstructure. This is because of the varying solubility of the fluorescent dye in the different phases, which is what causes the dye to accumulate in the more disordered LE phase. The arising domains, formed by the LC phase, develop different shapes, which continue to change with time as the monolayer rests. Besides chirality of lipids [KL00], the mechanical processes also influence the size and shape of the arising domains such as speed and strength of compression or waiting periods during multiple compression operations, [MV97], [KV96], [NBRK91]. With further compression, the monolayer can then be transferred into the crystalline phase.

Figures 2.4 and 2.5 show examples of the shapes and sizes of the LC domains that occur. Figure 2.4 shows a photograph of coexisting LE and LC regions in a lipid monolayer observed in an experiment in which the phase transition was induced by the subphase (which is water in our explanations) from below. See [BBF$^+$17] for details.

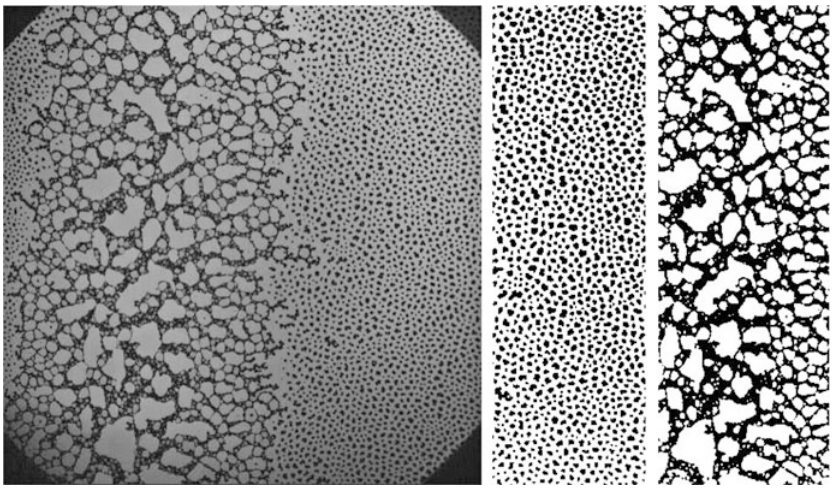

Figure 2.4: Coexistence of regions of LE and LC phases in a lipid monolayer with very different structure: (left) original photograph; (middle) contrast-enhanced piece of the right region of the original photograph; (right) contrast-enhanced piece of the left region of the original photograph. (Reprinted by permission from Springer Nature Customer Service Centre GmbH from [BBF$^+$17], Copyright Springer International Publishing AG (2017))

The effects of the chirality of the molecules on the domain structures when compressing a D-DPPC monolayer are illustrated in Figure 2.5. The “D” denotes a right-handed twist of the molecules, which is responsible for the direction of rotation of the domains (black coloured).

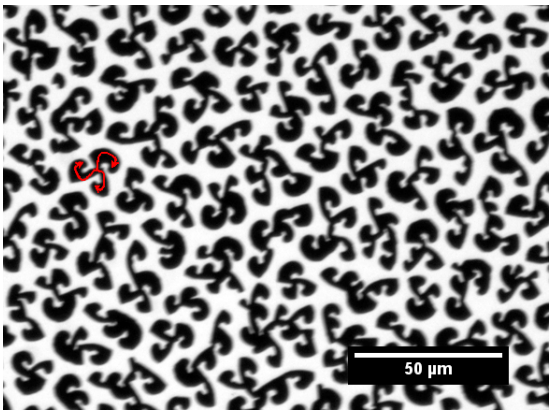

Figure 2.5: Coexistence of LE and LC phases in a D-DPPC monolayer forming characteristic chiral domains [Bur11].

By interpreting the lipid monolayer with its coexisting phases as a binary mixture, we use the mathematical model presented in the next section to describe the phase-separation process. Since the LC phase of the monolayer can be described as gel-like and has an already relatively densely packed and ordered molecular structure, we also consider the monolayer as a solid and use solid mechanics to describe the mechanical properties of the monolayer mathematically.

We want to emphasise the multiscale aspect of this setting at this point. Notice that the size of the LC domains is in the range of several µms (see e.g. figure 2.5), which differs from the scale of the mechanical deformation by approximately 5 orders of magnitude. Owing to the fact that the mechanical deformation takes place on a macrosopic scale whereas the phase separation happens on a microscopic level, a multiscale approach is imperative in the mathematical context.

2.2 The mathematical model

In this part we turn to the mathematical descripton of the just presented film-balance experiments. First, we consider the Cahn–Hilliard model, a model for describing separation processes. Since this model cannot capture the mechanical aspects of the experiments described in the previous section, we consider an extended model afterwards, the Cahn–Larché model. In the context of phase separation in lipid monolayers, the Cahn–Hilliard model has already been extended to take elastic effects into account. In [**?**], it was coupled with a viscoelastic fluid-flow model to study phase-separation processes in lipid monolayers for a surface-acoustic-wave-actuated fluid flow. As already motivated previously, instead of fluid mechanics, we will turn to solid mechanics for the extension of the introduced phase-field model.

2.2.1 The Cahn–Hilliard equation

The Cahn–Hilliard equation goes back to J. W. Cahn and J. E. Hilliard, see [CH58]. It is a fourth-order nonlinear equation, which was originally developed to model phase separation of binary alloys. Since then, however, the equation has found application in numerous fields, such as image processing [BHS09] or modelling tumor growth [GL17]. In addition, this phase-field model has already been adapted to model the separation process observed in lipid bilayers [BFL$^+$13], [Fra14]. Referring to that, we will briefly summarise the derivation of the Cahn–Hilliard equation in the context of the separation of a lipid mixture into two distinct phases.

We start with defining an order parameter $c \in [0,1]$ which describes the relative concentration of a binary mixture. Pure phases of the components correspond to $c = 0$ and $c = 1$. We introduce a local free energy f per volume. As can be seen in the descriped experiments, pure regions consisting of relatively strictly arranged molecules (LC phases) and regions of the less densely arranged molecules (LE phases) are formed during compression. Since nature tends to minimise its energy, the local free energy must take this circumstance into account and make local concentrations of pure phases to be energetically favourable. We assume f to be a continuous function and, further, we assume the order parameter c and its derivatives to be independent variables. This makes it possible to apply a Taylor series expansion in order to approximate f at some c_0 describing the concentration of a homogeneous mixture. We obtain

$$f(c, \nabla c, \nabla^2 c, \ldots) = f(c_0) + \sum_i L_i \partial_{x_i} c + \sum_{i,j} \kappa_{ij}^{(1)} \partial^2_{x_i x_j} c + \frac{1}{2} \sum_{i,j} \kappa_{ij}^{(2)} \partial_{x_i} c \, \partial_{x_j} c + \ldots \tag{2.2.1}$$

with

$$L_i = \frac{\partial f(c)}{\partial(\partial_{x_i} c)}\Big|_{c_0}, \quad \kappa_{ij}^{(1)} = \frac{\partial f(c)}{\partial(\partial^2_{x_i x_j} c)}\Big|_{c_0} \quad \text{and} \quad \kappa_{ij}^{(2)} = \frac{\partial f(c)}{\partial(\partial_{x_i} c)\,\partial(\partial_{x_j} c)}\Big|_{c_0}.$$

We now only consider even powers of ∇c, since, for symmetry reasons, f does not depend on the orientation of the gradient and thus (2.2.1) becomes

$$f(c, \nabla c, \nabla^2 c, \ldots) = f(c_0) + \kappa_1 \nabla^2 c + \kappa_2 (\nabla c)^2 + \ldots, \tag{2.2.2}$$

with

$$\kappa_1 = \frac{\partial f(c)}{\partial \nabla^2 c}\Big|_{c_0} \quad \text{and} \quad \kappa_2 = \frac{\partial^2 f(c)}{(\partial |\nabla c|)^2}\Big|_{c_0}.$$

Then, the total free energy of the homogeneous mixture occupying a given domain Ω can be

defined by

$$F(c_0) \simeq \int_\Omega f(c_0) + \kappa_1 \nabla^2 c + \kappa_2 (\nabla c)^2 \, \mathrm{d}x. \tag{2.2.3}$$

Integration by parts of the second term yields

$$\int_\Omega \kappa_1 \nabla^2 c \, \mathrm{d}x = -\int_\Omega \frac{d\kappa_1}{dc} (\nabla c)^2 \, \mathrm{d}x + \int_{\partial\Omega} \kappa_1 \nabla c \cdot n \, \mathrm{d}\sigma. \tag{2.2.4}$$

Since mass conservation is desirable, we require

$$\nabla c \cdot n = 0 \quad \text{on } \partial\Omega, \tag{2.2.5}$$

and therefore, the boundary term in (2.2.4) vanishes. Then the total free energy becomes

$$F(c_0) \simeq \int_\Omega f(c_0) + \frac{\lambda}{2} |\nabla c_0|^2 \, \mathrm{d}x, \tag{2.2.6}$$

where we have defined $\frac{\lambda}{2} := \kappa_2 - \frac{d\kappa_1}{dc}$. It is essential to define the total free energy for inhomogeneous concentrations c as well. For this purpose we extend the local free energy or redefine it for general concentrations. Specifically, we choose a double-well potential of the form

$$f(c) = \varphi \, c^2 (1-c)^2, \tag{2.2.7}$$

with a scaling parameter $\varphi > 0$, as shown in figure 2.6.

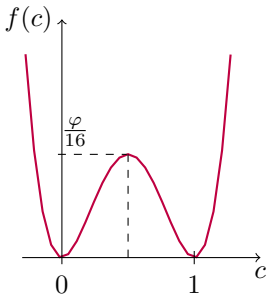

Figure 2.6: A double-well potential $f(c) = \varphi \, c^2 (1-c)^2$ describing the local free energy of a binary mixture.

The minimas of the double-well potential are achieved for $c = 0$ and $c = 1$, i.e. for pure phases. For homogeneous mixtures the local free energy is greater. Since nature tends to minimise its energy the local free energy can be considered as the driving force for phase separation of a homogeneous mixture. The larger the parameter φ is selected, the faster the phase separation progresses at the beginning of the process. The second term of the total free energy (2.2.6)

does only play a role at phase boundaries. In regions of pure phases, ∇c vanishes and does not contribute to the energy. Hence, this term penalises interfaces between two separated phases and makes large interfaces energetically unfavourable. So, at the beginning of the process, when we have a homogeneous mixture, the local free energy term causes the separation. Then after a certain time when inhomogeneities appear in the course of separation and domains of pure phases are formed, the second term emerges. It provides the minimisation of phase boundaries, which results in merger and growth of the domains, which form during the separation process. To describe this process formally, we introduce the chemical potential μ, which can be defined via the first variation of the total free energy with respect to c,

$$\int_\Omega \mu v \,\mathrm{d}x \coloneqq \int_\Omega \frac{\delta}{\delta c} F(c)\, v \,\mathrm{d}x = \int_\Omega f'(c)v - \lambda \nabla c \nabla v \,\mathrm{d}x, \quad \forall v \in C_0^\infty(\Omega), \tag{2.2.8}$$

and hence,

$$\mu = f'(c) + \lambda \Delta c. \tag{2.2.9}$$

According to Fick's law of diffusion, the mass flow is given by

$$j = -M \nabla \mu, \tag{2.2.10}$$

where M denotes the mobility. The balance law describes the change of the relative concentration in time:

$$\partial_t c = \nabla \cdot (M \nabla \mu). \tag{2.2.11}$$

Inserting now the chemical potential defined by (2.2.9), we obtain the Cahn–Hilliard equation, which describes the change of the relative concentration in time in a given domain Ω:

$$\partial_t c = \nabla \cdot \big(M \nabla \big(f'(c) - \lambda \Delta c\big)\big). \tag{2.2.12}$$

The mobility

We want to take a short look at the mobility M of the system, since it is not necessarily clear how mobility is related to standard physical parameters. This circumstance is noticeable during dimensional analysis, which we want to perform later. For $\Omega \subset \mathbb{R}^N$ this leads to the physical unit $\mathrm{m}^{N+2}\mathrm{J}^{-1}\mathrm{s}^{-1}$ for the mobility compared to e.g. $\mathrm{m}^2\mathrm{s}^{-1}$ for the diffusivity. In [KM94], the authors consider a mobility factor M and put this in relation to the diffusion coefficient D via

$$f'' M \approx D, \tag{2.2.13}$$

where f'' is the second derivative of the local free energy density f with respect to c. Assuming that the two phases have approximately the same diffusivity D, we choose a constant mobility factor of the form

$$M = \varphi_*^{-1} D, \tag{2.2.14}$$

where the dimensional factor φ_* denotes a characteristic value of the free energy of the system.

2.2.2 The Cahn–Larché system

The Cahn–Hilliard model cannot capture essential aspects of the experiments described in the previous section. The elastic properties of the lipids are not taken into account and deformations caused by external forces cannot be reproduced. In the following we extend the model from § 2.2.1 by contributions of linear elasticity. We will focus now on the Cahn–Larché system, which goes back to J. Cahn and F. Larché [LC82]. It is the resulting system of coupling the Cahn–Hilliard equation with the equations of linear elasticity and therefore mechanical properties can be taken into account. The elasticity tensor depends naturally on the order parameter c and the chemical potential of the Cahn–Hilliard equation is extended by a contribution derived from the elastic energy density. This model has also been extended and considered in a multiscale context: in [Mer05], a viscoelastic Cahn–Larché model is used to study the decomposition process in eutectic alloys.

We now give a very brief outline of the equations of linear elasticity. In solid mechanics, the current state of a body $\Omega \subset \mathbb{R}^N$ is described by a mapping

$$u \colon \Omega \to \mathbb{R}^N, \tag{2.2.15}$$

known as the deformation. Typically, for physical considerations, one has N equal to 2 or 3. If external forces affect the solid body, a point $x \in \Omega$ is moved to $x + u(x) \in \mathbb{R}^N$. If only small deformations are considered, as in our case, a linearised theory is applicable and we then consider only infinitesimal strains defined by

$$\mathcal{E}(u) = \frac{1}{2} \left(\nabla u + (\nabla u)^{\mathrm{T}} \right), \tag{2.2.16}$$

a symmetric tensor $\mathcal{E}(u) = (e_{ij}(u))_{1 \le i,j \le N} \in \mathbb{R}^{N \times N}$. In the case of the considered lipid monolayer, we have different elastic properties of the two phases. Thus, the elasticity tensor $\mathcal{A}(c)$, which contains the material parameters of the monolayer characterising the stiffness of the phases, naturally depends on the order parameter c. The deformation caused by the movable barrier on the film balance, i.e. the deformation of the monolayer, can therefore have different effects on the two phases.

In linear elasticity, the relation between strain and stress is described by Hooke's law and including eigenstrains we get

$$\mathcal{S} = \mathcal{A}(c)\big(\mathcal{E}(u) - \bar{\mathcal{E}}(c)\big). \tag{2.2.17}$$

By $\bar{\mathcal{E}}(c)$ we denote the eigenstrain of the monolayer. In general, this refers to a strain which is present in absence of any applied stress. This phenomenon occurs in the presence of inhomogeneities, such as thermal expansions, or as in our case, with phase transitions and leads to self-generated internal stress [Mur87]. The eigenstrain is often refered to as stress-free strain and, just like the elastic material parameters, it may be different for each phase. A natural choice is a multiple of the identity

$$\bar{\mathcal{E}}(c) = e(c)\mathbb{1}, \tag{2.2.18}$$

where the scalar valued function e specifies the eigenstrain behaviour at a particular phase state and $\mathbb{1} \in \mathbb{R}^{N\times N}$ is the second-order identity tensor. So, according to (2.2.18), the eigenstrain is uniform in all directions, which seems to be a common choice, see e.g. [Mur87], [FPL99], [Wei02]. Further, in the absence of external forces, a body is in elastic equilibrium if

$$-\nabla \cdot \mathcal{S} = 0 \quad \text{in } \Omega. \tag{2.2.19}$$

The dynamics of the system is now running also to minimise energy resulting from elastic tensions. The energy of the system must be extended by an elastic contribution. According to [Esh61], [Kha67] the elastic energy density, can be described by

$$\mathcal{W}(u,c) = \frac{1}{2}(\mathcal{E}(u) - \bar{\mathcal{E}}(c)) : \mathcal{A}(c)\,(\mathcal{E}(u) - \bar{\mathcal{E}}(c)). \tag{2.2.20}$$

The total free energy of the system (2.2.6) therefore extends to

$$F(c,u) = \int_\Omega f(c) - \frac{\lambda}{2}|\nabla c|^2 + \mathcal{W}(u,c)\,\mathrm{d}x. \tag{2.2.21}$$

Its first variation with respect to c is given by

$$\frac{\delta}{\delta c}\mathcal{W}(u,c) = \frac{1}{2}\big(\mathcal{E}(u) - \bar{\mathcal{E}}(c)\big) : \mathcal{A}'(c)\big(\mathcal{E}(u) - \bar{\mathcal{E}}(c)\big) - \bar{\mathcal{E}}'(c) : \mathcal{S}$$

and hence, the chemical potential (2.2.9) of the system is extended to

$$\mu = f'(c) - \lambda\Delta c - \bar{\mathcal{E}}'(c) : \mathcal{S} + \frac{1}{2}(\mathcal{E}(u) - \bar{\mathcal{E}}(c)) : \mathcal{A}'(c)(\mathcal{E}(u) - \bar{\mathcal{E}}(c)). \tag{2.2.22}$$

Inserting (2.2.22) into (2.2.11) leads to an extended Cahn–Hilliard equation:

$$\partial_t c = \nabla \cdot \Big(M \nabla \big(f'(c) - \lambda \Delta c - \bar{\mathcal{E}}'(c) : \mathcal{S} + \frac{1}{2} (\mathcal{E}(u) - \bar{\mathcal{E}}(c)) : \mathcal{A}'(c) (\mathcal{E}(u) - \bar{\mathcal{E}}(c)) \big) \Big). \tag{2.2.23}$$

If one supplements this equation with the equilibrium (2.2.19), which shall now be valid at any time t of a certain observation period $(0, T)$, one obtains the Cahn–Larché system:

$$\begin{aligned} \partial_t c =& \nabla \cdot \Big(M \nabla \big(f'(c) - \lambda \Delta c - \bar{\mathcal{E}}'(c) : \mathcal{S} \\ &\qquad + \frac{1}{2} (\mathcal{E}(u) - \bar{\mathcal{E}}(c)) : \mathcal{A}'(c) (\mathcal{E}(u) - \bar{\mathcal{E}}(c)) \big) \Big) \quad \text{in } \Omega \times (0,T), \\ 0 =& \nabla \cdot \Big(\mathcal{A}(c) \big(\mathcal{E}(u) - \bar{\mathcal{E}}(c) \big) \Big) \qquad \text{in } \Omega \times (0,T). \end{aligned} \tag{2.2.24, 2.2.25}$$

The consideration of the evolution equation (2.2.24) under the quasi-stationary equilibrium (2.2.25) is reasonable, since the mechanical equilibrium is reached much faster than the diffusion takes place. If we use our representation for the eigenstrain (2.2.18), then, since

$$\bar{\mathcal{E}}'(c) : \mathcal{S} = e'(c) \mathbb{1} : \mathcal{S} = e'(c) \operatorname{tr}(\mathcal{S}),$$

we can write the Cahn–Larché system as follows:

$$\begin{aligned} \partial_t c =& \nabla \cdot \Big(M \nabla \big(f'(c) - \lambda \Delta c - e'(c) \operatorname{tr}(\mathcal{S}) \\ &\qquad + \frac{1}{2} (\mathcal{E}(u) - e(c) \mathbb{1}) : \mathcal{A}'(c) (\mathcal{E}(u) - e(c) \mathbb{1}) \big) \Big) \quad \text{in } \Omega \times (0,T), \\ 0 =& \nabla \cdot \Big(\mathcal{A}(c) \big(\mathcal{E}(u) - e(c) \mathbb{1} \big) \Big) \qquad \text{in } \Omega \times (0,T). \end{aligned} \tag{2.2.26, 2.2.27}$$

Tensors in linear elasticity

Working with problems in mechanics requires the use of fourth-order tensors. In linear elasticity theory, the relationship between stress and strain is described by Hooke's law with the elasticity tensor. This tensor usually has certain symmetries. We will therefore have a brief look on how these have an effect and how they can be dealt with. For more details we refer to [CCS03].

Let A be a fourth-order tensor with components $a_{klmn} \in \mathbb{R}$, for $k, l, m, n = 1, \dots, N$, which

- is symmetric, i.e.

$$A^{\mathrm{T}} = A, \tag{2.2.28}$$

  where the components of the transposed tensor are given by $a^{\mathrm{T}}_{klmn} = a_{mnkl}$, for $k, l, m, n = 1, \dots, N$, and which

- fulfils the additional condition

$$AX^{\mathrm{T}} = AX, \tag{2.2.29}$$

for all second-order tensors $X = (x_{ij})_{1\leq i,j\leq N} \in \mathbb{R}^{N\times N}$, where the product AX is definded by $(AX)_{ij} = \sum_{k,l=1}^{N} a_{ijkl}x_{kl}$.

Then, from (2.2.29), it follows

$$a_{klmn} = a_{klnm} \tag{2.2.30}$$

and with (2.2.28) we get

$$a_{klmn} = a_{lkmn} = a_{klnm} = a_{mnkl}, \tag{2.2.31}$$

for all $k, l, m, n = 1, \ldots, N$. We denote this set of fourth-order tensors by L_4^{S}, i.e. those tensors that fulfill (2.2.28) and (2.2.29). These are the standard tensors in linear elasticity. Furthermore, from (2.2.29), it follows

$$(AX)^{\mathrm{T}} = (AX),$$

for any $X \in \mathbb{R}^{N\times N}$. A tensor $A \in L_4^{\mathrm{S}}$ thus symmetrises an arbitrary second-order tensor, or more precisely it holds that

$$AX = AX^{\mathrm{S}} \quad \text{and} \quad AX^{\mathrm{A}} = 0,$$

where $X = X^{\mathrm{S}} + X^{\mathrm{A}}$ denotes the decomposition of a second-order tensor X into a symmetric part $X^{\mathrm{S}} = \frac{1}{2}(X + X^{\mathrm{T}})$ and an antiysmmetric part $X^{\mathrm{A}} = \frac{1}{2}(X - X^{\mathrm{T}})$. Therefore, a tensor $A \in L_4^{\mathrm{S}}$, considered as a linear mapping from the set of second-order tensors into itself, cannot be injective. However, if we restrict A to the set of symmetric second-order tensors, we can get around this problem. We denote by $I \in \mathbb{R}^{N\times N}$ the symmetric fourth-order tensor with components defined by

$$I_{klmn} = \frac{1}{2}(\delta_{km}\delta_{ln} + \delta_{kn}\delta_{lm}), \quad 1 \leq k, l, m, n \leq N. \tag{2.2.32}$$

This tensor fulfils property (2.2.29), and hence, $I \in L_4^{\mathrm{S}}$. It holds that $AI = IA = A$, where the product of two fourth-order tensors is defined by $(AB)_{ijmn} = \sum_{k,l=1}^{N} a_{ijkl}b_{klmn}$. Thus, we call I the unit tensor in the space L_4^S. The inverse A^{-1} of a fourth-order tensor $A \in L_4^S$, if it exists, is defined by the relation

$$A^{-1}A = AA^{-1} = I.$$

Moreover, a fourth-order tensor A is called positive definite, if

$$X : AX \geq 0,$$

for all symmetric second-order tensors X and

$$X : AX = 0 \quad \Leftrightarrow \quad X = 0.$$

A positive definite tensor $A \in L_4^S$ is non-singular, i.e. its inverse A^{-1} exists. In addition, the inverse is also positive definite.

Remark 2.2.1.

(i) In the case of isotropic material, i.e. the mechanical properties are the same in all directions, the elastic properties can be described by two parameters $\lambda, \mu \in \mathbb{R}$. According to Hooke's law, the stress tensor $\mathcal{S} = \mathcal{A}\mathcal{E}$ can be represented by

$$\mathcal{S} = 2\,\mu\,\mathcal{E} + \lambda\,\mathrm{tr}(\mathcal{E})\,\mathbb{1}, \tag{2.2.33}$$

where λ and μ are known as the Lamé constants determining the elasticity tensor. If $\lambda > 0$ and $\mu > 0$, the corresponding elasticity tensor is positive definite.

(ii) In linear elasticity, the inverse of the elasticity or stiffness tensor is known as the compliance tensor.

Identification of the setting

In the following, we specify some parameters, conditions and requirements in order to determine the setting in which we want to work. For the modelling of the concrete experiments described in section 2.1, we choose a rectangular domain $\Omega \subset \mathbb{R}^2$, representing the area of the water trough of the film balance on which the lipid monolayer is examined, and with boundary $\partial\Omega =: \Gamma = \Gamma_0 \cup \Gamma_g \cup \Gamma_s$, with boundary parts Γ_0, Γ_g and Γ_s as illustrated in figure 2.7.

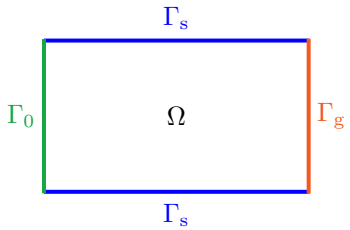

Figure 2.7: Domain Ω with boundary parts Γ_0, Γ_g and Γ_s.

In order to keep mathematics more general, in the following chapters we consider a bounded domain $\Omega \subset \mathbb{R}^N$ with Lipschitz continuous boundary $\Gamma := \partial\Omega$ with pairwise disjoint boundary parts Γ_0, Γ_g and Γ_s such that $\Gamma = \Gamma_0 \cup \Gamma_\mathrm{g} \cup \Gamma_\mathrm{s}$.

By n we denote the outer unit normal and by τ the unit tangential vector on Γ and we consider the processes in the time interval $S = (0, T)$, where $T > 0$. At any time, the lipid monolayer remains on the film balance and cannot pass over the edges. Thus, we choose no-flux conditions for the relative concentration c and the chemical potential μ on the whole boundary Γ,

$$\nabla c \cdot n = 0 \quad \text{on } \Gamma \times S, \tag{2.2.34}$$

$$\nabla \mu \cdot n = 0 \quad \text{on } \Gamma \times S. \tag{2.2.35}$$

The force applied by the controllable barrier and compressing the lipid monolayer is modelled by applying a boundary force g on Γ_g, hence,

$$\mathcal{S}n = g \quad \text{on } \Gamma_\mathrm{g} \times S. \tag{2.2.36}$$

On the opposite boundary part Γ_0 we do not want any deformation and hence we require

$$u = 0 \quad \text{on } \Gamma_0 \times S. \tag{2.2.37}$$

Also, we do not want any deformation of the monolayer beyond the lateral edges in the normal direction. Therefore, on the side part of the boundary Γ_s we set

$$u \cdot n = 0 \quad \text{on } \Gamma_\mathrm{s} \times S, \tag{2.2.38}$$

and a free-slip condition as well, namely

$$\tau \cdot \mathcal{S}n = 0 \quad \text{on } \Gamma_\mathrm{s} \times S, \tag{2.2.39}$$

These conditions describe that the monolayer cannot expand past the lateral edges and does not adhere there when compressed. It would also have been possible to set the free-slip condition (2.2.39) also on the boundary part Γ_0 instead of the Dirichlet condition $u = 0$. However, the boundary condition (2.2.37) ensures the uniqueness of u. Setting the displacement equal to zero on Γ_0 means a fixing of the elastic medium. This is valid here, since the lipid film is not pushed along this boundary part. However, the choice of the free-slip condition on Γ_0 would not change the following analytical results; the displacement would only have to be uniquely determined by an additional condition. Besides, the non-uniqueness in u is not the deciding factor anyway, since u itself will have no effect on the evolution of c, because only $\mathcal{E}(u)$ enters the evolution equation for c.

We complete the system with an appropriate initial condition for c,

$$c(\,\cdot\,,0) = c^{\mathrm{in}}(\cdot) \quad \text{in } \Omega, \tag{2.2.40}$$

describing the initial homogeneous relative concentration of the mixture, i.e. the initial homogeneous state of the monolayer.

The elasticity tensor

We assume the two phases of the monolayer to have different elastic properties and hence we denote the elasticity tensor describing the elastic properties of the LE phase by $\mathcal{A}^{\mathrm{E}}$ and the elasticity tensor of the elastically harder phase LC phase by $\mathcal{A}^{\mathrm{C}}$. Each of the two pure lipid phases is isotropic, and so are the two component tensors. Then, following [Wei02], for the lipid mixture, we consider

$$\mathcal{A}(c) \coloneqq \mathcal{A}^{\mathrm{E}} + d(c)\left(\mathcal{A}^{\mathrm{C}} - \mathcal{A}^{\mathrm{E}}\right), \tag{2.2.41}$$

an elasticity tensor depending on the relative concentration of the mixture, which is simply an interpolation of the two component tensors. The interpolation function d should be defined such that

$$d(0) = 0, \quad d(1) = 1, \quad d'(0) = 0, \quad d'(1) = 0,$$

for instance

$$d(x) = \begin{cases} 0, & x < 0, \\ -2x^3 + 3x^2, & 0 \le x \le 1, \\ 1, & x > 1. \end{cases} \tag{2.2.42}$$

With this we have also determined that $c = 0$ corresponds to the elastically softer LE phase and $c = 1$ corresponds to the elastically stiffer LC phase. We assume positive definiteness for the individual component tensor, i.e. for each $i \in \{\mathrm{E}, \mathrm{C}\}$ we asume the existence of positive numbers $\alpha^i > 0$ such that

$$\alpha^i \left|X\right|^2 \le \mathcal{A}^i\, X : X, \tag{2.2.43}$$

for any symmetric matrix $X \in \mathbb{R}^{N\times N}$. Further, we assume the usual symmetry conditions in linear elasticity theory (2.2.31), i.e. for $\mathcal{A}^i = (a^i_{ijkh})_{1\le i,j,k,h\le N}$, $i \in \{\mathrm{E}, \mathrm{C}\}$, we require

$$a^i_{ijkh} = a^i_{ijhk} = a^i_{jikh} = a^i_{khij}. \tag{2.2.44}$$

Obviously, the interpolated tensor defined by (2.2.41) is also positive definite and fulfils the symmetry condition (2.2.44).

Existence of weak solutions

In the following, we want to summerise in short the existence result from Garcke, stated in [Gar00], adopted to our setting. In [Gar00], the author studied phase separation in multi-component alloys in the presence of elastic interactions. There, he considered the Cahn–Larché system stated as system of second-order differential equations. Adapted to our setting of a binary mixture where the relative concentration is described by the order parameter c and adapted to our notation, the system looks as follows:

$$\begin{aligned} \partial_t c &= M\Delta\mu, \\ \mu &= f'(c) + \lambda\Delta c - \bar{\mathcal{E}}'(c) : \mathcal{S} + \frac{1}{2}(\mathcal{E}(u) - \bar{\mathcal{E}}(c)) : \mathcal{A}'(c)(\mathcal{E}(u) - \bar{\mathcal{E}}(c)), \\ 0 &= \nabla \cdot \mathcal{S}, \\ \mathcal{S} &= \mathcal{A}(c)\,(\mathcal{E}(u) - \bar{\mathcal{E}}(c)), \end{aligned} \tag{2.2.45}$$

completed by the same boundary conditions for c and μ as chosen by us, a condition to the stress in normal direction on the whole boundary $\partial\Omega$ and an initial condition $c(\,\cdot\,, 0) = c_0 \in H^1(\Omega)$.

Before we recall the definition of a weak solution of the above system, we specify two function spaces, namely the space of all infinitesimal rigid displacements

$$X = \{u \in (H^1(\Omega))^N \mid \text{there exist } b \in \mathbb{R}^N, A \in \mathbb{R}^{N\times N} \text{ with } A^{\mathrm{T}} = -A \text{ such that } u(x) = Ax + b\}$$

and the space orthogonal to it

$$X^{\perp} = \{v \in (H^1(\Omega))^N \mid (v, u)_{H^1(\Omega)} = 0 \text{ for all } u \in X\}.$$

Definition 2.2.2 (Weak solution, [Gar00])**.** *A triple*

$$(c, \mu, u) \in L^2(0, T; H^1(\Omega)) \times L^2(0, T; H^1(\Omega)) \times L^2(0, T; X^{\perp}) \tag{2.2.46}$$

with $f'(c) \in L^1(\Omega \times (0, T))$ is called a weak solution of the system (2.2.45)*, completed by the specified boundary and initial value conditions, if and only if*

(i)

$$\int_0^T \int_\Omega \partial_t\varphi_1\,(c - c_0)\,\mathrm{d}x\,\mathrm{d}\tau = \int_0^T \int_\Omega M\nabla\mu\nabla\varphi_1\,\mathrm{d}x\,\mathrm{d}\tau,$$

for all $\varphi_1 \in L^2(0, T; H^1(\Omega))$ with $\partial_t\varphi_1 \in L^2(\Omega \times (0, T))$ and $\varphi_1(T) = 0$,

(ii)

$$\int_0^T \int_\Omega \mu\, \varphi_2 \,\mathrm{d}x\,\mathrm{d}\tau$$
$$= \int_0^T \int_\Omega \Big(f'(c) - \lambda\Delta c - \bar{\mathcal{E}}'(c) : \mathcal{S} + \frac{1}{2}(\mathcal{E}(u) - \bar{\mathcal{E}}(c)) : \mathcal{A}'(c)(\mathcal{E}(u) - \bar{\mathcal{E}}(c))\Big)\, \varphi_2 \,\mathrm{d}x\,\mathrm{d}\tau,$$

for all $\varphi_2 \in L^2(0,T;H^1(\Omega)) \cap L^\infty(\Omega \times (0,T))$ *and*

(iii)

$$\int_0^T \int_\Omega \Big(\mathcal{A}(c)(\mathcal{E}(u) - e(c)\mathbb{1})\Big) : \nabla\psi \,\mathrm{d}x\,\mathrm{d}\tau = \int_0^T \int_{\partial\Omega} g\,\psi \,\mathrm{d}\sigma\,\mathrm{d}\tau,$$

for all $\psi \in L^2(0,T;[H^1(\Omega)]^N)$.

Under the conditions stated in [Gar00], which are fulfiled in our setting, the existence of weak solutions in the sense of definition 2.2.2 with the following properties is proven.

Theorem 2.2.3 (Existence of weak solutions, [Gar00])**.** *There exists a weak solution of the system* (2.2.45) *in the sense of definition 2.2.2, such that*

$$\begin{aligned} c &\in C^{0,\frac{1}{4}}(0,T;L^2(\Omega)), \\ \partial_t c &\in L^2(0,T;(H^1(\Omega))'), \\ u &\in L^\infty(0,T;[H^1(\Omega)]^N). \end{aligned} \tag{2.2.47}$$

This solution is uniquely determined if the elasticity tensor is equal for each phase.

Moreover, according to [Gar00], there exists a $p > 2$, such that $\nabla u \in L^\infty(0,T;(L^p(\Omega))^{N\times N})$, which, together with the Sobolev embedding, in the two-dimensional case, i.e. $N = 2$, implies, that there exists a number $\alpha > 0$, such that $u \in L^\infty(0,T;(C^{0,\alpha}(\Omega))^2)$.

We would like to emphasise that the framework in [Gar00] was kept more general and even the case of a logarithmic free energy was considered, but we just wanted to briefly summarise the results concerning our setting.

2.3 Multiscale setting

In § 2.1, we have already pointed out the multiscale aspect of the considered physical process. Now, we would like to go into this aspect again in more detail. As we will see in the next

chapter, this, together with the assumption of a periodic framework, will allow us to work in the framework of periodic homogenisation.

With regard to experimental observations, we assume the evolving microstructure of the pattern to have an intrinsic length scale associated with it. We introduce a characteristic macroscopic length scale L, representing the order of magnitude of the size of the film balance and corresponding to the macroscopic process, and a characteristic microscopic length scale l, which corresponds to the order of magnitude of the scale on which the phase separation is observable, and we write

$$\epsilon = \frac{l}{L}. \tag{2.3.1}$$

It is clear that it holds $\epsilon \ll 1$. Then, the order parameter c, which describes the microstructure, is assumed to depend on two independent spatial variables, x, associated with the macroscale and $\frac{x}{\epsilon}$, associated with the microscale. We denote this with an ϵ in the index and write

$$c_\epsilon(x,t) = c(x, x/\epsilon, t). \tag{2.3.2}$$

We achieve this circumstance by choosing an initial value for c_ϵ, depending on the macroscopic variable x and on the microscopic variable $\frac{x}{\epsilon}$. Due to the dependency on the order parameter, this also applies to the elasticity tensor $\mathcal{A}(c_\epsilon)$, which implies an analogue spatial dependence of the displacement field and hence, we write $u_\epsilon = u$.

2.4 Non-dimensionalisation and scaling

As already mentioned, in this thesis we deal with the special scaled variant of the Cahn–Larché system, given by (1.0.1). With this scaled system, separation processes on the microscopic scale can be described under the influence of mechanical processes that take place on a macroscopic scale. This scaling is justified in the following.

The usual form of the Cahn–Larché system (2.2.26), (2.2.27) as introduced in § 2.2.2 does not take into account that the processes we consider take place on different scales. Therefore, it is necessary to do a non-dimensionalisation under inclusion of different involved characteristic lengths (cf. e.g. [AJH90], [PB09], [PB05], [Mei08]). Also, we have different time scales and in view of the strong difference here, we already consider the system in quasi-stationary setting for the mechanics. At this point, however, we would like to take a step back and consider the

mechanics dynamically. The starting point for the non-dimensionalisation is now therefore

$$\begin{aligned}\partial_{t_\mathrm{d}} c_\epsilon =& \nabla \cdot \big(M \nabla \big(f'(c_\epsilon) - \lambda \Delta c - e'(c_\epsilon) \operatorname{tr}(\mathcal{S}) \\ &+ \frac{1}{2} (\mathcal{E}(u_\epsilon) - e(c_\epsilon)\mathbb{1}) : \mathcal{A}'(c_\epsilon)(\mathcal{E}(u_\epsilon) - e(c_\epsilon)\mathbb{1}) \big) \big),\end{aligned} \tag{2.4.1}$$

$$\varrho\, \partial_{t_\mathrm{m}}^2 u_\epsilon = \nabla \cdot \big(\mathcal{A}(c_\epsilon)(\mathcal{E}(u_\epsilon) - e(c_\epsilon)\mathbb{1}) \big), \tag{2.4.2}$$

where ϱ denotes the density and $M = D/\varphi_*$ from (2.2.14), where D is the diffusivity. Further, t_d and t_m denote the time variables corresponding to diffusion and mechanics, respectively, as we now distinguish the times. It turns out that a non-dimensionalisation of (2.4.1) and (2.4.2) taking into account the characteristic macroscopic length scale L and the characteristic microscopic length scale l introduced in section 2.3, results in a system scaled by powers of ϵ and which is suitable for application of techniques of periodic homogenisation.

We further define characteristic microscopic lengths associated with the diffusion and the mechanics, l_d and l_m, respectively, and express them as a multiple of the geometric microscopic length l. We choose $l_\mathrm{d} = \frac{1}{10}\, l$ and $l_\mathrm{m} = l$, since the mechanics happens on the whole microscopic length scale whereas the diffusion scale is typically a little shorter. The characteristic time for the diffusion is then defined by

$$T_\mathrm{d} \coloneqq \frac{l_d^r\, L^{2-r}}{D_\mathrm{ref}}, \tag{2.4.3}$$

and the characteristic time for the mechanics by

$$T_\mathrm{m} \coloneqq \Big(\frac{l_m^s L^{2-s} \varrho_\mathrm{ref}}{\sigma_\mathrm{ref}} \Big)^{1/2}, \tag{2.4.4}$$

both depending on powers of the two different characteristic length scales. The respective influence of the different characteristic lengths is regulated by exponents depending on parameters $r, s \in [0, 2]$, which we have to determine later. With D_ref, σ_ref and ϱ_ref we denote reference values corresponding to the diffusivity, the stiffness and the density, respectively, such that

$$\frac{D}{D_\mathrm{ref}} = 1 \quad \text{and} \quad \frac{\varrho}{\varrho_\mathrm{ref}} = 1.$$

With the dimensionless macroscopic space variable $\tilde{x} \coloneqq x/L$ and the time variable $\tilde{t}_\mathrm{d} \coloneqq t_\mathrm{d}/T_\mathrm{d}$, from (2.4.1) and $D = M\varphi_*$, we get

$$\begin{aligned}\frac{1}{T_\mathrm{d}}\, \partial_{\tilde{t}_d} c_\epsilon = \frac{1}{L} \tilde{\nabla} \cdot \Big(D \frac{1}{L} \tilde{\nabla} \big(& \varphi_*^{-1} f'(c_\epsilon) - \varphi_*^{-1} \lambda \frac{1}{L^2} \tilde{\Delta} c - \varphi_*^{-1} e'(c_\epsilon) \operatorname{tr}(\mathcal{S}) \\ &+ \frac{1}{2} \varphi_*^{-1} (\mathcal{E}(u_\epsilon) - e(c_\epsilon)\mathbb{1}) : \mathcal{A}'(c_\epsilon)(\mathcal{E}(u_\epsilon) - e(c_\epsilon)\mathbb{1}) \big) \Big).\end{aligned}$$

With (2.4.3), we obtain

$$\partial_{\tilde{t}_d} c_\epsilon = \frac{l^r L^{2-r}}{10^r L^2}\,\tilde{\Delta}\Big(\varphi_*^{-1} f'(c_\epsilon) - \varphi_*^{-1}\lambda\frac{1}{L^2}\tilde{\Delta}c - \varphi_*^{-1} e'(c_\epsilon)\,\mathrm{tr}(\mathcal{S}) + \frac{1}{2}\varphi_*^{-1}(\mathcal{E}(u_\epsilon) - e(c_\epsilon)\mathbb{1}) : \mathcal{A}'(c_\epsilon)(\mathcal{E}(u_\epsilon) - e(c_\epsilon)\mathbb{1})\Big),$$

which, recalling that $\epsilon = \frac{l}{L}$, can be written as

$$\partial_{\tilde{t}_d} c_\epsilon = \epsilon^r\, 10^{-r}\,\tilde{\Delta}\Big(\tilde{f}'(c_\epsilon) - \epsilon^2\tilde{\lambda}\tilde{\Delta}c - e'(c_\epsilon)\,\mathrm{tr}(\tilde{\mathcal{S}}) + \frac{1}{2}(\mathcal{E}(u_\epsilon) - e(c_\epsilon)\mathbb{1}) : \tilde{\mathcal{A}}'(c_\epsilon)(\mathcal{E}(u_\epsilon) - e(c_\epsilon)\mathbb{1})\Big),$$

where we have defined the dimensionless quantities as follows

$$\tilde{f}'(c_\epsilon) \coloneqq \varphi_*^{-1} f'(c_\epsilon), \quad \tilde{\lambda} \coloneqq \varphi_*^{-1}\epsilon^{-2}L^{-2}\lambda, \quad \tilde{\mathcal{A}}'(c_\epsilon) \coloneqq \varphi_*^{-1}\mathcal{A}'(c_\epsilon) \tag{2.4.5}$$

and

$$\tilde{\mathcal{S}} \coloneqq \varphi_*^{-1}\,\mathcal{S} = \varphi_*^{-1}\,\mathcal{A}(c_\epsilon)\big(\mathcal{E}(u_\epsilon) - e(c_\epsilon)\mathbb{1}\big) = \tilde{\mathcal{A}}(c_\epsilon)\big(\mathcal{E}(u_\epsilon) - e(c_\epsilon)\mathbb{1}\big), \tag{2.4.6}$$

with

$$\tilde{\mathcal{A}}(c_\epsilon) \coloneqq \varphi_*^{-1}\mathcal{A}(c_\epsilon). \tag{2.4.7}$$

All quantities with a tilde denote dimensionless quantities, where $\tilde{f}'(c_\epsilon)$ is of order 1. Note that the strain is already dimensionless. Further, we have made use of the fact that the magnitude of the line tension λ is much smaller than the free energy level. In order to account for this and to compensate the length scale associated with the Laplacian, a factor ϵ^2 is explicitly taken out.

With regard to the mechanical equation (2.4.2) we set $\tilde{u} \coloneqq \frac{u}{L}$ and with the dimensionless time variable $\tilde{t}_\mathrm{m} \coloneqq t_\mathrm{m}/T_\mathrm{m}$ we get

$$\varrho\,\frac{L}{T_\mathrm{m}^2}\,\partial^2_{\tilde{t}_m}\tilde{u}_\epsilon = \frac{1}{L}\tilde{\nabla}\cdot\big(\mathcal{A}(c_\epsilon)(\mathcal{E}(u_\epsilon) - e(c_\epsilon)\mathbb{1})\big). \tag{2.4.8}$$

This then results in

$$\partial^2_{\tilde{t}_m}\tilde{u}_\epsilon = \epsilon^s\,\tilde{\nabla}\cdot\big(\hat{\mathcal{A}}(c_\epsilon)(\mathcal{E}(u_\epsilon) - e(c_\epsilon)\mathbb{1})\big), \tag{2.4.9}$$

with dimensionless elasticity tensor

$$\hat{\mathcal{A}}(c_\epsilon) = \sigma_\mathrm{ref}^{-1}\mathcal{A}(c_\epsilon). \tag{2.4.10}$$

Since we want to non-dimensionalise the elasticity tensor in a common way, we put the two

different dimensionless variants (2.4.7) and (2.4.10) in relation to each other and get

$$\hat{\mathcal{A}}(c_\epsilon) = \sigma_{\text{ref}}^{-1}\,\mathcal{A}(c_\epsilon) = \sigma_{\text{ref}}^{-1}\,\varphi_*\,\tilde{\mathcal{A}}(c_\epsilon) =: \kappa\,\tilde{\mathcal{A}}(c_\epsilon). \tag{2.4.11}$$

In summary, we can state the following dimensionless and scaled system:

$$\begin{aligned}\partial_{\tilde{t}_{\text{d}}} c_\epsilon = \epsilon^r\,10^{-r}\,\tilde{\Delta}\,\Big(&\tilde{f}'(c_\epsilon) - \epsilon^2\tilde{\lambda}\tilde{\Delta}c - e'(c_\epsilon)\,\text{tr}(\tilde{\mathcal{S}}) \\ &+ \frac{1}{2}(\mathcal{E}(u_\epsilon) - e(c_\epsilon)\mathbb{1}) : \tilde{\mathcal{A}}'(c_\epsilon)(\mathcal{E}(u_\epsilon) - e(c_\epsilon)\mathbb{1})\Big),\end{aligned} \tag{2.4.12}$$

$$\partial_{\tilde{t}_{\text{m}}}^2\,\tilde{u}_\epsilon = \epsilon^s\,\kappa\,\tilde{\nabla}\cdot\Big(\tilde{\mathcal{A}}(c_\epsilon)\big(\mathcal{E}(u_\epsilon) - e(c_\epsilon)\mathbb{1}\big)\Big), \tag{2.4.13}$$

with a positive dimensionless constant $\kappa := \sigma_{\text{ref}}^{-1}\,\varphi_*$ that ensures the unification of the dimensionless elasticity tensor in the equations above. The other way around, setting $\tilde{\mathcal{A}}(c_\epsilon) = \kappa^{-1}\,\hat{\mathcal{A}}(c_\epsilon)$, of course, can also be chosen.

Identification of the parameters r, s:

Special attention must now be paid to the different characteristic times, since they depend on different powers of the scaling parameter ϵ. Further, to represent the diffusion and the mechanics on a common time scale, we need to match the characteristic times and want to unify them as well as possible. Therefore, we require

$$T_{\text{d}} \approx T_{\text{m}}. \tag{2.4.14}$$

Motivated from the film-balance setup, we choose $L = 1\,\text{m}$ as characteristic length corresponding to the macroscopic process and $l = 10^{-4}\,\text{m}$ as characteristic microscopic length scale. Unfortunately, as already mentioned, there are currently no complete parameter sets of measurement data from experiments available. Within the context of the film-balance experiments, a lipid monolayer seems to be a sensitive system and in the literature, the values of the physical quantities may vary depending on the specific lipid or lipids, the phase state of the monolayer, temperature and even on the measuring method. However, we are only interested in the orders of magnitude to get an approximate estimate of the characteristic times. Considering typical values of the diffusion coefficient, we choose $1\,\mu\text{m}^2\,\text{s}^{-1}$ as characteristic value [GFBH09]. Hence, we obtain

$$T_{\text{d}} = \frac{10^{-r}\,l^r L^{2-r}}{D_{\text{ref}}} = 10^{-5r+12}.$$

Assuming that one DPPC-molecule occupies an area of approximately $1/70 \cdot 10^{-20}\,\text{m}^2$ in the beginnig of the phase transition [TPMS10] and with the molar mass of DPPC, which is $734.04 \cdot 10^{-3}\,\text{kg mol}^{-1}$ [SA19], we calculate a characteristic value of the order of magnitude $\approx 10^{-2}\,\text{kg m}^{-2}$ for the density of a lipid monolayer. With 10^{-1}N m^{-1} as characteristic value

of the stiffness of a lipid monolayer [Ste05], we get

$$T_{\mathrm{m}} = \Big(\frac{l^s L^{2-s} \varrho_{\mathrm{ref}}}{\sigma_{\mathrm{ref}}}\Big)^{1/2} = 10^{\frac{1}{2}(-4s-1)},$$

which, with regard to the definition interval of the parameters, leads to $r = 2$ and $s = 0$. Note that, with this scaling, we still consider the mechanics too slow compared to the diffusion and therefore we turn to the quasi-stationary setting again. Dropping the tildes for a simpler notation and better clarity, we get the following dimensionless and scaled system:

$$\begin{aligned} \partial_t c_\epsilon = \epsilon^2\, 10^{-2}\, \Delta \Big(& f'(c_\epsilon) - \epsilon^2 \lambda \Delta c - e'(c_\epsilon)\, \mathrm{tr}(\mathcal{S}) \\ & + \frac{1}{2}(\mathcal{E}(u_\epsilon) - e(c_\epsilon)\mathbb{1}) : \mathcal{A}'(c_\epsilon)(\mathcal{E}(u_\epsilon) - e(c_\epsilon)\mathbb{1}) \Big), \end{aligned} \tag{2.4.15}$$

$$0 = \kappa\, \nabla \cdot \Big(\mathcal{A}(c_\epsilon)\, (\mathcal{E}(u_\epsilon) - e(c_\epsilon)\mathbb{1}) \Big). \tag{2.4.16}$$

With this system we have now a system which takes the different scales into account by its scaling by exponents of ϵ. It is the starting point for our following considerations. Note that so far no assumption has been made about the periodicity of the microstructure, but only about the existence of macroscopic and microscopic characteristic lengths. Whenever we speak about this system in what follows, we mean these equations completed by the boundary and initial conditions (2.2.34) – (2.2.40).

In the further course of our considerations, we will refrain from carrying the constants 10^{-2} and κ until chapter 7, in which we deal with numerical simulations.

2.5 Linearisation

We end this chapter by deriving a linear scaled Cahn–Larché system, which we deal with in more detail in § 4.2.2 and in chapters 5 and 6. Let $c_{n,\epsilon}$ and $u_{n,\epsilon}$ denote general solutions of the scaled Cahn–Larché system (2.4.15), (2.4.16). Then, we consider $c_{n,\epsilon} + h\,\tilde{c}_\epsilon$ and $u_{n,\epsilon} + h\,\tilde{u}_\epsilon$, for a small $h > 0$ and functions $\tilde{c}_\epsilon,\ \tilde{u}_\epsilon$ having the same multiscale character as described in § 2.3, to obtain a linear system for $\tilde{c}_\epsilon$ and $\tilde{u}_\epsilon$. First, we linearise the stress tensor $\mathcal{S}_\epsilon$ and write

$$\mathcal{S}_\epsilon = \mathcal{S}_{n,\epsilon} + h\,\tilde{\mathcal{S}}_\epsilon + \mathcal{O}(h^2), \tag{2.5.1}$$

with the stress tensor in the nonlinear solutions

$$\mathcal{S}_{n,\epsilon} \coloneqq \mathcal{A}(c_{n,\epsilon})\big(\mathcal{E}(u_{n,\epsilon}) - e(c_{n,\epsilon})\mathbb{1}\big) \tag{2.5.2}$$

and the linearised stress

$$\tilde{\mathcal{S}}_\epsilon \coloneqq \mathcal{A}(c_{n,\epsilon})\big(\mathcal{E}(\tilde{u}_\epsilon) - e'(c_{n,\epsilon})\tilde{c}_\epsilon \mathbb{1}\big) + \mathcal{A}'(c_{n,\epsilon})\tilde{c}_\epsilon\big(\mathcal{E}(u_{n,\epsilon}) - e(c_{n,\epsilon})\mathbb{1}\big). \tag{2.5.3}$$

For the extended Cahn–Hilliard equation (2.4.15) we get

$$\begin{aligned}
&\partial_t(c_{n,\epsilon} + h\tilde{c}_\epsilon) \\
&= \epsilon^2\Delta\Big[f'(c_{n,\epsilon}) - \epsilon^2\lambda\Delta c_{n,\epsilon} - e'(c_{n,\epsilon})\operatorname{tr}(\mathcal{S}_{n,\epsilon}) \\
&\qquad + \frac{1}{2}(\mathcal{E}(u_{n,\epsilon}) - e(c_{n,\epsilon})\mathbb{1}) : \mathcal{A}'(c_{n,\epsilon})(\mathcal{E}(u_{n,\epsilon}) - e(c_{n,\epsilon})\mathbb{1})\Big] \\
&+ h\,\epsilon^2\Delta\Big[f''(c_{n,\epsilon})\tilde{c}_\epsilon - \epsilon^2\lambda\Delta\tilde{c}_\epsilon - e'(c_{n,\epsilon})\operatorname{tr}(\tilde{\mathcal{S}}_\epsilon) - e''(c_{n,\epsilon})\tilde{c}_\epsilon\operatorname{tr}(\mathcal{S}_{n,\epsilon}) \\
&\qquad + \big(\mathcal{E}(u_{n,\epsilon}) - e(c_{n,\epsilon})\mathbb{1}\big) : \mathcal{A}'(c_{n,\epsilon})\big(\mathcal{E}(\tilde{u}_\epsilon) - e'(c_{n,\epsilon})\tilde{c}_\epsilon\mathbb{1}\big) \\
&\qquad + \frac{1}{2}\big(\mathcal{E}(u_{n,\epsilon}) - e(c_{n,\epsilon})\mathbb{1}\big) : \mathcal{A}''(c_{n,\epsilon})\tilde{c}_\epsilon\big(\mathcal{E}(u_{n,\epsilon}) - e(c_{n,\epsilon})\mathbb{1}\big)\Big] \\
&+ \mathcal{O}(h^2).
\end{aligned} \tag{2.5.4}$$

Neglecting the second order terms, from (2.5.1) and (2.5.4) we can read off linear equations for the perturbations $\tilde{c}_\epsilon$ and $\tilde{u}_\epsilon$:

$$\begin{aligned}
\partial_t\tilde{c}_\epsilon = \epsilon^2\Delta\Big(&f''(c_{n,\epsilon})\tilde{c}_\epsilon - \epsilon^2\lambda\Delta\tilde{c}_\epsilon - e'(c_{n,\epsilon})\operatorname{tr}(\tilde{\mathcal{S}}_\epsilon) - e''(c_{n,\epsilon})\tilde{c}_\epsilon\operatorname{tr}(\mathcal{S}_{n,\epsilon}) \\
&+ \big(\mathcal{E}(u_{n,\epsilon}) - e(c_{n,\epsilon})\mathbb{1}\big) : \mathcal{A}'(c_{n,\epsilon})\big(\mathcal{E}(\tilde{u}_\epsilon) - e'(c_{n,\epsilon})\tilde{c}_\epsilon\mathbb{1}\big) \\
&+ \frac{1}{2}\big(\mathcal{E}(u_{n,\epsilon}) - e(c_{n,\epsilon})\mathbb{1}\big) : \mathcal{A}''(c_{n,\epsilon})\tilde{c}_\epsilon\left(\mathcal{E}(u_{n,\epsilon}) - e(c_{n,\epsilon})\mathbb{1}\right)\Big) \qquad \text{in } \Omega\times S,
\end{aligned} \tag{2.5.5}$$

$$\begin{aligned}
0 = \nabla\cdot\Big(&\mathcal{A}(c_{n,\epsilon})\big(\mathcal{E}(\tilde{u}_\epsilon) - e'(c_{n,\epsilon})\tilde{c}_\epsilon\mathbb{1}\big) \\
&+ \mathcal{A}'(c_{n,\epsilon})\tilde{c}_\epsilon\big(\mathcal{E}(u_{n,\epsilon}) - e(c_{n,\epsilon})\mathbb{1}\big)\Big) \quad \text{in } \Omega\times S.
\end{aligned} \tag{2.5.6}$$

The boundary conditions are also linearised, which leads to

$$\begin{aligned}
\nabla\tilde{c}_\epsilon\cdot n &= 0 \quad \text{on } \Gamma\times S,\\
\nabla\tilde{\mu}_\epsilon\cdot n &= 0 \quad \text{on } \Gamma\times S,\\
\tilde{u}_\epsilon &= 0 \quad \text{on } \Gamma_0\times S,\\
\tilde{\mathcal{S}}_\epsilon n &= g \quad \text{on } \Gamma_{\mathrm{g}}\times S,\\
\tilde{u}_\epsilon\cdot n &= 0 \quad \text{on } \Gamma_{\mathrm{s}}\times S,\\
\tau\cdot\tilde{\mathcal{S}}_\epsilon n &= 0 \quad \text{on } \Gamma_{\mathrm{s}}\times S,
\end{aligned} \tag{2.5.7}$$

with

$$\begin{aligned}\tilde{\mu}_\epsilon = {} & f''(c_{n,\epsilon})\tilde{c}_\epsilon - \epsilon^2\lambda\Delta\tilde{c}_\epsilon - e'(c_{n,\epsilon})\operatorname{tr}(\mathcal{S}_\epsilon) - e''(c_{n,\epsilon})\tilde{c}_\epsilon \operatorname{tr}(\mathcal{S}_{n,\epsilon}) \\ & + \big(\mathcal{E}(u_{n,\epsilon}) - e(c_{n,\epsilon})\mathbb{1}\big) : \mathcal{A}'(c_{n,\epsilon})\big(\mathcal{E}(\tilde{u}_\epsilon) - e'(c_{n,\epsilon})\tilde{c}_\epsilon\mathbb{1}\big) \\ & + \frac{1}{2}\big(\mathcal{E}(u_{n,\epsilon}) - e(c_{n,\epsilon})\mathbb{1}\big) : \mathcal{A}''(c_{n,\epsilon})\tilde{c}_\epsilon\,\big(\mathcal{E}(u_{n,\epsilon}) - e(c_{n,\epsilon})\mathbb{1}\big)\end{aligned}$$

denoting the linearised chemical potential. In the following, whenever we talk about the linear Cahn–Larché system, we mean the equations (2.5.5) and (2.5.6) completed by the boundary conditions (2.5.7) and a suitable initial condition for $\tilde{c}_\epsilon$.

In the following, we will drop all tildes for ease of notation and more clarity. From now on, we denote the solutions of the linearised scaled Cahn–Larché system by c_ϵ and u_ϵ, the solutions of the nonlinear scaled quasi-stationary Cahn–Larché system (2.4.15), (2.4.16) completed with the corresponding intitial and boundary conditions, are still referred to as $c_{n,\epsilon}$ and $u_{n,\epsilon}$.

3 Periodic homogenisation

In this chapter, we introduce the framework of periodic homogenisation and explain the terminology as well as the notation we use. The concept of periodic homogenisation was first introduced to treat problems involving composite materials having an approximately periodic structure, but it can also be applied to problems involving periodically oscillating coefficients. In the case of a composite material with a periodic structure, the idea of periodic homogenisation can be illustrated particularly well, so let us first briefly concentrate on this.

Let $\Omega \subset \mathbb{R}^N$ be a bounded domain. We consider a periodic paving of Ω by a so-called unit cell $Y \subset \mathbb{R}^N$, scaled by a small parameter $\epsilon > 0$. This unit cell, also called reference cell, represents the microstructure in case of a composite material or it gives the periodicity in case of periodically oscillating coefficients. In view of the application considered in this thesis, Y shows a representative section of the pattern of the evolving microstructure. In terms of the assumption in section 2.3, this means that the order parameter c_ϵ is periodic on Y with respect to the $\frac{x}{\epsilon}$-variable. We define $\Omega_\epsilon \subset \Omega$, the resulting paved domain, as

$$\Omega_\epsilon := \bigcup_{k \in \mathbb{Z}^N} \epsilon(k + Y) \cap \Omega.$$

Further, we define the unit cell by $Y = (0, l_1) \times (0, l_2) \times \ldots \times (0, l_N) \subset \mathbb{R}^N$, where $l_1, l_2, \ldots, l_N \in \mathbb{R}$ are positive numbers.

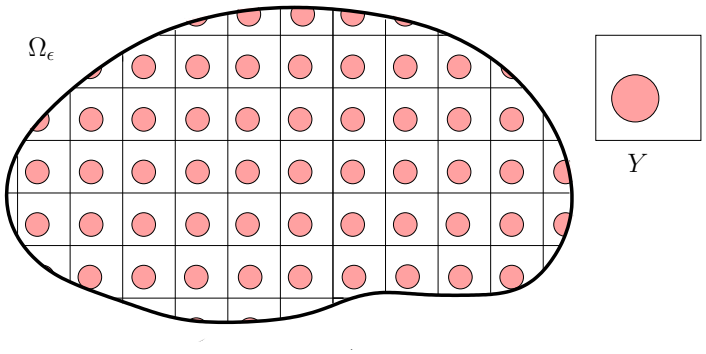

Figure 3.1: bounded domain $\Omega_\epsilon \subset \mathbb{R}^2$ with Y-periodic structure

Figure 3.1 shows a domain with a periodic paving by $\epsilon\, Y$. Introducing a characteristic mi-

croscopic length l, representing the size of the microstructure (e.g. the diameter of Y) and a characteristic macroscopic length L, giving the size of Ω_ϵ, we set $\epsilon := \frac{l}{L}$. Therefore, we can say that ϵ describes the heterogeneity of the material: the smaller ϵ, the finer is the structure of the domain Ω_ϵ. Imagine now a physical problem including different material parameters for the individual components of the composite, modelled by a partial differential equation on Ω_ϵ. To fix ideas, we consider the following second-order linear model problem, which is actually a family of problems indexed by ϵ:

$$\begin{aligned} -\nabla \cdot (A_\epsilon(x)\nabla u_\epsilon) &= f \quad \text{in } \Omega_\epsilon, \\ u_\epsilon &= 0 \quad \text{on } \partial\Omega_\epsilon, \end{aligned} \tag{3.0.1}$$

where u_ϵ is the unknown function, which, for example, describes temperature in case of a heat-conduction problem or a certain concentration in case of a diffusion problem. Due to their strong heterogeneities, one usually is not interested in how the coefficient A_ϵ or the unknown u_ϵ look in detail, one would rather like to know what the material properties are or the unknown physical quantity look like on a macroscopic level. This is also appreciated from a numerical point of view, because a sufficiently precise resolution of the fine microstructure would result in an enormous amount of computing effort.

Periodic homogenisation now deals with the question what happens if the scaling parameter ϵ tends towards zero. Thus, as illustrated in figure 3.2, the domain loses its fine structure.

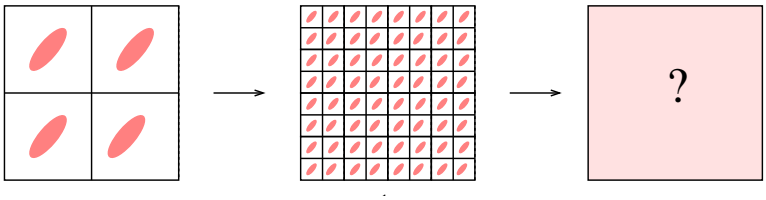

Figure 3.2: Illustration of the refinement of a periodic microstructure in course of the homogenisation process

Laxly spoken, this limit process corresponds to the idea of making the heterogeneous material more and more homogeneous and thus to obtain the so-called effective coefficients A_0 describing the material properties of the composite material as a whole. Figure 3.3 illustrates the result of this limit process for the described film-balance experiments. Macroscopically, the phase-separation process is not visible, but on the microscale it is.

So, in the course of periodic homogenisation, for a given partial differential equation describing a problem on a domain of approximately periodic microstructure or including periodic rapidly oscillating coefficients, one hopes to derive a limit equation, which describes the problem and its solution macroscopically.

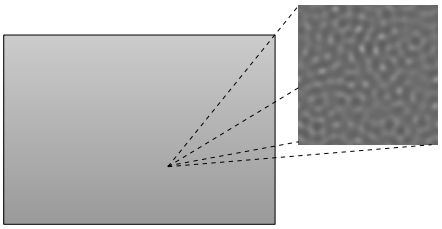

Figure 3.3: Schematic drawing of the top view of the water trough of the film balance (macroscopic domain) together with a zoom-in representing a volume element showing the evolving microstructure

Homogenisation is a wide field and it encompasses numerous methods. In the following, we restrict ourselves only to the methods and results we need. We present two methods of the framework of periodic homogenisation. We start with a procedure that is well suited to get an idea of what the homogenised system might look like in a relatively fast way. This is done under the assumption that the unknowns can be represented as an asymptotic expansion in ϵ. After, we will introduce the framework of two-scale convergence, with which we can derive a homogenisation result analytically rigorously and verify the results developed with the method of asymptotic expansions.

For further mathematically rigorous homogenisation techniques in a periodic framework, we would also like to refer to the method of oscillating test functions, developed by Tartar, based on the construction of problem-adapted periodically oscillating test functions [Tar78], and the method of periodic unfolding, based on conversion to convergence in L^p-spaces [CDG18]. But homogenisation is not restricted to the periodic case and can be applied to problems without conditions on periodicity of geometry or coefficients, such as the notion of Γ-convergence associated to homogenisation in the context of calculus of variations [DM93], [Bra02]. Furthermore, we would like to refer to the concept G-convergence for the convergence of sequences of symmetric operators or a generalisation thereof, the H-convergence, applicable to sequences of non-symmetric operators [Pan13], [MT97]. For an overview of the different techniques we refer to [CD99] and [ZKO94].

3.1 The method of asymptotic expansions

In order to get a first idea how a limit problem may look like, one can use the method of two-scale asymptotic expansions. This method is extremely useful since it can also be applied

to complex problems to obtain a first formal homogenisation result in a relatively simple way. Unfortunatelly, it is only heuristic and does not yield a rigorous proof of the homogenisation process. But nevertheless this procedure is very promising, as we will show later. For what follows, we refer to [CD99] and [Hor97].

To fix ideas and explain best how this method works, we demonstrate it by applying it to the following model problem. Let $\Omega \subset \mathbb{R}^N$ be, just as in all following chapters, a bounded domain with smooth boundary $\partial\Omega$. Introducing a reference cell Y as above, we consider the coefficient matrix $A(y) = (a_{ij}(y))_{1\leq i,j\leq N}$ with components $a_{ij} \in L^\infty(Y)$ extended Y-periodically to $\mathbb{R}^N$ for all $i, j = 1, \ldots, N$. Further, we assume there exists two positive constants $\alpha, \beta \in \mathbb{R}$, with $0 < \alpha \leq \beta$, such that

$$\alpha|\xi|^2 \leq \sum_{i,j=1}^{N} a_{ij}\,\xi_i\,\xi_j \leq \beta|\xi|^2, \tag{3.1.1}$$

for all $\xi = (\xi_1, \xi_2, \ldots, \xi_N)^{\mathrm{T}} \in \mathbb{R}^N$. Then we set

$$a_{ij}^\epsilon(x) \coloneqq a_{ij}(\frac{x}{\epsilon}) \quad \text{a.e. in } \mathbb{R}^N,$$

and write $A_\epsilon = (a_{ij}^\epsilon)_{1\leq i,j\leq N}$. We consider the familiy of boundary-value problems

$$\mathcal{L}_\epsilon u_\epsilon = f \quad \text{in } \Omega, \tag{3.1.2}$$

$$u_\epsilon = 0 \quad \text{on } \partial\Omega, \tag{3.1.3}$$

with $\mathcal{L}_\epsilon = -\nabla \cdot (\nabla A_\epsilon)$ and the right-hand side f given in $H^{-1}(\Omega)$.

Now, we set $y \coloneqq \frac{x}{\epsilon}$ and postulate the variables x and y to be independent. For $x \in \Omega$, then $\frac{x}{\epsilon}$ specifies a point in Y. Therefore we refer to y as the microscopic variable and x as the macroscopic one. We assume the unknown u_ϵ to possess a two-scale asymptotic expansion in ϵ of the form

$$u_\epsilon(x) = \sum_{i=0}^{\infty} \epsilon^i u_i(x, y), \tag{3.1.4}$$

with sufficiently smooth coefficient functions u_i, such that

(i) $u_i(x, y)$ is defined for $x \in \Omega$, $y \in Y$,

(ii) and $u_i(x, \cdot)$ as well as its derivatives are Y-periodic,

for $i \geq 0$. Justifying this step is the main goal in rigorous homogenisation theory.

For a function $v = v(x, y)$ depending on two variables in the way as introduced as above, we consider $v_\epsilon \coloneqq v(\cdot, \frac{\cdot}{\epsilon})$, depending only on the variable x. Then, the derivative is given by

$$\frac{\partial}{\partial x_i} v_\epsilon(x) = \frac{\partial}{\partial x_i} v(x, \frac{x}{\epsilon}) + \epsilon^{-1} \frac{\partial}{\partial y_i} v(x, \frac{x}{\epsilon}). \tag{3.1.5}$$

In the following, we will also write ∇_x and ∇_y for the gradient with respect to x and y, respectively. Inserting the expansion (3.1.4) and taking into account the derivative law (3.1.5), we can write equation (3.1.2) in the following form:

$$\epsilon^{-2} L_0 u_0 + \epsilon^{-1} \big(L_1 u_0 + L_0 u_1\big) + \epsilon^0 \big(L_2 u_0 + L_1 u_1 + L_0 u_2\big) + \epsilon^1 \ \ldots = f, \tag{3.1.6}$$

with

$$\begin{aligned}
L_0 &= -\sum_{i,j=1}^{N} \frac{\partial}{\partial y_i}(a_{ij}(y)\frac{\partial}{\partial y_j}),\\
L_1 &= -\sum_{i,j=1}^{N} \frac{\partial}{\partial x_i}(a_{ij}(y)\frac{\partial}{\partial y_j}) - \sum_{i,j=1}^{N} \frac{\partial}{\partial y_i}(a_{ij}(y)\frac{\partial}{\partial x_j}),\\
L_2 &= -\sum_{i,j=1}^{N} \frac{\partial}{\partial x_i}(a_{ij}(y)\frac{\partial}{\partial x_j}).
\end{aligned}$$

Since ϵ is a parameter getting smaller and smaller, we deduce the following system of partial differential equations:

$$\begin{aligned}
L_0 u_0 &= 0 \ \text{ in } Y\\
u_0 &\quad Y\text{-periodic}
\end{aligned} \tag{3.1.7}$$

$$\begin{aligned}
L_0 u_1 &= -L_1 u_0 \ \text{ in } Y\\
u_1 &\quad Y\text{-periodic in } y
\end{aligned} \tag{3.1.8}$$

$$\begin{aligned}
L_0 u_2 &= f - L_2 u_0 - L_1 u_1 \ \text{ in } Y\\
u_2 &\quad Y\text{-periodic in } y
\end{aligned} \tag{3.1.9}$$

and for $k \geq 3$:

$$\begin{aligned}
L_0 u_k &= -L_2 u_{k-2} - L_1 u_{k-1} \ \text{ in } Y\\
u_k &\quad Y\text{-periodic in } y.
\end{aligned} \tag{3.1.10}$$

Notice the special structure of this system: with each further equation there comes a further unknown coefficient function of the expansion (3.1.4) and we can successively solve the equations. To do so we take a closer look on the first problem of the series above which reads

as

$$\begin{aligned} \nabla_y \cdot \left(A \nabla_y u_0\right) &= 0 \quad \text{in } Y, \\ u_0 \quad & Y\text{-periodic in } y. \end{aligned}$$

Multiplying the equation with u_0, integrating over Y and by parts and using property (3.1.1) yields

$$\alpha \left\|\nabla_y u_0\right\|^2 \leq \int_Y A(y) \left(\nabla_y u_0\right)^2 \mathrm{d}y = 0.$$

Therefrom we conclude $\nabla_y u_0 \equiv 0$ which implies

$$u_0 = u_0(x), \tag{3.1.11}$$

i.e. u_0, the first term of the expansion (3.1.4), depends only on the macroscopic variable x and not on y. Hence, u_0 does not oscillate on the microscale and is therefore expected to be the homogenised solution. Next we want to find an equation which u_0 fulfils on the macroscopic domain Ω. If we can achieve this, we hope that we have found the homogenised or effective equation. The next problem we want to solve is problem (3.1.8), written as

$$\nabla_y \cdot \left(A \nabla_y u_1\right) = -\nabla_y \cdot \left(A \nabla_x u_0\right) \quad \text{in } Y, \tag{3.1.12}$$

$$u_1 \quad Y\text{-periodic in } y, \tag{3.1.13}$$

which we consider as a problem for the unknown u_1, since we already earned some information about u_0. The task now is to express u_1 in terms of u_0. At this point, we need to introduce the following auxiliary problems, well-known as the cell problems, since they are defined on the unit cell Y.

The cell problems

The cell problems are periodic auxiliary problems defined on the unit cell Y. By solving these, microscopic information can be extracted.

Let e_j be the j-th unit vector in $\mathbb{R}^N$. For each $j = 1, \ldots, N$, we want to find a function $\omega_j = \omega_j(y)$ such that

$$\nabla_y \cdot \left(A \nabla_y \omega_j\right) = -\nabla_y \cdot \left(A e_j\right) \quad \text{in } Y, \tag{3.1.14}$$

$$\omega_j \quad Y\text{-periodic.} \tag{3.1.15}$$

The following proposition, a consequence of Fredholms alternative, provides the existence and uniqueness of a weak solution of the cell problem (3.1.14), (3.1.15) in $H^1_{\#}(Y)/\mathbb{R}$ (# denotes

Y-periodicity).

Proposition 3.1.1. *Let $f \in L^2_{\#}(Y)$ be a periodic function. There exists a solution in $H^1_{\#}(Y)$, unique up to an additive constant, of*

$$-\nabla \cdot \big(A\,\nabla w\big) = f \quad \text{in } Y, \tag{3.1.16}$$

$$w \quad Y\text{-periodic}, \tag{3.1.17}$$

if and only if $\int_Y f(y)\,\mathrm{d}y = 0$.

Due to the Y-periodicity of the coefficients a_{ij}, $1 \le i,j \le N$, the integral over Y of the right-hand side of (3.1.14) vanishes by applying Gauss's theorem and hence, the condition of proposition 3.1.1 is fulfilled.

Now we consider (3.1.12). According to proposition 3.1.1, this problem has a unique solution (up to an additive constant). We rewrite the right-hand side as

$$\begin{aligned} \nabla_y \cdot (A\,\nabla_y u_1) &= -\nabla_y \cdot (A\,\nabla_x u_0) \\ &= -\sum_{i,j} \partial_{y_i} a_{ij}\,\partial_{x_j} u_0. \end{aligned} \tag{3.1.18}$$

Writing the cell equation (3.1.14) componentwise, multiplying both sides by $\partial_{x_j} u_0$ and summing up over j, we get

$$\sum_{i,j=1}^{N} \partial_{y_i}\big(a_{ij}\,\partial_{y_j}\omega_j\,\partial_{x_j} u_0\big) = -\sum_{i,j=1}^{N} \partial_{y_i} a_{ij}\,\partial_{x_j} u_0. \tag{3.1.19}$$

This enables us to compare the cell problems with equation (3.1.12). Considering (3.1.18) and (3.1.19), we can easily read off a representation of the function u_1 in terms of u_0, namely

$$u_1 = \sum_{j=1}^{N} \omega_j\,\partial_{x_j} u_0 \tag{3.1.20}$$

Actually, u_1 is merely defined up to the addition of a constant function depending only on x, but this does not matter since, as we will see, only its gradient $\nabla_y u_1$ is included in the homogenised equation. The last problem of the considered series we are interested in is problem (3.1.9). We integrate the equation over Y and obtain

$$\begin{aligned} &-\int_Y \nabla_y \cdot \big(A(y)\nabla_y u_2(x,y) + A(y)\nabla_x u_1(x,y)\big)\,\mathrm{d}y \\ &\quad -\int_Y \nabla_x \cdot \big(A(y)\nabla_x u(x) + A(y)\nabla_y u_1(x,y)\big)\,\mathrm{d}y = |Y|\,f(x). \end{aligned} \tag{3.1.21}$$

The first integral term vanishes due to the Y-periodicity of A and of the functions u_1 and $\nabla_y u_2$:

$$\begin{aligned}&\int_Y \nabla_y \cdot \big(A(y)\nabla_y u_2(x,y) + A(y)\nabla_x u_1(x,y)\big)\,\mathrm{d}y\\ &= \int_{\partial Y} \big(A(y)\nabla_y u_2(x,y) + A(y)\nabla_x u_1(x,y)\big)\cdot n\,\mathrm{d}y = 0.\end{aligned}$$

Using the representation (3.1.20), we write

$$\partial_{y_i} u_1(x,y) = \sum_{j=1}^{N} \partial_{y_i}\omega_j(y)\,\partial_{x_j} u_0(x),$$

and therefore, from equation (3.1.21), we obtain

$$-\sum_{i,j,k=1}^{N} \partial_{x_i} \int_Y a_{ij}(y)\,\big(\partial_{x_j} u_0(x) + \partial_{y_j}\omega_k(y)\,\partial_{x_k} u_0(x)\big)\,\mathrm{d}y = |Y|\,f(x), \tag{3.1.22}$$

which can also be written as

$$-\sum_{i,j,k=1}^{N} \partial_{x_i} \int_Y a_{ij}(y)\,\big(\delta_{jk} + \partial_{y_j}\omega_k(y)\big)\,\mathrm{d}y\;\partial_{x_k} u_0(x) = |Y|\,f(x). \tag{3.1.23}$$

With this equation we have now found an equation, which is valid for the macroscopic function u_0. We introduce the abbreviation

$$a_{ik}^{\mathrm{hom}} = \frac{1}{|Y|}\sum_{j=1}^{N} \int_Y a_{ij}(y)\big(\delta_{jk} + \partial_{y_j}\omega_k(y)\big)\,\mathrm{d}y, \tag{3.1.24}$$

where we have now defined the coefficients of the so-called homogenised or effective tensor $A^{\mathrm{hom}} := (a_{ik}^{\mathrm{hom}})_{1\le i,k\le N}$. The homogenised problem is stated in the proposition below.

Proposition 3.1.2 (The homogenised problem)**.**
The homogenisation of problem (3.1.2), (3.1.3) *is given by*

$$\begin{aligned}-\nabla\cdot\big(A^{\mathrm{hom}}\,\nabla u(x)\big) &= f(x) \quad \text{in } \Omega,\\ u(x) &= 0 \qquad \text{on } \partial\Omega.\end{aligned} \tag{3.1.25}$$

Here, we have completed the homogenised equation (3.1.23) with the same boundary conditions as the ϵ-dependent problem. The homogenised tensor A^{hom} describes the effective properties. Note that this tensor is constant and does not depend on the choice of the macroscopic domain Ω, on the boundary condition or the right-hand side term f.

The applied method is useful to get a quick idea of what the homogenised problem will probably look like, but, as mentioned previously, it is unfortunately only heuristic and a further step is needed to prove the convergence of the sequence u_ϵ to u. An analytic technique, which provides a mathematically rigorous proof of the homogenisation result, is the aim of the next part.

3.2 Two-scale convergence

In the following we will present the concept of two-scale convergence, a special type of weak convergence in L^p-spaces. This concept of convergence takes oscillations on the microscale into account and goes back to Nguetseng [Ngu89] and Allaire [All92]. Most of the results presented in this section are taken from [All92], [CS99] and [LNW02], which we refer to for more details.

Considering again our model equation (3.1.2), as already mentioned, the aim of periodic homogenisation is to find the limit differential operator $\mathcal{L}_0$, such that

$$\mathcal{L}_0 u_0 = f \quad \text{in } \Omega, \tag{3.2.1}$$

which is referred to as the homogenised equation. Using two-scale convergence, one proceeds as follows: appropriate a-priori estimates of u_ϵ, the sequence of solutions of the ϵ-indexed family of partial differential equations (3.1.2), enables one to identify a limit function u_0, so that at least a subsequence of u_ϵ converges to u_0 in the two-scale sense. Then, one passes to the limit in each term of the partial differential equation and obtains an equation which is fulfilled by the limit function u_0.

Unless stated otherwise, in the following $\Omega \subset \mathbb{R}^N$ is a bounded and open set and $p \in (1, \infty)$. Furthermore, whenever we extract a subsequence, for brevity, we always denote it by the sequence itself. We start with the definition of two-scale convergence in $L^p(\Omega)$.

Definition 3.2.1 (Two-scale convergence)**.**
A sequence of functions u_ϵ in $L^p(\Omega)$, with $1 < p < \infty$, two-scale converges to a limit $u_0 \in L^p(\Omega \times Y)$ if

$$\lim_{\epsilon \to 0} \int_\Omega u_\epsilon(x) \phi(x, \frac{x}{\epsilon}) \, \mathrm{d}x = \frac{1}{|Y|} \int_\Omega \int_Y u_0(x, y) \phi(x, y) \, \mathrm{d}y \, \mathrm{d}x,$$

for any $\phi \in C_0^\infty(\Omega; C_\#^\infty(Y))$. In this case, we write

$$u_\epsilon \overset{\text{2s.}}{\rightharpoonup} u_0.$$

In the definition, we take special testfunctions which are Y-periodic with respect to the microscopic variable. This class of testfunctions can be enlarged, for example one can choose functions in $L^q(\Omega; C_\#(Y))$, with $1 < q < \infty$, such that $\frac{1}{p} + \frac{1}{q} = 1$. There are several discussions about the question which regularity of test functions is necessary to capture the largest possible amount, see e.g [All92], [LNW02]. In any case, there is a criterion that makes a function an "admissible" test function in the above definition 3.2.1:

Definition 3.2.2 (Admissible test function)**.**
A function, $\phi \in L^p(\Omega \times Y)$, which is Y-periodic in y and which satisfies

$$\lim_{\epsilon \to 0} \int_\Omega |\phi(x, \frac{x}{\epsilon})|^p \, \mathrm{d}x = \int_\Omega \int_Y |\phi(x, y)|^p \, \mathrm{d}y \, \mathrm{d}x \tag{3.2.2}$$

is called an admissible test function.

Of course we are now interested in criteria which enable us to conclude that a given sequence in $L^p(\Omega)$ is two-scale convergent. The next compactness theorem ensures the existence of a two-scale limit of a sequence bounded in $L^p(\Omega)$.

Theorem 3.2.3 (Compactness in $L^p(\Omega)$)**.**
For each bounded sequence u_ϵ in $L^p(\Omega)$, there exists a subsequence, which two-scale converges to a function $u_0 \in L^p(\Omega \times Y)$.

There are several proofs for this theorem, see for example [All92], for $p = 2$, or [LNW02], for $1 < p < \infty$. When working with partial differential equations, derivatives usually also appear. Therefore, the next two compactness results are very helpful.

Theorem 3.2.4 (Compactness of the gradient)**.**
Let u_ϵ be a sequence in $W^{1,p}(\Omega)$ such that u_ϵ converges weakly to a limit $u_0 \in W^{1,p}(\Omega)$. Then u_ϵ two-scale converges to u_0 and there exists a function $u_1 \in L^p(\Omega; W^{1,p}_\#(Y))$ such that, up to a subsequence,

$$\nabla u_\epsilon \overset{2s.}{\rightharpoonup} \nabla u_0 + \nabla_y u_1.$$

For the proof we refer to [LNW02]. Since we are dealing with a fourth-order equation the following non-standard result is also required.

Proposition 3.2.5 (Compactness of 2nd order derivatives)**.**
Let u_ϵ, $\epsilon \, \partial_{x_i} u_\epsilon$ and $\epsilon^2 \, \partial^2_{x_i x_j} u_\epsilon$ be bounded sequences in $L^p(\Omega)$, respectively. Then, there exists a function $u_0 \in L^p(\Omega; W^{2,p}_\#(Y))$, such that, up to a subsequence,

$$\begin{aligned} u_\epsilon &\overset{2s.}{\rightharpoonup} u_0, \\ \epsilon \, \partial_{x_i} u_\epsilon &\overset{2s.}{\rightharpoonup} \partial_{y_i} u_0, \\ \epsilon^2 \, \partial^2_{x_i x_j} u_\epsilon &\overset{2s.}{\rightharpoonup} \partial^2_{y_i y_j} u_0. \end{aligned}$$

Proof. From [All92] we already know that for sequences u_ϵ and $\epsilon\,\partial_{x_i} u_\epsilon$ bounded in $L^p(\Omega)$, there exists a function $u_0 \in L^p(\Omega; W^{1,p}_{\#}(Y))$, such that, up to a subsequence, u_ϵ and $\epsilon\,\partial_{x_i} u_\epsilon$ two-scale-converge to u_0 and $\partial_{y_i} u_0$, respectively. Since $\epsilon^2\,\partial^2_{x_i x_j} u_\epsilon$ is also bounded in $L^p(\Omega)$, we can extract a subsequence, still denoted by $\epsilon^2\,\partial^2_{x_i x_j} u_\epsilon$, and there exists a function $w \in L^p(\Omega \times Y)$ such that this subsequence two-scale converges to w, i.e.

$$\lim_{\epsilon\to 0} \int_\Omega \epsilon^2\,\partial^2_{x_i x_j} u_\epsilon(x)\,\psi(x, \frac{x}{\epsilon})\,\mathrm{d}x = \frac{1}{|Y|} \int_\Omega \int_Y w(x,y)\psi(x,y)\,\mathrm{d}y\,\mathrm{d}x \tag{3.2.3}$$

for any admissible test function $\psi \in C^\infty_0(\Omega, C^\infty_{\#}(Y))$. Integrating the left-hand side in (3.2.3) by parts and passing to the limit yields

$$\lim_{\epsilon\to 0} \int_\Omega \epsilon\,\partial_{x_i} u_\epsilon(x)\,[\partial_{y_j}\psi(x, \frac{x}{\epsilon}) + \epsilon \partial_{x_j}\psi(x, \frac{x}{\epsilon})]\,\mathrm{d}x = \frac{1}{|Y|} \int_\Omega \int_Y \partial_{y_i} u_0(x,y) \partial_{y_j}\,\psi(x,y)\,\mathrm{d}y\,\mathrm{d}x.$$

With (3.2.3) we get

$$\lim_{\epsilon\to 0} \int_\Omega \epsilon^2\,\partial^2_{x_i x_j} u_\epsilon(x)\psi(x, \frac{x}{\epsilon})\,\mathrm{d}x = -\frac{1}{|Y|} \int_\Omega \int_Y \partial_{y_i} u_0(x,y) \partial_{y_j}\psi(x,y)\,\mathrm{d}y\,\mathrm{d}x. \tag{3.2.4}$$

Integrating the right-hand side of (3.2.4) by parts yields the desired result,

$$\lim_{\epsilon\to 0} \int_\Omega \epsilon^2\,\partial^2_{x_i x_j} u_\epsilon(x)\psi(x, \frac{x}{\epsilon})\,\mathrm{d}x = \frac{1}{|Y|} \int_\Omega \int_Y \partial^2_{y_i y_j} u_0(x,y)\psi(x,y)\,\mathrm{d}y\,\mathrm{d}x,$$

and we identify $\partial^2_{y_i y_j} u_0$ as the two-scale limit of $\epsilon^2\,\partial^2_{x_i x_j} u_\epsilon$ and hence, $u_0 \in L^p(\Omega; W^{2,p}_{\#}(Y))$. □

The next theorem gives a link between two-scale convergence and normal weak convergence in $L^p(\Omega)$.

Theorem 3.2.6. *Let u_ϵ be a bounded sequence in $L^p(\Omega)$, which two-scale converges to its limit $u_0 \in L^p(\Omega \times Y)$. Then,*

(i) u_ϵ converges weakly in $L^p(\Omega)$ to $u := \int_Y u_0(x,y)\,dy$ and

(ii) $\lim_{\epsilon\to 0} \|u_\epsilon\|_{L^p(\Omega)} \geq \|u_0\|_{L^p(\Omega\times Y)} \geq \|u\|_{L^p(\Omega)}$.

Hence, a bounded two-scale convergent sequence also converges weakly in $L^p(\Omega)$. To proof the weak convergence of the sequence towards u one simply chooses a testfunction $\varphi = \varphi(x)$ independent of the variable y in definition 3.2.1. The second statement of theorem 3.2.6 states that more information is contained in the two-scale limit than in the weak one. For the proof we refer to [LNW02].

Two-scale convergence can be strengthened. In the literature one sometimes talks about strong convergence in the two-scale sense. This terminology can be justified since it enables us to pass to the limit of products of sequences as we will see in proposition 3.2.8.

Definition 3.2.7 (Strong two-scale convergence)**.**
A sequence u_ϵ in $L^p(\Omega)$ is said to two-scale converge strongly to a limit $u_0 \in L^p(\Omega \times Y)$ if u_ϵ two-scale converges to u_0 in $L^p(\Omega)$ and

$$\lim_{\epsilon \to 0} \|u_\epsilon\|_{L^p(\Omega)} = \|u_0\|_{L^p(\Omega \times Y)} .$$

Then, we write $u_\epsilon \xrightarrow{\text{2s.}} u_0$.
Moreover, if the Y-periodic extension of u_0 belongs to $L^p(\Omega, C_\#(Y))$, we have

$$\lim_{\epsilon \to 0} \left\| u_\epsilon(\cdot) - u_0(\cdot, \frac{\cdot}{\epsilon}) \right\|_{L^p(\Omega)} = 0.$$

We remark that all admissible test functions two-scale converge strongly by definition. The next theorem enables to pass to the limit of products of several two-scale converging sequences. This result is an extension of the well-known result that the product of one strongly convergent with one weakly convergent sequence converges towards the product of their two-scale limits in the sense of distributions, see e.g. [All92] or [LNW02].

Proposition 3.2.8 (Convergence of products)**.**
Let $\Omega \subset \mathbb{R}^N$ be a bounded domain and $u_\epsilon^{(i)}$ bounded sequences in $L^{p_i}(\Omega)$, for $i \in \{1, \dots, n\}$ and $p^{(i)} \in (1, \infty)$, which two-scale converge strongly to limit functions $u_0^{(i)} \in L^{p_i}(\Omega \times Y)$, respectively. Then, for any bounded sequence w_ϵ in $L^q(\Omega)$, with $q \in (1, \infty)$ such that $\frac{1}{q} + \sum_i \frac{1}{p^{(i)}} \leq 1$, which two-scale converges to $w_0 \in L^q(\Omega \times Y)$, the following convergence holds:

$$\begin{aligned} \lim_{\epsilon \to 0} \int_\Omega & u_\epsilon^{(1)}(x) \dots u_\epsilon^{(n)}(x)\, w_\epsilon(x)\, \varphi(x)\, \mathrm{d}x \\ & = \frac{1}{|Y|} \int_\Omega \int_Y u_0^{(1)}(x,y) \dots u_0^{(n)}(x,y)\, w_0(x,y)\, \varphi(x)\, \mathrm{d}y\, \mathrm{d}x, \end{aligned} \tag{3.2.5}$$

for every $\varphi \in C^\infty(\Omega)$.

Proof. We proof this result for the product of two strongly and one weakly two-scale converging sequences, i.e. $n = 2$. The proof of the general case, for $n > 2$, can be continued successively.

For $i = 1, 2$, let $\varphi_k^{(i)} \in C^\infty(\Omega; C^\infty_\#(Y))$ be sequences such that $\varphi_k^{(i)} \to u_0^{(i)}$ in $L^{p_i}(\Omega \times Y)$ and $\varphi \in C^\infty(\Omega)$. We split the product of the sequences as follows

$$\begin{aligned} u_\epsilon^{(1)} u_\epsilon^{(2)}\, w_\epsilon &= \big(u_\epsilon^{(1)} - \varphi_k^{(1)}\big) u_\epsilon^{(2)} w_\epsilon + \varphi_k^{(1)} u_\epsilon^{(2)} w_\epsilon \\ &= \big(u_\epsilon^{(1)} - \varphi_k^{(1)}\big) u_\epsilon^{(2)} w_\epsilon + \varphi_k^{(1)} \big(u_\epsilon^{(2)} - \varphi_k^{(2)}\big) w_\epsilon + \varphi_k^{(1)} \varphi_k^{(2)} w_\epsilon. \end{aligned} \tag{3.2.6}$$

It is easy to see that this decompositon can be continued successively if further strongly converging consequences are added to the product on left-hand side of (3.2.6). We multiply by φ, integrate over Ω and subtract the right-hand side of (3.2.5) from both sides and obtain with the triangle inequality

$$\begin{aligned} &\Big| \int_\Omega u_\epsilon^{(1)}(x)\, u_\epsilon^{(2)}(x)\, w_\epsilon(x)\, \varphi(x)\, \mathrm{d}x \\ &\qquad - \frac{1}{|Y|} \int_\Omega \int_Y u_0^{(1)}(x,y)\, u_0^{(2)}(x,y)\, w_0(x,y)\, \varphi(x)\, \mathrm{d}y\, \mathrm{d}x \Big| \\ \leq\ &\Big| \int_\Omega \big[u_\epsilon^{(1)}(x) - \varphi_k^{(1)}(x, \frac{x}{\epsilon})\big]\, u_\epsilon^{(2)}(x)\, w_\epsilon(x)\, \varphi(x)\, \mathrm{d}x \Big| \\ &\quad + \Big| \int_\Omega \varphi_k^{(1)}(x, \frac{x}{\epsilon})\, \big[u_\epsilon^{(2)}(x) - \varphi_k^{(2)}(x, \frac{x}{\epsilon})\big]\, w_\epsilon(x)\, \varphi(x)\, \mathrm{d}x \Big| \\ &\quad + \Big| \int_\Omega \varphi_k^{(1)}(x, \frac{x}{\epsilon})\, \varphi_k^{(2)}(x, \frac{x}{\epsilon})\, w_\epsilon(x)\, \varphi(x)\, \mathrm{d}x \\ &\qquad - \frac{1}{|Y|} \int_\Omega \int_Y u_0^{(1)}(x,y)\, u_0^{(2)}(x,y)\, w_0(x,y)\, \varphi(x)\, \mathrm{d}y\, \mathrm{d}x \Big|. \end{aligned} \tag{3.2.7}$$

We consider the last term in (3.2.7) and pass to the limit, first for $\epsilon \to 0$ and after for $k \to \infty$. We get

$$\lim_{\epsilon \to 0} \int_\Omega \varphi_k^{(1)}(x, \frac{x}{\epsilon})\, \varphi_k^{(2)}(x, \frac{x}{\epsilon})\, w_\epsilon(x)\, \varphi(x)\, \mathrm{d}x = \frac{1}{|Y|} \int_\Omega \int_Y \varphi_k^{(1)}(x,y)\, \varphi_k^{(2)}(x,y)\, w_0(x,y)\, \varphi(x)\, \mathrm{d}y\, \mathrm{d}x,$$

since w_ϵ two-scale converges to w_0 and $\varphi_k^{(1)} \varphi_k^{(2)} \varphi$ is an admissible test function. Therefore, as k tends to zero, we get

$$\begin{aligned} \lim_{k \to \infty} \lim_{\epsilon \to 0} \Big| &\int_\Omega \varphi_k^{(1)}(x, \frac{x}{\epsilon})\, \varphi_k^{(2)}(x, \frac{x}{\epsilon})\, w_\epsilon(x)\, \varphi(x)\, \mathrm{d}x \\ &- \frac{1}{|Y|} \int_\Omega \int_Y u_0^{(1)}(x,y)\, u_0^{(2)}(x,y)\, w_0(x,y)\, \varphi(x)\, \mathrm{d}y\, \mathrm{d}x \Big| = 0 \end{aligned}$$

and hence, the third term in (3.2.7) vanishes. Using Hölder's inequality, for the first term of the right-hand side we get

$$\begin{aligned}
&\Big| \int_\Omega \big[u_\epsilon^{(1)}(x) - \varphi_k^{(1)}(x, \frac{x}{\epsilon})\big]\, u_\epsilon^{(2)}(x)\, w_\epsilon(x)\, \varphi(x)\, \mathrm{d}x \Big| \\
&\leq c(\Omega) \sup_{x\in\Omega} |\varphi(x)| \, \Big\| u_\epsilon^{(1)} - \varphi_k^{(1)} \Big\|_{L^{p_1}(\Omega)} \, \Big\| u_\epsilon^{(2)} \Big\|_{L^{p_2}(\Omega)} \, \|w_\epsilon\|_{L^q(\Omega)} \\
&\leq C \, \Big\| u_\epsilon^{(1)} - \varphi_k^{(1)} \Big\|_{L^{p_1}(\Omega)},
\end{aligned}$$

with a constant $c(\Omega) = |\Omega|^{1-\frac{1}{p_1}-\frac{1}{p_2}-\frac{1}{q}}$. Here we have used that $u_\epsilon^{(2)}$ and w_ϵ are bounded in $L^{p_2}(\Omega)$ and $L^q(\Omega)$, respectivley. For the next term we get in an analogous way

$$\Big| \int_\Omega \varphi_k^{(1)}(x, \frac{x}{\epsilon}) \, \big[u_\epsilon^{(2)}(x) - \varphi_k^{(2)}(x, \frac{x}{\epsilon})\big]\, w_\epsilon(x)\, \varphi(x)\, \mathrm{d}x \Big| \leq C \, \Big\| u_\epsilon^{(2)} - \varphi_k^{(2)} \Big\|_{L^{p_2}(\Omega)}.$$

If

$$\lim_{k\to\infty} \lim_{\epsilon\to 0} \Big\| u_\epsilon^{(1)} - \varphi_k^{(1)} \Big\|_{L^{p_1}(\Omega)} = 0, \quad \lim_{k\to\infty} \lim_{\epsilon\to 0} \Big\| u_\epsilon^{(2)} - \varphi_k^{(2)} \Big\|_{L^{p_2}(\Omega)} = 0 \tag{3.2.8}$$

our proof is done. At this point we refer to [LNW02] where (3.2.8) is shown very precisely using the Clarkson inequalities. □

For the sake of clarity, we have not included time here, since time only plays the role of a parameter in our setting. Therefore, all results can be adapted to the time-dependent case, cf. [Hal97], [CS99], [PS08]. For example, we get:

Proposition 3.2.9. *For a sequence of functions u_ϵ bounded in $L^p((0,T)\times\Omega)$, with $p \in (1,\infty)$, there exists a function $u_0 \in L^p((0,T)\times\Omega\times Y)$, such that a subsequence, still denoted by u_ϵ, two-scale converges to u_0, i.e.*

$$\lim_{\epsilon\to 0} \int_0^T \int_\Omega u_\epsilon(t,x)\, \phi(t,x,\frac{x}{\epsilon})\, \mathrm{d}x\, \mathrm{d}t = \frac{1}{|Y|} \int_0^T \int_\Omega \int_Y u_0(t,x,y)\, \phi(t,x,y)\, \mathrm{d}y\, \mathrm{d}x\, \mathrm{d}t,$$

for any $\phi \in C_0^\infty((0,T)\times\Omega; C_\#^\infty(Y))$.

Before we end this part, we would like to put into perspective the ansatz (3.1.4) from the previous part.

Remark 3.2.10. *In view of the stated compactness results, the ansatz of asymptotic expansions therefore seems quite reasonable:*

(i) If a function provides a representation of the form

$$u_\epsilon(x) = \sum_{i=0}^{\infty} \epsilon^i u_i(x, y), \tag{3.2.9}$$

with smooth and Y-periodic (with respect to y) functions u_i, $i \geq 0$, then the sequence u_ϵ two-scale converges to u_0.

(ii) If a function provides a representation of the form (3.2.9) with $u_0 = u_0(x)$, then, the sequence ∇u_ϵ two-scale converges to $\nabla u_0 + \nabla_y u_1$.

4 Formal periodic homogenisation

So far, in § 2.4, we considered a scaled Cahn–Larché system which describes a certain phase-separation process. Since the different length scales that occur are taken into account by its scaling by exponents of ϵ, it is suitable for the application of multiscale techniques. The nonlinear and the linearised system are to be understood as families of systems indexed by ϵ. Thus, both systems provide a sequence of solutions, respectively. In the following, first, we derive a system which is suspected to be a limit system, as ϵ tends to zero, of the fully nonlinear system (2.4.15), (2.4.16) in the course of periodic homogenisation. Therefore, we use the method of two-scale asymptotic expansions which provides a sensibly justified result of the homogenisation process. After, we do the same for the linear system (2.5.5), (2.5.6). In preparation for this, we first introduce the cell problems for linear elasticity.

4.1 The cell problems in linear elasticity

Since we are dealing with linear elasticity, we are working with higher-order tensors and thus the cell problems differ from those of chapter 3.1. Since we want to turn to periodic homogenisation, we now introduce, in preparation, a familiy of periodic boundary-value problems posed on the unit cell Y, including a fourth-order, symmetric and positive definite tensor $\mathcal{A}$, which are the cell problems in linear elasticity. For detailed information of these problems, we refer to [CD99] where the homogenisation result for the equations in linear elasticity was proven using Tartar's oscillating test functions.

Let $\Omega \subset \mathbb{R}^N$ be a bounded domain and $Y = (0, l_1) \times (0, l_2) \times \ldots \times (0, l_N) \subset \mathbb{R}^N$, with positive numbers $l_1, \ldots, l_N$. We want to specify a certain class of fourth-order tensors, which plays an important role in elasticity.

Definition 4.1.1. *Let $\mathcal{O} \subset \mathbb{R}^N$ be an open and bounded set and $\alpha, \beta \in \mathbb{R}$ such that $0 < \alpha < \beta$. We denote by $\mathcal{M}(\alpha, \beta, \mathcal{O})$ the set of fourth-order tensors $C = (c_{ijkl})_{1 \le i,j,k,l \le N}$, which fulfil*

(i) $c_{ijkl} \in L^\infty(\mathcal{O})$, *for* $i, j, k, l = 1, \ldots, N$,

(ii) $c_{ijkl} = c_{jikl} = c_{ijlk} = c_{klij}$, *for* $i, j, k, l = 1, \ldots, N$,

(iii) $\alpha \big|X\big|^2 \le CXX$, *for any symmetric matrix* X,

(iv) $\big|CX\big| \le \beta \big|X\big|$, *for any matrix* X,

almost everywhere on $\mathcal{O}$.

We have adopted this definition from [CD99], but added the additional symmetry condition (2.2.30).

Let $\mathcal{A} = \mathcal{A}(y)$, with $\mathcal{A} = (a_{ijkh})_{1\leq i,j,k,h\leq N}$, be a fourth-order tensor, such that $\mathcal{A} \in \mathcal{M}(\alpha, \beta, Y)$ and a_{ijkh} being Y-periodic, for $i, j, k, h = 1, \dots, N$. For any $l, m \in \{1, \dots, N\}$ we define the vector-valued function $\lambda^{lm} = (\lambda_k^{lm})_{1\leq k\leq N} \in \mathbb{R}^N$ by

$$\lambda_k^{lm}(y) \coloneqq y_m \delta_{kl}, \quad y \in Y, \quad k = 1, \dots, N,$$

with y_m being the m-th component of $y \in Y$. Then, for each $l, m = 1, \dots, N$, we want to find a vector-valued function ω^{lm}, which solves the following cell problem:

$$\begin{aligned} -\nabla_y \cdot \big(\mathcal{A}\, \mathcal{E}_y(\omega^{lm})\big) = \nabla_y \cdot \big(\mathcal{A}\, \mathcal{E}_y(\lambda^{lm})\big) \quad \text{in } Y, \\ \omega^{lm} \quad Y\text{-periodic in } y. \end{aligned} \tag{4.1.1}$$

Or considering the weak form, we want to find $\omega^{lm} \in [H^1_{\#}(Y)]^N$, such that

$$-\int_Y \mathcal{A}(y)\, \mathcal{E}(\omega^{lm}) : \mathcal{E}(v)\, \mathrm{d}y = \int_Y \mathcal{A}(y)\, \mathcal{E}(\lambda^{lm}) : \mathcal{E}(v)\, \mathrm{d}y \tag{4.1.2}$$

for every $v \in (H^1_{\#}(Y))^N$.

According to the notation used so far, we write $\mathcal{E}_x$ and $\mathcal{E}_y$, where the subscripts indicate the partial derivatives with respect to the variables x and y, respectively.

Remark 4.1.2. *For $\mathcal{A} \in \mathcal{M}(\alpha, \beta, Y)$, there exists a solution of a cell problem* (4.1.2) *according to proposition 3.1.1. This can be quickly seen by applying Gauss's theorem to the componentwise representation of the right-hand side of* (4.1.1)*. Further, the solution is unique up to an additive constant.*

Remark 4.1.3. *The cell problems can be interpreted as follows. They give information about the behaviour of a small representative section of the macroscopic domain, body or material. The right-hand side of* (4.1.1) *can be interpreted as a volume force. So, one is interessted in how the displacement field looks like, when applying certain volume forces on a small section of a body or a domain which is representative for the microstructure. By rewriting the cell equation, the term $\mathcal{E}_y(\lambda^{lm})$ can also be interpretated as an enforced eigenstrain and one is interested in the displacement or the strain which occurs when equilibrium is achieved.*

4.2 Formal derivation of a distributed-microstructure model

Now we turn to periodic homogenisation. In what follows, first formally homogenise the nonlinear system (2.4.15), (2.4.16) and then the linear system (2.5.5), (2.5.6) using the method of two-scale asymptotic expansions introduced in section 3.1. It turns out, that the systems derived in this way are of the so-called distributed-microstructure type. We explain this term in the next part.

4.2.1 The nonlinear case

Now we assume the unknowns of (2.4.15) and (2.4.16) to have an asymptotic expansion in ϵ of the form

$$c_{n,\epsilon}(x,t) = \sum_{i=0}^{\infty} \epsilon^i \, c_{n,i}(x, \frac{x}{\epsilon}, t) \tag{4.2.1}$$

and

$$u_{n,\epsilon}(x,t) = \sum_{i=0}^{\infty} \epsilon^i \, u_{n,i}(x, \frac{x}{\epsilon}, t), \tag{4.2.2}$$

whereby the coefficient functions $c_{n,i}$ and $u_{n,i}$ are smooth and these as well as their derivatives are Y-periodic with respect to the second argument. Recall that the derivatives obey the law

$$\partial_x \mapsto \partial_x + \epsilon^{-1} \, \partial_y, \tag{4.2.3}$$

In addition to the indexed gradient and strain, we also use the notation Δ_{xx}, Δ_{xy}, and Δ_{yy} for the Laplacian operator with respect to the variables specified in the index.

Next, we insert the expansions (4.2.1) and (4.2.2) into the scaled Cahn–Larché system (2.4.15), (2.4.16) and identify the coefficients of the different ϵ-powers. As seen in section 3.1, this procedure leads to a series of partial differential equations:

The ϵ^{-2}-coefficient, provided by the mechanical equation, gives

$$\nabla_y \cdot \big(\mathcal{A}(c_{n,0}) \, \mathcal{E}_y(u_{n,0}) \big) = 0 \quad \text{in } \Omega \times Y \times S. \tag{4.2.4}$$

Multiplying this equation by u_0 and integrating over Y and by parts yields

$$\int_Y \mathcal{A}(c_{n,0}) \, \mathcal{E}_y(u_{n,0}) : \mathcal{E}_y(u_{n,0}) \, \mathrm{d}y = 0,$$

where the boundary integral vanishes due to the Y-periodicity of the derivatives of $u_{n,0}$ and

the components of $\mathcal{A}$. Since $\mathcal{A}$ is positive definite, we get

$$\alpha \left\| \mathcal{E}_y(u_{n,0}) \right\|^2 \leq \int_Y \mathcal{A}(c_{n,0})\, \mathcal{E}_y(u_{n,0}) : \mathcal{E}_y(u_{n,0})\, \mathrm{d}y = 0,$$

which implies $\mathcal{E}_y(u_{n,0}) = 0$ and hence,

$$u_{n,0} = u_{n,0}(x,t) \tag{4.2.5}$$

depends only on the macroscopic variable x and on time. So, we have found a candidate describing the macroscopic deformation. The ϵ^{-1}-term gives

$$\begin{aligned} \nabla_y \cdot \big(\mathcal{A}(c_{n,0})(\mathcal{E}_x(u_{n,0}) + \mathcal{E}_y(u_{n,1}) - e(c_{n,0})\mathbb{1}) + c_{n,1}\mathcal{A}'(c_{n,0})\mathcal{E}_y(u_{n,0})\big) \\ + \nabla_x \cdot \big(\mathcal{A}(c_{n,0})\mathcal{E}_y(u_{n,0})\big) = 0, \end{aligned} \tag{4.2.6}$$

which we consider as an equation for the unknown $u_{n,1}$. Using (4.2.5) and the Y-periodicity of $u_{n,1}$ we get a well-posed problem

$$\begin{aligned} -\nabla_y \cdot \big(\mathcal{A}(c_{n,0})\,(\mathcal{E}_y(u_{n,1}) - e(c_{n,0})\mathbb{1})\big) = \nabla_y \cdot \big(\mathcal{A}(c_{n,0})\,\mathcal{E}_x(u_{n,0})\big) \quad \text{in } \Omega \times Y \times S, \\ u_{n,1} \quad Y\text{-periodic in } y. \end{aligned} \tag{4.2.7}$$

For our further considerations we need to work with the componentwise representation of this equation, namely

$$\begin{aligned} -\sum_{j=1}^{N} \partial_{y_j} \sum_{k,h=1}^{N} \big(a_{ijkh}(c_{n,0})\,(e_{khy}(u_{n,0}) - e(c_{n,0})\delta_{kh})\big) \\ = -\sum_{j=1}^{N} \partial_{y_j} \sum_{k,h=1}^{N} \big(a_{ijkh}(c_{n,0})\, e_{khx}(u_{n,0})\big), \end{aligned} \tag{4.2.8}$$

for $i = 1, \ldots, N$. As in section 3.1, at this step we want to gain a representation of the function $u_{n,1}$ in terms of $u_{n,0}$. Therefore, we need the auxiliary problems (4.1.1) for the mechanics, which we also consider now in component-wise form:

$$-\sum_{j=1}^{N} \partial_{y_j} \sum_{k,h} a_{ijkh}(c_{n,0})\, e_{khy}(\omega^{lm}) = \sum_{j=1}^{N} \partial_{y_j} \sum_{k,h} a_{ijkh}(c_{n,0})\, e_{khx}(\lambda^{lm}), \tag{4.2.9}$$

for $i = 1, \ldots, N$. Recall that the right-hand side is defined as $(\lambda^{lm}(y))_k = y_m \delta_{kl}$ for $l, m = 1, \ldots, N$. By using the identity

$$\sum_{k,h=1}^{N} a_{ijkh}(c_{n,0})\, e_{khx}(\lambda^{lm}) = a_{ijlm}, \tag{4.2.10}$$

for $i, j, l, m = 1, \dots, N$, we can write (4.2.9) as

$$-\sum_{j=1}^{N} \partial_{y_j} \sum_{k,h} a_{ijkh}(c_{n,0})\, e_{khy}(\omega^{lm}) = \sum_{j=1}^{N} \partial_{y_j}\, a_{ijlm}(c_{n,0}), \quad 1 \le i \le N. \tag{4.2.11}$$

Multiplying both sides of (4.2.11) with $e_{lmx}(u_{n,0})$ and summing up over l and m yields

$$\begin{aligned} -\sum_{j=1}^{N} \partial_{y_j} \Big(\sum_{k,h=1}^{N} a_{ijkh}(c_{n,0}) \sum_{l,m=1}^{N} e_{khy}(\omega^{lm})\, e_{lmx}(u_{n,0}) \Big) \\ = \sum_{j=1}^{N} \partial_{y_j} \sum_{l,m=1}^{N} a_{ijlm}(c_{n,0}) e_{lmx}(u_{n,0}), \end{aligned} \tag{4.2.12}$$

for $i = 1, \dots, N$. Now we can compare both equations, namely (4.2.12) and (4.2.8) and from the left-hand sides we can directly read off a representation for $u_{n,1}$ in terms of $u_{n,0}$ with the help of the solutions of the cell problems. We obtain

$$e_{khy}(u_{n,1}) - e(c_{n,0})\delta_{kh} = \sum_{l,m=1}^{N} e_{lmx}(u_{n,0})\, e_{khy}(\omega^{lm}), \quad 1 \le k, h \le N,$$

and therefore, we get

$$e_{ijy}(u_{n,1}) = \sum_{l,m=1}^{N} e_{lmx}(u_{n,0})\, e_{ijy}(\omega^{lm}) + e(c_{n,0})\delta_{ij}, \quad 1 \le i, j \le N. \tag{4.2.13}$$

Taking into account that $\mathcal{E}_y(u_{n,0}) = 0$, the ϵ^0-term leads to

$$\begin{aligned} \partial_t c_{n,0} = \Delta_y \Big(& f'(c_{n,0}) - \lambda \Delta_y c_{n,0} - e'(c_{n,0}) \operatorname{tr} \left[\mathcal{A}(c_{n,0})(\mathcal{E}_x(u_{n,0}) + \mathcal{E}_y(u_{n,1}) - e(c_{n,0})\mathbb{1}) \right] \\ & + \frac{1}{2} (\mathcal{E}_x(u_{n,0}) + \mathcal{E}_y(u_{n,1}) - e(c_{n,0})\mathbb{1}) : \mathcal{A}'(c_{n,0}) \left(\mathcal{E}_x(u_{n,0}) + \mathcal{E}_y(u_{n,1}) - e(c_{n,0})\mathbb{1} \right) \Big) \end{aligned}$$

and

$$\begin{aligned} 0 = \nabla_y \cdot \Big(& \mathcal{A}(c_{n,0})(\mathcal{E}_x(u_{n,1}) + \mathcal{E}_y(u_{n,2}) - e'(c_{n,0}) c_{n,1} \mathbb{1}) \\ & + c_{n,1} \mathcal{A}'(c_{n,0})(\mathcal{E}_x(u_{n,0}) + \mathcal{E}_y(u_{n,1}) - e(c_{n,0})\mathbb{1}) \Big) \\ + \nabla_x \cdot \Big(& \mathcal{A}(c_{n,0})(\mathcal{E}_x(u_{n,0}) + \mathcal{E}_y(u_{n,1}) - e(c_{n,0})\mathbb{1}) \Big). \end{aligned} \tag{4.2.14}$$

Now, integrating the mechanical equation (4.2.14) in a componentwise form over Y, we obtain

the system

$$\begin{aligned}\partial_t c_{n,0} = \Delta_y \Big(& f'(c_{n,0}) - \lambda \Delta_y c_{n,0} - e'(c_{n,0}) \operatorname{tr}\left[\mathcal{A}(c_{n,0})(\mathcal{E}_x(u_{n,0}) + \mathcal{E}_y(u_{n,1}) - e(c_{n,0})\mathbb{1})\right] \\ & + \frac{1}{2}(\mathcal{E}_x(u_{n,0}) + \mathcal{E}_y(u_{n,1}) - e(c_{n,0})\mathbb{1}) \\ & \qquad : \mathcal{A}'(c_{n,0})\left(\mathcal{E}_x(u_{n,0}) + \mathcal{E}_y(u_{n,1}) - e(c_{n,0})\mathbb{1}\right)\Big),\end{aligned} \tag{4.2.15}$$

$$0 = \frac{1}{|Y|} \sum_{j=1}^{N} \partial_{x_j} \int_Y \sum_{k,h=1}^{N} a_{ijkh}(c_{n,0}) \left(e_{khx}(u_{n,0}) + e_{khy}(u_{n,1}) - e(c_{n,0})\delta_{kh}\right) \mathrm{d}y, \tag{4.2.16}$$

for $i = 1, \dots, N$. Thereby, the integral of the first expression of the right-hand side of (4.2.14) vanishes due to the Y-periodicity of the involved functions. Next, we insert (4.2.13), the representation for $\mathcal{E}_y(u_{n,1})$, into (4.2.16):

$$\begin{aligned}0 &= \frac{1}{|Y|} \sum_{j=1}^{N} \partial_{x_j} \int_Y \sum_{k,h=1}^{N} a_{ijkh}(c_{n,0}) \big(e_{khx}(u_{n,0}) + e_{khy}(u_{n,1}) - \delta_{kh} e(c_{n,0})\big) \,\mathrm{d}y \\ &= \frac{1}{|Y|} \sum_{j=1}^{N} \partial_{x_j} \int_Y \sum_{k,h=1}^{N} a_{ijkh}(c_{n,0}) \big(e_{khx}(u_{n,0}) + \sum_{l,m=1}^{N} e_{lmx}(u_{n,0})\, e_{khy}(\omega^{lm})\big) \,\mathrm{d}y \\ &= \frac{1}{|Y|} \sum_{j=1}^{N} \partial_{x_j} \int_Y \sum_{l,m,k,h=1}^{N} a_{ijlm}(c_{n,0}) \big(\delta_{lk}\delta_{mh} + e_{lmy}(\omega^{kh})\big) \,\mathrm{d}y \; e_{khx}(u_{n,0}),\end{aligned} \tag{4.2.17}$$

for $i = 1, \dots, N$. In this, we have now found an equation for the macroscopic part of the deformation $u_{n,0}$, which motivates to define the effective or homogenised elasticity tensor

$$\mathcal{A}^{\mathrm{hom}} = (a^{\mathrm{hom}}_{ijkh})_{1 \le i,j,k,h \le N} \tag{4.2.18}$$

by its components

$$a^{\mathrm{hom}}_{ijkh} \coloneqq \frac{1}{|Y|} \int_Y \sum_{l,m=1}^{N} a_{ijlm}(c_{n,0}) \big(\delta_{lk}\delta_{mh} + e_{lmy}(\omega^{kh})\big) \,\mathrm{d}y, \tag{4.2.19}$$

for $i, j, k, h = 1, \dots, N$, and write (4.2.17) as macroscopic equation:

$$0 = \nabla_x \cdot \left(\mathcal{A}^{\mathrm{hom}}\, \mathcal{E}_x(u_{n,0})\right) \quad \text{in } \Omega.$$

Furthermore, to use tensor notation for better clarity, we write

$$\mathcal{E}_\omega = \left(e^{\omega}_{lmkh}\right)_{1 \le l,m,k,h \le N}, \quad \text{with} \quad e^{\omega}_{lmkh} = e_{lmy}(\omega^{kh}), \tag{4.2.20}$$

and we also use the identity tensor $\mathcal{I} \in L^{\mathrm{S}}_4$,

$$\mathcal{I} = \big(\mathcal{I}_{lmkh}\big)_{1\le l,m,k,h\le N}, \quad \text{with} \quad \mathcal{I}_{lmkh} = \frac{1}{2}(\delta_{lm}\delta_{kh} + \delta_{mh}\delta_{lk}). \tag{4.2.21}$$

Now we can state the formally homogenised system, given by

$$\begin{aligned} \partial_t c_{n,0} =& \Delta_y \Big(f'(c_{n,0}) - \lambda \Delta_y c_{n,0} - e'(c_{n,0}) \operatorname{tr}\left[\mathcal{A}(c_{n,0})(\mathcal{I}+\mathcal{E}_\omega)\,\mathcal{E}_x(u_{n,0})\right] \\ &+ \frac{1}{2}(\mathcal{I}+\mathcal{E}_\omega)\,\mathcal{E}_x(u_{n,0}) : \mathcal{A}'(c_{n,0})\,(\mathcal{I}+\mathcal{E}_\omega)\,\mathcal{E}_x(u_{n,0})\Big) \quad \text{in } \Omega\times Y\times S, \end{aligned} \tag{4.2.22}$$

$$0 = \nabla_x \cdot \big(\mathcal{A}^{\mathrm{hom}}\,\mathcal{E}_x(u_{n,0})\big) \qquad \text{in } \Omega\times S. \tag{4.2.23}$$

The remaining unknowns of this limit system are c_0 and u_0, the coefficient functions of the first terms of the expansions, whereby only c_0 still depends on the microscopic variable y. Hence, the extended Cahn–Hilliard equation of the limit system (4.2.22) lives in the unit cell Y, whereas the equation for the mechanics (4.2.23) is defined on the macroscopic domain Ω. This fits well with the considerations of the experiments: the mechanics taks place on the macroscopic scale whereas the process of phase separation happens on a microsopic level. There is a special term for such a micro–macro system, which we discuss in more detail below in order to understand the system (4.2.22), (4.2.23) better.

Distributed-microstructure model

The system above is of the so-called distributed-microstructure type. In such a model, a unit cell is identified for each macroscopic point, on which the local equations are solved, cf. [AJH90], [Sho91], [Sho93], [Hor97], [Mei08]. We have a global or macroscopic equation (4.2.23) for the global or macroscopic unknown u_0, coupled with a local or microscopic equation (4.2.22) for the local or microscopic unknown c_0. At each point $x \in \Omega$, there is identified a microscopic cell Y_x. The local equation (4.2.22) as well as the cell equations (4.1.1) have to be solved in every unit cell Y_x associated with each global point $x \in \Omega$. On Y_x, therefore, a microstructure can be seen which is representative near $x \in \Omega$ (see figure 4.1). In particular, the microstructure can evolve differently at each global point.

Remark 4.2.1. *As such a structure of the limit problem is a typical result for coupled systems where one process occurs on the macroscopic scale and the other one on the microscopic scale, such distributed-microstructure models have been postulated a priori in such situations. The main difficulty in the analysis of such problems comes from the fact that the solution spaces are of the non-standard form $L^p(\Omega, H^1_\#(Y_x))$ where the space $H^1_\#(Y_x)$ depends on $x \in \Omega$. We refer to [Mei08] for details.*

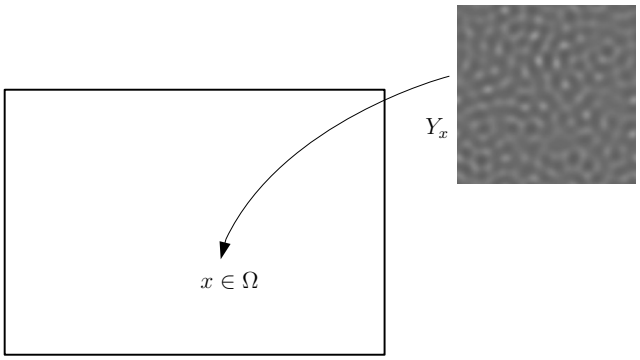

Figure 4.1: Macroscopic domain and microscopic cell Y_x associated to $x \in \Omega$

Note, that the homogenised tensor depends through c_0 on both variables, on x and on y. Properties of the homogenised tensor are discussed in more detail in section 6.1. Notice further, that the homogenised mechanical equation does not contain the eigenstrain explicitly anymore. Self-generated tensions on the microscale are thus macroscopically averaged out. However, this information is still indirectly absorbed via the cell solutions and thus enters the effective tensor as well as the homogenised equation describing the separation process on the microscale.

4.2.2 The linear case

Now we turn to the linear case and we assume the unknown functions of the system (2.5.5), (2.5.6) to have an asymptotic expansion of the same form as in the nonlinear case,

$$c_\epsilon(x,t) = \sum_{i=0}^{\infty} \epsilon^i \, c_i(x,y,t), \quad u_\epsilon(x,t) = \sum_{i=0}^{\infty} \epsilon^i \, u_i(x,y,t). \tag{4.2.24}$$

As before, we insert the expansions (4.2.24) into the equations (2.5.5) and (2.5.6) and compare the coefficients of the several ϵ-powers. The ϵ^{-2}-terms gives

$$\nabla_y \cdot \big(\mathcal{A}(c_{n,\epsilon})\, \mathcal{E}_y(u_0)\big) = 0.$$

This implies $\mathcal{E}_y(u_0) = 0$, as in the nonlinear case, and hence we conclude that u_0 does not depend on y. The ϵ^{-1}-terms yields

$$\begin{aligned} -\nabla_y \cdot \Big(\mathcal{A}(c_{n,\epsilon}) \left(\mathcal{E}_y(u_1) - e'(c_{n,\epsilon}) c_0 \mathbb{1}\right) + \mathcal{A}'(c_{n,\epsilon}) c_0 \big(\mathcal{E}(u_{n,\epsilon}) - e(c_{n,\epsilon})\mathbb{1}\big)\Big) \\ = \nabla_y \cdot \Big(\mathcal{A}(c_{n,\epsilon}) \mathcal{E}_x(u_0)\Big), \end{aligned} \tag{4.2.25}$$

which we consider as an equation for the unknown u_1. For the following calculations, we use the componentwise representation

$$\begin{aligned} -\sum_{j=1}^{N}\partial_{y_j}\sum_{k,h=1}^{N}\big(a_{ijkh}\left(e_{khy}(u_1)-\delta_{kh}e'(c_{n,\epsilon})c_0\right)+a'_{ijkh}c_0\big(e_{kh}(u_{n,\epsilon})-\delta_{kh}e(c_{n,\epsilon})\big)\big) \\ =\sum_{j=1}^{N}\partial_{y_j}\sum_{k,h=1}^{N}\big(a_{ijkh}\,e_{khx}(u_0)\big), \end{aligned} \tag{4.2.26}$$

for $i=1,\dots,N$. In order to develop a representation of u_1 or for the microscopic strain $\mathcal{E}_y(u_1)$, we use the cell problems introduced in 4.1. As in the nonlinear case, in order to compare these with the ϵ^{-1}-equation, we consider (4.2.12), which we state here again:

$$-\sum_{j=1}^{N}\partial_{y_j}\sum_{k,h=1}^{N}a_{ijkh}\sum_{l,m=1}^{N}e_{khy}(\omega^{lm})\,e_{lmx}(u_0)=\sum_{j=1}^{N}\partial_{y_j}\sum_{l,m=1}^{N}a_{ijlm}e_{lmx}(u_0). \tag{4.2.27}$$

With view to the left-hand sides, we can read off

$$\begin{aligned} \sum_{k,h=1}^{N}a_{ijkh}e_{khy}(u_1)=\sum_{k,h=1}^{N}a_{ijkh}\sum_{l,m=1}^{N}e_{khy}(\omega^{lm})\,e_{lmx}(u_0)+\sum_{k,h=1}^{N}a_{ijkh}\delta_{kh}e'(c_{n,\epsilon})c_0 \\ -\sum_{k,h=1}^{N}a'_{ijkh}c_0\big(e_{kh}(u_{n,\epsilon})-e(c_{n,\epsilon})\delta_{kh}\big) \end{aligned} \tag{4.2.28}$$

or, using tensor notation,

$$\begin{aligned} \mathcal{A}(c_{n,\epsilon})\mathcal{E}_y(u_1)=\mathcal{A}(c_{n,\epsilon})\mathcal{E}_\omega\,\mathcal{E}_x(u_0)+\mathcal{A}(c_{n,\epsilon})e'(c_{n,\epsilon})c_0\mathbb{1} \\ -\mathcal{A}'(c_{n,\epsilon})c_0\big(\mathcal{E}(u_{n,\epsilon})-e(c_{n,\epsilon})\mathbb{1}\big). \end{aligned} \tag{4.2.29}$$

Multiplying (4.2.29) by $\mathcal{A}^{-1}(c_{n,\epsilon})$, the inverse of the elasticity tensor, we get

$$\mathcal{E}_y(u_1)=\mathcal{E}_\omega\,\mathcal{E}_x(u_0)+e'(c_{n,\epsilon})c_0\mathbb{1}-\mathcal{A}^{-1}(c_{n,\epsilon})\mathcal{A}'(c_{n,\epsilon})(\mathcal{E}(u_{n,\epsilon})-e(c_{n,\epsilon})\mathbb{1})\,c_0. \tag{4.2.30}$$

According to the positive definiteness of $\mathcal{A}$ and § 2.2.2, the inverse $\mathcal{A}^{-1}$ exists. As discussed

in § 2.2.2, it is uniquely defined by $\mathcal{A}^{-1}\mathcal{A} = \mathcal{I}$. The ϵ^0-term gives

$$\begin{aligned}\partial_t c_0 = \Delta_y\Big(& f''(c_{n,\epsilon})c_0 - \lambda\Delta_y c_0 \\ & - e'(c_{n,\epsilon})\operatorname{tr}\big[\mathcal{A}(c_{n,\epsilon})\big(\mathcal{E}_x(u_0) + \mathcal{E}_y(u_1) - e'(c_{n,\epsilon})c_0\mathbb{1}\big)\big] \\ & - e'(c_{n,\epsilon})\operatorname{tr}\big[\mathcal{A}'(c_{n,\epsilon})c_0\big(\mathcal{E}(u_{n,\epsilon}) - e(c_{n,\epsilon})\mathbb{1}\big)\big] - e''(c_{n,\epsilon})c_0\operatorname{tr}\mathcal{S}_{n,\epsilon} \\ & + \big(\mathcal{E}(u_{n,\epsilon}) - e(c_{n,\epsilon})\mathbb{1}\big) : \mathcal{A}'(c_{n,\epsilon})\big(\mathcal{E}_x(u_0) + \mathcal{E}_y(u_1) - e'(c_{n,\epsilon})c_0\mathbb{1}\big) \\ & + \frac{1}{2}\big(\mathcal{E}(u_{n,\epsilon}) - e(c_{n,\epsilon})\mathbb{1}\big) : \mathcal{A}''(c_{n,\epsilon})c_0\big(\mathcal{E}(u_{n,\epsilon}) - e(c_{n,\epsilon})\mathbb{1}\big)\Big)\end{aligned} \tag{4.2.31}$$

and

$$\begin{aligned}0 = {} & \nabla_x\cdot\Big(\mathcal{A}(c_{n,\epsilon})\big(\mathcal{E}_x(u_0) + \mathcal{E}_y(u_1) - e'(c_{n,\epsilon})c_0\mathbb{1}\big) \\ & \qquad + \mathcal{A}'(c_{n,\epsilon})c_0\big(\mathcal{E}(u_{n,\epsilon}) - e(c_{n,\epsilon})\mathbb{1}\big)\Big) \\ & + \nabla_y\cdot\Big(\mathcal{A}(c_{n,\epsilon})\big(\mathcal{E}_x(u_1) + \mathcal{E}_y(u_2) - e'(c_{n,\epsilon})c_1\mathbb{1}\big) \\ & \qquad + \mathcal{A}'(c_{n,\epsilon})c_1\big(\mathcal{E}(u_{n,\epsilon}) - e(c_{n,\epsilon})\mathbb{1}\big)\Big).\end{aligned} \tag{4.2.32}$$

We average the mechanical part (4.2.32) componentwise over Y and get

$$\begin{aligned}0 = \sum_{j=1}^{N}\partial_{x_j}\frac{1}{|Y|}\int_Y \sum_{k,h=1}^{N} & a'_{ijkh}(c_{n,\epsilon})\,c_0\,\big(e_{kh}(u_{n,\epsilon}) - \delta_{kh}e(c_{n,\epsilon})\big) \\ & + a_{ijkh}(c_{n,\epsilon})\,\big(e_{khx}(u_0) + e_{khy}(u_1) - \delta_{kh}e'(c_{n,\epsilon})c_0\big)\,\mathrm{d}y.\end{aligned} \tag{4.2.33}$$

The second term of the right-hand side of (4.2.32) vanishes by integrating due to the Y-periodicity of the involved functions and coefficients. Using the representation (4.2.29), from (4.2.33) we obtain

$$\begin{aligned}0 &= \sum_{j=1}^{N}\partial_{x_j}\frac{1}{|Y|}\int_Y \sum_{k,h=1}^{N} a_{ijkh}(c_{n,\epsilon})\,\big(e_{khx}(u_0) + \sum_{l,m=1}^{N} e_{khy}(\omega^{lm})\,e_{lmx}(u_0)\big)\,\mathrm{d}y \\ &= \sum_{j=1}^{N}\partial_{x_j}\frac{1}{|Y|}\int_Y \sum_{k,h,l,m=1}^{N} a_{ijkh}(c_{n,\epsilon})\,\big(\delta_{lk}\delta_{mh} + e_{khy}(\omega^{lm})\big)\,\mathrm{d}y\;e_{lmx}(u_0).\end{aligned}$$

We use the same abbreviation as in § 4.2 and define the homogenised tensor $\mathcal{A}^{\mathrm{hom}}$, which describes the effective elastic properties of the monolayer, by

$$a^{\mathrm{hom}}_{ijlm} = \frac{1}{|Y|}\int_Y \sum_{k,h=1}^{N} a_{ijkh}(c_{n,\epsilon})\,\big(\delta_{lk}\delta_{mh} + e_{khy}(\omega^{lm})\big)\,\mathrm{d}y. \tag{4.2.34}$$

With the identities (4.2.29) and (4.2.30) and using tensor notation (4.2.20) and (4.2.21), we can state the formally homogenised linear Cahn–Larché system:

$$
\begin{aligned}
\partial_t c_0 = \Delta_y \Big(& f''(c_{n,\epsilon}) c_0 - \lambda \Delta_y c_0 \\
& - e'(c_{n,\epsilon}) \operatorname{tr} \big(\mathcal{A}(c_{n,\epsilon})(\mathcal{I} + \mathcal{E}_\omega) \mathcal{E}_x(u_0) \big) - e''(c_{n,\epsilon}) c_0 \operatorname{tr} \mathcal{S}_{n,\epsilon} \\
& + \big(\mathcal{E}(u_{n,\epsilon}) - e(c_{n,\epsilon}) \mathbb{1} \big) : \mathcal{A}'(c_{n,\epsilon})(\mathcal{I} + \mathcal{E}_\omega) \mathcal{E}_x(u_0)) \\
& - \big(\mathcal{E}(u_{n,\epsilon}) - e(c_{n,\epsilon}) \mathbb{1} \big) : \mathcal{A}'(c_{n,\epsilon}) \big(\mathcal{A}^{-1}(c_{n,\epsilon}) \mathcal{A}'(c_{n,\epsilon}) c_0 (\mathcal{E}(u_{n,\epsilon}) - e(c_{n,\epsilon}) \mathbb{1}) \big) \\
& + \frac{1}{2} \big(\mathcal{E}(u_{n,\epsilon}) - e(c_{n,\epsilon}) \mathbb{1} \big) : \mathcal{A}''(c_{n,\epsilon}) c_0 \big(\mathcal{E}(u_{n,\epsilon}) - e(c_{n,\epsilon}) \mathbb{1} \big) \Big) \quad \text{in } \Omega \times Y \times S,
\end{aligned} \tag{4.2.35}
$$

$$
0 = \nabla_x \cdot \big(\mathcal{A}^{\mathrm{hom}} \mathcal{E}_x(u_0) \big) \quad \text{in } \Omega \times S. \tag{4.2.36}
$$

This limit system has the same structure as the limit system in the nonlinear case (4.2.22), (4.2.23) and has in particular the structure of a distributed-microstructure model. The only remaining unknowns are the first terms of the asymtotic expansions, c_0 and u_0. The limit order parameter c_0 depends on the microscopic space variable y and the equation describing the phase separation (4.2.35) in the reference element on the microscale includes only derivatives with respect to y, whereas the limit displacement u_0 describes a purely macroscopic phenomenon. The solutions of the cell problems enter into the components of the homogenised elasticity tensor as well as into the equation for the phase separation. The mechanical equation (4.2.36) and also the formally homogenised tensor (4.2.34) are the same as in the nonlinear case.

5 Well-posedness of the linear Cahn–Larché system

In this chapter, we examine the linearised Cahn–Larché system (2.5.5), (2.5.6). We first make some assumptions and state the weak formulation of the linear system. After, we give an a-priori estimate for every $\epsilon > 0$, which enables the homogenisation process in the next chapter. Further, for every $\epsilon > 0$, we proof the existence and uniqueness of a weak solution using theory about linear differential–algebraic equations.

5.1 Weak setting

As we want to work in a weak setting, we introduce now some function spaces, specify some assumptions and thus also state the notation we use. Then, we will have all tools to state the weak formulation of the linear scaled Cahn–Larché system.

Let $\Omega \subset \mathbb{R}^N$ be a bounded domain with Lipschitz-continuous boundary $\partial\Omega = \Gamma$ such that $\Gamma = \Gamma_0 \cup \Gamma_s \cup \Gamma_g$ with pairwise disjoint parts $\Gamma_0, \Gamma_s, \Gamma_0$, cf. § 2.2.2. In the following, we denote by

$$(u, v)_\Omega = \int_\Omega u(x)\, v(x)\, \mathrm{d}x \quad \text{and} \quad (u, v)_{\Omega,t} = \int_0^t (u(s), v(s))_\Omega \, \mathrm{ds}$$

the scalar products on $L^2(\Omega)$ and $L^2\left((0,t), L^2(\Omega)\right)$ for $t \in [0,T]$, respectively, and the abbreviation $\|\cdot\|_\Omega \coloneqq \|\cdot\|_{L^2(\Omega)}$ for the standard norm on $L^2(\Omega)$ as well as $\|u\|^2_{\Omega,t} \coloneqq \int_0^t (u(\tau),\, u(\tau))_\Omega \, \mathrm{d}\tau$. We define the function space

$$V(\Omega) \coloneqq \{v \in H^2(\Omega) \mid \nabla v \cdot n = 0 \text{ on } \Gamma\},$$

equipped with the norm

$$\|v\|_{V(\Omega)} \coloneqq \left(\|v\|^2_\Omega + \|\Delta v\|^2_\Omega\right)^{1/2}, \quad v \in V,$$

which is equivalent to the standard norm on $H^2(\Omega)$ (see remark 5.2.7), and

$$W(\Omega) \coloneqq \{w \in [H^1(\Omega)]^N \mid w = 0 \text{ on } \Gamma_0,\ w \cdot n = 0 \text{ on } \Gamma_s\},$$

provided with the standard norm on $[H^1(\Omega)]^N$. For the unknown functions, we need the function spaces

$$\begin{aligned}\mathcal{V}(\Omega) &\coloneqq L^2\left(S, V(\Omega)\right),\\ \mathcal{W}(\Omega) &\coloneqq L^2\left(S, W(\Omega)\right).\end{aligned}$$

For matrix-valued functions $A = (a_{ij})_{1\le i,j\le N}, B = (b_{ij})_{1\le i,j\le N} \in [L^2(\Omega)]^{N\times N}$, we define the scalar product

$$(A\,, B)_{F,\Omega} \coloneqq \int_\Omega A : B \,\mathrm{d}x,$$

and the norm

$$\|A\|_{F,\Omega}^2 \coloneqq (A\,, A)_{F,\Omega}$$

as well as

$$\|D\|_{M,\Omega}^2 = N^2 \max_{i,j} \|d_{ij}\|_{L^\infty(\Omega)}^2,$$

for $D = (d_{ij})_{1\le i,j\le N} \in [L^\infty(\Omega)]^{N\times N}$. Whenever we use a standard norm of a matrix- or vector-valued function, this is to be understood in the following averaged componentenwise sense,

$$\|v\|_{L^p(\Omega)}^p = \sum_{i=1}^N \|v_i\|_{L^p(\Omega)}^p, \quad \|v\|_{H^1(\Omega)}^2 = \sum_{i=1}^N \|v_i\|_{H^1(\Omega)}^2 \quad \text{and} \quad \|M\|_\Omega^2 = \sum_{i,j=1}^N \|m_{ij}\|_\Omega^2,$$

for $v = (v_1, \dots, v_N)^{\mathrm{T}} \in \mathbb{R}^N$, $M = (m_{ij})_{1\le i,j\le N} \in \mathbb{R}^{N\times N}$, $p \in [1, \infty)$. Note that $\|M\|_{F,\Omega}^2 = \int_\Omega M : M \,\mathrm{d}x = \|M\|_\Omega^2$.

Further, we denote the dual pairing of $V(\Omega)'$ and $V(\Omega)$ by $\langle \cdot\,, \cdot \rangle_{V(\Omega)}$ and , in abuse of notation, we sometimes write $\langle \cdot\,, \cdot \rangle_{V(\Omega)} = (\,\cdot\,, \cdot\,)_\Omega$. Moreover, we use the trace operator

$$\gamma\colon H^1(\Omega) \to L^2(\Gamma), \quad u \mapsto u_{|\Gamma}$$

if we want to restrict a function $u \in H^1(\Omega)$ to the boundary of Ω and for the sake of simplicity, however, we simply write u instead of $\gamma(u)$ for functions $u \in H^1(\Omega)$.

Now we need to make concrete assumptions on the solutions to the nonlinear ϵ-dependent problem. These are denoted by $c_{n,\epsilon}$ and $u_{n,\epsilon}$ and we assume them as well as the partial derivatives of the displacement to be bounded with respect to space and time, hence

$$\begin{aligned} c_{n,\epsilon} &\in L^\infty(\Omega \times S), \\ u_{n,\epsilon} &\in [L^\infty(\Omega \times S)]^N, \\ \nabla u_{n,\epsilon} &\in [L^\infty(\Omega \times S)]^{N\times N}. \end{aligned} \tag{5.1.1}$$

We consider the interpolated tensor $\mathcal{A}$ defined by (2.2.41) with constant tensors $\mathcal{A}^i$, $i \in \{\mathrm{E}, \mathrm{C}\}$ corresponding to the two phases, specified in § 2.2.2, such that there exist $\alpha^i, \beta^i \in \mathbb{R}$, with $0 < \alpha^i < \beta^i$, such that $\mathcal{A}^i \in M(\alpha^i, \beta^i, \Omega)$. Then, there exist $\alpha, \beta \in \mathbb{R}$, with $0 < \alpha < \beta$, such that

$$\mathcal{A}(c_{n,\epsilon}(\,\cdot\,, t)) \in \mathcal{M}(\alpha, \beta, \Omega), \tag{5.1.2}$$

$t \in S$. Note, that the derivatives $\mathcal{A}'(c_{n,\epsilon})$ and $\mathcal{A}''(c_{n,\epsilon})$ do not necessarily fulfil property *(iii)* of definition 4.1.1, but the other three ones of this tensor class. In particular, there exist two numbers $\beta', \beta'' > 0$ such that

$$\big|\mathcal{A}'(c_{n,\epsilon})X\big| \le \beta'\big|X\big| \quad \text{and} \quad \big|\mathcal{A}''(c_{n,\epsilon})X\big| \le \beta''\big|X\big|, \tag{5.1.3}$$

for any $X \in \mathbb{R}^{N\times N}$.

For the eigenstrain $\bar{\mathcal{E}}(c) = e(c)\mathbb{1}$ we first choose the same type of interpolation as for the elasticity tensor, i.e.

$$e(c)\mathbb{1} \coloneqq \big(e_\mathrm{E} + d(c)(e_\mathrm{C} - e_\mathrm{E})\big)\mathbb{1}, \tag{5.1.4}$$

with constants $e_\mathrm{E}, e_\mathrm{C} \in \mathbb{R}$ describing the eigenstrain behaviour of the corresponding lipid phase, and with the interpolation function $d(\cdot)$ defined by (2.2.42).

Finally, we choose the initial value $c^\mathrm{in} \in L^2(\Omega)$ and for the boundary force term we assume $g \in L^2(S, [H^{-1/2}(\Gamma_g)]^N)$. For ease of notation, we simply write

$$\langle \cdot, \cdot \rangle_{\Gamma_\mathrm{g}} \coloneqq \langle \cdot, \cdot \rangle_{H^{-1/2}(\Gamma_g), H^{1/2}(\Gamma_g)},$$

whenever we need the pairing of $[H^{1/2}(\Gamma_g)]^N$ with its dual space. Now we can state the equations in their weak form:

Find $(c_\epsilon, u_\epsilon) \in \mathcal{V}(\Omega) \times \mathcal{W}(\Omega)$ with $c_\epsilon(\,\cdot\,, 0) = c^{\text{in}}$ in Ω, such that

$$\begin{aligned}
&\big(\partial_t c_\epsilon, \varphi\big)_\Omega - \epsilon^2\big(f''(c_{n,\epsilon})c_\epsilon\,, \Delta\varphi\big)_\Omega + \epsilon^4\big(\lambda\Delta c_\epsilon\,, \Delta\varphi\big)_\Omega \\
&+ \epsilon^2\big(e'(c_{n,\epsilon})\,\mathrm{tr}(\mathcal{S}_\epsilon)\,, \Delta\varphi\big)_\Omega + \epsilon^2\big(e''(c_{n,\epsilon})c_\epsilon\,\mathrm{tr}(\mathcal{S}_{n,\epsilon})\,, \Delta\varphi\big)_\Omega \\
&- \epsilon^2\big((\mathcal{E}(u_{n,\epsilon}) - e(c_{n,\epsilon})\mathbb{1}) : \mathcal{A}'(c_{n,\epsilon})(\mathcal{E}(u_\epsilon) - e'(c_{n,\epsilon})c_\epsilon\mathbb{1})\,, \Delta\varphi\big)_\Omega \\
&- \epsilon^2\frac{1}{2}\big((\mathcal{E}(u_{n,\epsilon}) - e(c_{n,\epsilon})\mathbb{1}) : \mathcal{A}''(c_{n,\epsilon})c_\epsilon\,(\mathcal{E}(u_{n,\epsilon}) - e(c_{n,\epsilon})\mathbb{1})\,\Delta\varphi\big)_\Omega = 0,
\end{aligned} \tag{5.1.5}$$

and

$$\begin{aligned}
&\big(\mathcal{A}(c_{n,\epsilon})\,(\mathcal{E}(u_\epsilon) - e'(c_{n,\epsilon})c_\epsilon\mathbb{1}), \mathcal{E}(\psi)\big)_{F,\Omega} \\
&+ \big(\mathcal{A}'(c_{n,\epsilon})\,c_\epsilon\,(\mathcal{E}(u_{n,\epsilon}) - e(c_{n,\epsilon})\mathbb{1}), \mathcal{E}(\psi)\big)_{F,\Omega} - \langle g, \psi\rangle_{\Gamma_g} = 0,
\end{aligned} \tag{5.1.6}$$

for any $(\phi, \psi) \in V(\Omega) \times W(\Omega)$ and a.e. $t \in S$.

The next proposition tells us that the time derivative of a function c_ϵ satisfying equation (5.1.5) is an element of $L^2(S, V'(\Omega))$.

Proposition 5.1.1. *For every $\epsilon > 0$ and functions $(c_\epsilon, u_\epsilon) \in \mathcal{V}(\Omega) \times \mathcal{W}(\Omega)$ satisfying the equations* (5.1.5) *and* (5.1.6)*, it holds that $\partial_t c_\epsilon \in L^2(S, V'(\Omega))$.*

Proof. For almost every $t \in S$ we have

$$\begin{aligned}
&\|\partial_t c_\epsilon\|_{V'(\Omega)} = \\
&= \sup_{\varphi\in V(\Omega),\ \|\varphi\|_{V(\Omega)}=1} \langle\partial_t c_\epsilon, \varphi\rangle_{V(\Omega)} \\
&= \sup_{\varphi\in V(\Omega),\ \|\varphi\|_{V(\Omega)}=1} \Big\{\epsilon^2\big(f''(c_{n,\epsilon})\,c_\epsilon, \Delta\varphi\big)_\Omega - \epsilon^4\lambda\big(\Delta c_\epsilon, \Delta\varphi\big)_\Omega \\
&\qquad - \epsilon^2\big(e'(c_{n,\epsilon})\,\mathrm{tr}(\mathcal{S}_\epsilon), \Delta\varphi\big)_\Omega - \epsilon^2\big(e''(c_{n,\epsilon})c_\epsilon\,\mathrm{tr}(\mathcal{S}_{n,\epsilon}), \Delta\varphi\big)_\Omega \\
&\qquad + \epsilon^2\big((\mathcal{E}(u_{n,\epsilon}) - e(c_{n,\epsilon})\mathbb{1}) : \mathcal{A}'(c_{n,\epsilon})(\mathcal{E}(u_\epsilon) - e'(c_{n,\epsilon})c_\epsilon\mathbb{1}),\ \Delta\varphi\big)_\Omega \\
&\qquad + \frac{1}{2}\epsilon^2\big((\mathcal{E}(u_{n,\epsilon}) - e(c_{n,\epsilon})\mathbb{1}) : \mathcal{A}''(c_{n,\epsilon})c_\epsilon\,(\mathcal{E}(u_{n,\epsilon}) - e(c_{n,\epsilon})\mathbb{1}),\ \Delta\varphi\big)_\Omega\Big\}.
\end{aligned} \tag{5.1.7}$$

First we take a closer look at the trace terms. Remember that

$$\mathcal{S}_\epsilon = \mathcal{A}(c_{n,\epsilon})\big(\mathcal{E}(u_\epsilon) - e'(c_{n,\epsilon})c_\epsilon\mathbb{1}\big) + \mathcal{A}'(c_{n,\epsilon})c_\epsilon\big(\mathcal{E}(u_{n,\epsilon}) - e(c_{n,\epsilon})\mathbb{1}\big) \tag{5.1.8}$$

and the identity

$$\operatorname{tr} \mathcal{S}_\epsilon = \mathcal{S}_\epsilon : \mathbb{1}$$

and hence, we can estimate

$$\big(\mathcal{S}_\epsilon \,,\, \mathbb{1}\Delta\varphi\big)_{F,\Omega} \;\leq\; \|\mathcal{S}_\epsilon\|_{F,\Omega}\, \|\mathbb{1}\Delta\varphi\|_{F,\Omega}\,.$$

For the norm of the linear stress tensor, we get

$$\begin{aligned}
\|\mathcal{S}_\epsilon\|_{F,\Omega} &= \big\|\mathcal{A}(c_{n,\epsilon})\big(\mathcal{E}(u_\epsilon) - e'(c_{n,\epsilon})c_\epsilon \mathbb{1}\big) + \mathcal{A}'(c_{n,\epsilon})c_\epsilon\big(\mathcal{E}(u_{n,\epsilon}) - e(c_{n,\epsilon})\mathbb{1}\big)\big\|_{F,\Omega} \\
&\leq \beta\big(\, \|\mathcal{E}(u_\epsilon)\|_{F,\Omega} + \|e'(c_{n,\epsilon})c_\epsilon \mathbb{1}\|_{F,\Omega}\,\big) + \beta'\, \|c_\epsilon(\mathcal{E}(u_{n,\epsilon}) - e(c_{n,\epsilon})\mathbb{1})\|_{F,\Omega} \\
&\leq \beta\big(\, \|\mathcal{E}(u_\epsilon)\|_{\Omega} + N\, \|e'(c_{n,\epsilon})\|_{L^\infty(\Omega)}\, \|c_\epsilon\|_{\Omega}\,\big) + \beta'\, \|\mathcal{E}(u_{n,\epsilon}) - e(c_{n,\epsilon})\mathbb{1}\|_{M,\Omega}\, \|c_\epsilon\|_{\Omega}\,,
\end{aligned} \tag{5.1.9}$$

where we applied the inequalities of Minkowski and Hölder as well as the boundedness of $\mathcal{A}$ and its first derivative. With (5.1.9), we obtain

$$\begin{aligned}
&\epsilon^2\big(e'(c_{n,\epsilon})\, \mathcal{S}_\epsilon \,,\, \mathbb{1}\Delta\varphi\big)_{F,\Omega} \\
&\quad\leq \epsilon^2\, \|e'(c_{n,\epsilon})\, \mathcal{S}_\epsilon\|_{F,\Omega}\, \|\mathbb{1}\Delta\varphi\|_{F,\Omega} \\
&\quad\leq \epsilon^2\, \|e'(c_{n,\epsilon})\|_{L^\infty(\Omega)}\, \big(\beta\, \|\mathcal{E}(u_\epsilon)\|_{\Omega} + N\, \|e'(c_{n,\epsilon})\|_{L^\infty(\Omega)}\, \|c_\epsilon\|_{\Omega}\,\big)\, N\, \|\Delta\varphi\|_{\Omega} \\
&\qquad + \epsilon^2\, \|e'(c_{n,\epsilon})\|_{L^\infty(\Omega)}\, \beta'\, \|\mathcal{E}(u_{n,\epsilon}) - e(c_{n,\epsilon})\mathbb{1}\|_{M,\Omega}\, \|c_\epsilon\|_{\Omega}\; N\, \|\Delta\varphi\|_{\Omega} \\
&\quad\leq \epsilon^2\, C\, \big(\, \|\mathcal{E}(u_\epsilon)\|_{\Omega} + \|c_\epsilon\|_{\Omega}\,\big)\, \|\Delta\varphi\|_{\Omega}\,.
\end{aligned} \tag{5.1.10}$$

Analogous to this, we get

$$\begin{aligned}
&\epsilon^2\big(e''(c_{n,\epsilon})\, c_\epsilon\, \mathcal{S}_{n,\epsilon} \,,\, \mathbb{1}\Delta\varphi\big)_{F,\Omega} \\
&\quad\leq \epsilon^2\, \|e''(c_{n,\epsilon})\|_{L^\infty(\Omega)}\, \|c_\epsilon\|_{\Omega}\, \beta\, \|\mathcal{E}(u_{n,\epsilon}) - e(c_{n,\epsilon})\mathbb{1})\|_{M,\Omega}\, N\, \|\Delta\varphi\|_{\Omega} \\
&\quad\leq \epsilon^2\, C\, \|c_\epsilon\|_{\Omega}\, \|\Delta\varphi\|_{\Omega}\,.
\end{aligned} \tag{5.1.11}$$

For the next term, we get the following estimate, using the same inequalities as above,

$$\begin{aligned}
&\epsilon^2 \int_\Omega \big(\mathcal{E}(u_{n,\epsilon}) - e(c_{n,\epsilon})\mathbb{1}\big) : \mathcal{A}'(c_{n,\epsilon})\big(\mathcal{E}(u_\epsilon) - e'(c_{n,\epsilon})c_\epsilon(x,t)\mathbb{1}\big)\,\Delta\varphi(x)\,\mathrm{d}x \\
&\qquad \le \epsilon^2 \left\|\Delta\varphi(\mathcal{E}(u_{n,\epsilon}) - e(c_{n,\epsilon})\mathbb{1})\right\|_{F,\Omega} \left\|\mathcal{A}'(c_{n,\epsilon})(\mathcal{E}(u_\epsilon) - e'(c_{n,\epsilon})c_\epsilon\mathbb{1})\right\|_{F,\Omega} \\
&\qquad \le \epsilon^2 \left\|\Delta\varphi\right\|_\Omega \left\|\mathcal{E}(u_{n,\epsilon}) - e(c_{n,\epsilon})\mathbb{1}\right\|_{M,\Omega} \beta'\big(\left\|\mathcal{E}(u_\epsilon)\right\|_\Omega + N\left\|e'(c_{n,\epsilon})\right\|_{L^\infty(\Omega)}\left\|c_\epsilon\right\|_\Omega\big) \\
&\qquad \le \epsilon^2 C\,\big(\left\|\mathcal{E}(u_\epsilon)\right\|_\Omega + \left\|c_\epsilon\right\|_\Omega\big)\left\|\Delta\varphi\right\|_\Omega,
\end{aligned} \tag{5.1.12}$$

and the last term of the right-hand side of (5.1.7) in an analogous way. The remaining first two terms in (5.1.7) are estimated using Hölder's inequality. Altogether we obtain

$$\begin{aligned}
\left\|\partial_t c_\epsilon\right\|_{V'(\Omega)} &= \sup_{\varphi\in V(\Omega),\ \|\varphi\|_{V(\Omega)}=1} \langle \partial_t c_\epsilon, \varphi\rangle_{V'(\Omega),V(\Omega)} \\
&\le \sup_{\varphi\in V(\Omega),\ \|\varphi\|_{V(\Omega)}=1} \Big\{\epsilon^2 \left\|f''(c_{n,\epsilon})\right\|_{L^\infty(\Omega)} \left\|c_\epsilon\right\|_\Omega \left\|\Delta\varphi\right\|_\Omega + \epsilon^4\lambda \left\|\Delta c_\epsilon\right\|_\Omega \left\|\Delta\varphi\right\|_\Omega \\
&\qquad\qquad + \epsilon^2 C\,\big(\left\|\mathcal{E}(u_\epsilon)\right\|_\Omega + \left\|c_\epsilon\right\|_\Omega\big)\left\|\Delta\varphi\right\|_\Omega\Big\} \\
&\le \sup_{\varphi\in V(\Omega),\ \|\varphi\|_{V(\Omega)}=1} \Big\{C\,\big(\epsilon^4\left\|\Delta c_\epsilon\right\|_\Omega + \epsilon^2\left\|\mathcal{E}(u_\epsilon)\right\|_\Omega + \epsilon^2\left\|c_\epsilon\right\|_\Omega\big)\left\|\Delta\varphi\right\|_\Omega\Big\} \\
&\le \sup_{\varphi\in V(\Omega),\ \|\varphi\|_{V(\Omega)}=1} \Big\{C\,\big(\epsilon^4\left\|\Delta c_\epsilon\right\|_\Omega + \epsilon^2\left\|\mathcal{E}(u_\epsilon)\right\|_\Omega + \epsilon^2\left\|c_\epsilon\right\|_\Omega\big)\left\|\varphi\right\|_{V(\Omega)}\Big\}.
\end{aligned}$$

Because $c_\epsilon \in \mathcal{V}(\Omega)$, $u_\epsilon \in \mathcal{W}(\Omega)$ and $\|\varphi\|_{V(\Omega)} = 1$, the right-hand side is bounded for almost every $t \in S$. □

5.2 A-priori estimates

This part is devoted to show uniform boundedness of the sequences of the solution components of the scaled linear Cahn–Larché system, c_ϵ and u_ϵ, as well as for sequences depending on their derivatives. This result will enable us in section 6.1 to pass to the limit in the sense of two-scale convergence. Therefore, we start by recalling two variants of Korn's inequality as well as the inequality of Poincaré, which are important for the mechanics, as well as a trace inequality. The following results, which we cite from [Sch13] and [CD99], enable us to estimate the norm of the displacement.

Proposition 5.2.1 (Korn's inequality with boundary values)**.**
Let $\Omega \subset \mathbb{R}^N$ be a bounded domain with Lipschitz-boundary and $\Gamma_D \subset \partial\Omega$ a part of the boundary with $(N-1)$-dimensional Hausdorff measure $|\Gamma_D| > 0$. Then, there exists a constant $C > 0$ such that for any function $u \in [H^1(\Omega)]^N$ with $u = 0$ on Γ_D

$$\int_\Omega |\nabla u|^2 \,\mathrm{d}x \leq C \int_\Omega |\mathcal{E}(u)|^2 \,\mathrm{d}x.$$

In the course of periodic homogenisation we need the following version of Korns inequality.

Proposition 5.2.2 (Korn's inequality for periodic boundary conditions)**.**
Let $Y = (0, l_1) \times \ldots \times (0, l_N) \subset \mathbb{R}^N$. Then, there exists a constant $C > 0$ such that for any function $u \in [V_\#(Y)]^N$, where $V_\#(Y) = \{v \in H^1_\#(Y) \mid \int_Y v \,\mathrm{d}y = 0\}$, the following applies:

$$\int_Y |\nabla u|^2 \,\mathrm{d}y \leq C \int_Y |\mathcal{E}(u)|^2 \,\mathrm{d}y.$$

Proposition 5.2.3 (Poincaré inequality with control on a boundary part)**.**
Let $\Omega \subset \mathbb{R}^N$ be a bounded domain with Lipschitz-boundary and $u \in W^{1,p}(\Omega)$, $p \in [1, \infty)$, be function satisfying one of the following properties:

(i) $u = 0$ *on* $\partial\Omega$,

(ii) $\int_\Omega u \,\mathrm{d}x = 0$,

(iii) $\int_\Gamma u = 0$, *for* $\Gamma \subset \partial\Omega$ *with non-vanishing* $(N-1)$*-dimensional Hausdorff measure.*

Then, there exists a constant $C > 0$ such that

$$\|u\|_{W^{1,p}(\Omega)} \leq C \|\nabla u\|_{L^p(\Omega)}.$$

Proposition 5.2.4 (Trace inequality)**.**
Let Ω be a bounded domain with Lipschitz continuous boundary $\partial\Omega$. Then, there exists a constant $c_\gamma > 0$, depending on Ω, such that

$$\|\gamma(u)\|_{H^{1/2}(\partial\Omega)} \leq c_\gamma \|u\|_{H^1(\Omega)}.$$

for any function $u \in H^1(\Omega)$.

Remark 5.2.5. *In the following, we also make use of a weighted version of the well-known Young's inequality: For $a, b \in \mathbb{R}$ and $\delta > 0$ we have*

$$ab \leq \frac{\delta}{2} a^2 + \frac{1}{2\delta} b^2.$$

Now we want to state our boundedness result.

Proposition 5.2.6 (Boundedness)**.**
There exists a constant $C > 0$, independent of ϵ, such that

$$\|c_\epsilon\|_\Omega^2 + \|\epsilon \nabla c_\epsilon\|_{\Omega,t}^2 + \left\|\epsilon^2 \Delta c_\epsilon\right\|_{\Omega,t}^2 + \|u_\epsilon\|_{H^1(\Omega),t}^2 \leq C, \tag{5.2.1}$$

for almost every $t \in S$.

Proof. Starting with equation (5.1.6), we show first that u_ϵ is bounded in $\mathcal{W}(\Omega)$ if c_ϵ is bounded in $L^2(S, L^2(\Omega))$. Therefore, we use u_ϵ as test function in (5.1.6) and get

$$\begin{aligned} &\big(\mathcal{A}(c_{n,\epsilon})\left(\mathcal{E}(u_\epsilon) - e'(c_{n,\epsilon})c_\epsilon \mathbb{1}\right), \mathcal{E}(u_\epsilon)\big)_{F,\Omega} \\ &\quad + \big(\mathcal{A}'(c_{n,\epsilon})\, c_\epsilon \left(\mathcal{E}(u_{n,\epsilon}) - e(c_{n,\epsilon})\mathbb{1}\right), \mathcal{E}(u_\epsilon)\big)_{F,\Omega} - \langle g, u_\epsilon \rangle_{\Gamma_g} = 0. \end{aligned} \tag{5.2.2}$$

Rearanging terms yields

$$\begin{aligned} \big(\mathcal{A}(c_{n,\epsilon})\mathcal{E}(u_\epsilon), \mathcal{E}(u_\epsilon)\big)_{F,\Omega} = &\big(\mathcal{A}(c_{n,\epsilon})e'(c_{n,\epsilon})c_\epsilon \mathbb{1}, \mathcal{E}(u_\epsilon)\big)_{F,\Omega} \\ &+ \big(\mathcal{A}'(c_{n,\epsilon})c_\epsilon(\mathcal{E}(u_{n,\epsilon}) - e(c_{n,\epsilon})\mathbb{1}), \mathcal{E}(u_\epsilon)\big)_{F,\Omega} + \langle g, u_\epsilon \rangle_{\Gamma_g}. \end{aligned} \tag{5.2.3}$$

We estimate the left-hand side of (5.2.3) by using the postitive definiteness of $\mathcal{A}$ as well as Korn's and Poincaré's inequality:

$$\big(\mathcal{A}(c_{n,\epsilon})\,\mathcal{E}(u_\epsilon), \mathcal{E}(u_\epsilon)\big)_\Omega \geq \alpha \left\|\mathcal{E}(u_\epsilon)\right\|_{F,\Omega}^2 \geq \frac{\alpha}{2} \left\|\mathcal{E}(u_\epsilon)\right\|_{F,\Omega}^2 + \frac{\alpha}{2} C \left\|u_\epsilon\right\|_{H^1(\Omega)}^2. \tag{5.2.4}$$

Next we consider the first two terms of the right-hand side of (5.2.3), which can be estimated by applying Young's inequality and using (5.1.2). We get

$$\begin{aligned} \big(\mathcal{A}(c_{n,\epsilon})e'(c_{n,\epsilon})c_\epsilon \mathbb{1}\,, \mathcal{E}(u_\epsilon)\big)_{F,\Omega} \leq\ & \left\|\mathcal{A}(c_{n,\epsilon})e'(c_{n,\epsilon})c_\epsilon \mathbb{1}\right\|_{F,\Omega} \left\|\mathcal{E}(u_\epsilon)\right\|_{F,\Omega} \\ \leq\ & \beta N \left\|e'(c_{n,\epsilon})\right\|_{L^\infty(\Omega)} \left\|c_\epsilon\right\|_\Omega \left\|\mathcal{E}(u_\epsilon)\right\|_{F,\Omega} \\ \leq\ & \frac{1}{2\delta}\beta^2 N^2 \left\|e'(c_{n,\epsilon})\right\|_{L^\infty(\Omega)}^2 \left\|c_\epsilon\right\|_\Omega^2 + \frac{\delta}{2} \left\|\mathcal{E}(u_\epsilon)\right\|_{F,\Omega}^2 \end{aligned} \tag{5.2.5}$$

and

$$\begin{aligned}
&\big(\mathcal{A}'(c_{n,\epsilon})\left(\mathcal{E}(u_{n,\epsilon}) - e(c_{n,\epsilon})\mathbb{1}\right)c_\epsilon\,, \mathcal{E}(u_\epsilon)\big)_{F,\Omega} \\
&\leq \ \big\|\mathcal{A}'(c_{n,\epsilon})\big(\mathcal{E}(u_{n,\epsilon}) - e(c_{n,\epsilon})\mathbb{1}\big)c_\epsilon\big\|_{F,\Omega}\ \|\mathcal{E}(u_\epsilon)\|_{F,\Omega} \\
&\leq \ \beta'\,\|\mathcal{E}(u_{n,\epsilon}) - e(c_{n,\epsilon})\mathbb{1}\|_{M,\Omega}\,\|c_\epsilon\|_\Omega\ \|\mathcal{E}(u_\epsilon)\|_{F,\Omega} \\
&\leq \ \frac{1}{2\delta}(\beta')^2\,\|\mathcal{E}(u_{n,\epsilon}) - e(c_{n,\epsilon})\mathbb{1}\|^2_{M,\Omega}\,\|c_\epsilon\|^2_\Omega + \frac{\delta}{2}\,\|\mathcal{E}(u_\epsilon)\|^2_{F,\Omega}\,.
\end{aligned} \tag{5.2.6}$$

For the boundary term, we obtain

$$\begin{aligned}
\langle g, u_\epsilon\rangle_{\Gamma_g} &\leq \|g\|_{H^{-1/2}(\Gamma_g)}\,\|u_\epsilon\|_{H^{1/2}(\Gamma_g)} \ \leq \ c_\gamma\ \|g\|_{H^{-1/2}(\Gamma_g)}\,\|u_\epsilon\|_{H^1(\Omega)} \\
&\leq \frac{c_\gamma}{2\delta}\,\|g\|^2_{H^{-1/2}(\Gamma_g)} + \frac{c_\gamma\delta}{2}\,\|u_\epsilon\|^2_{H^1(\Omega)}\,,
\end{aligned} \tag{5.2.7}$$

where $c_\gamma > 0$ is the constant from the trace inequality. Further, we have used Young's inequality. Combining now (5.2.4) – (5.2.7), we can absorb the terms with u_ϵ and $\mathcal{E}(u_\epsilon)$:

$$\begin{aligned}
&(\alpha - 2\delta)\,\|\mathcal{E}(u_\epsilon)\|^2_{F,\Omega} + (C\alpha - c_\gamma\delta)\,\|u_\epsilon\|^2_{H^1(\Omega)} \\
&\leq \ \frac{1}{\delta}\Big(\beta^2 N^2\,\|e'(c_{n,\epsilon})\|^2_{L^\infty(\Omega)} + (\beta')^2\,\|\mathcal{E}(u_{n,\epsilon}) - e(c_{n,\epsilon})\mathbb{1}\|^2_{M,\Omega}\Big)\,\|c_\epsilon\|^2_\Omega \\
&\quad + \frac{c_\gamma}{\delta}\,\|g\|^2_{H^{-1/2}(\Gamma_g)}\,.
\end{aligned} \tag{5.2.8}$$

Integration with respect to time from 0 to t, $t \in (0, T]$, and δ small enough, gives the following intermediate result:

$$\|\mathcal{E}(u_\epsilon)\|^2_{\Omega,t} + \|u_\epsilon\|^2_{H^1(\Omega),t} \leq C\,\|c_\epsilon\|^2_{\Omega,t} + C_1\,\|g\|^2_{H^{-1/2}(\Gamma_g),t}\,, \tag{5.2.9}$$

for some constants $C, C_1 > 0$, independent of ϵ. Hence, $\mathcal{E}(u_\epsilon)$ and u_ϵ are bounded in $L^2(S, [L^2(\Omega)]^{N\times N})$ and $\mathcal{W}(\Omega)$, respectively, if c_ϵ is bounded in $L^2(S, L^2(\Omega))$. To show this, we use c_ϵ as test function in (5.1.5) and integrate from 0 to t, $t \in (0, T]$:

$$\begin{aligned}
&\frac{1}{2}\,\|c_\epsilon(t)\|^2_\Omega - \frac{1}{2}\,\|c_\epsilon(0)\|^2_\Omega - \epsilon^2\big(f''(c_{n,\epsilon})c_\epsilon\,, \Delta c_\epsilon\big)_{\Omega,t} + \epsilon^4\lambda\,\|\Delta c_\epsilon\|^2_{\Omega,t} \\
&+ \epsilon^2\big(e'(c_{n,\epsilon})\,\mathrm{tr}(\mathcal{S}_\epsilon)\,, \Delta c_\epsilon\big)_{\Omega,t} + \epsilon^2\big(e''(c_{n,\epsilon})c_\epsilon\,\mathrm{tr}(\mathcal{S}_{n,\epsilon})\,, \Delta c_\epsilon\big)_{\Omega,t} \\
&- \epsilon^2\big((\mathcal{E}(u_{n,\epsilon}) - e(c_{n,\epsilon})\mathbb{1}) : \mathcal{A}'(c_{n,\epsilon})(\mathcal{E}(u_\epsilon) - e'(c_{n,\epsilon})c_\epsilon\mathbb{1})\,, \Delta c_\epsilon\big)_{\Omega,t} \\
&- \epsilon^2\frac{1}{2}\big((\mathcal{E}(u_{n,\epsilon}) - e(c_{n,\epsilon})\mathbb{1}) : \mathcal{A}''(c_{n,\epsilon})c_\epsilon\,(\mathcal{E}(u_{n,\epsilon}) - e(c_{n,\epsilon})\mathbb{1})\,, \Delta c_\epsilon\big)_{\Omega,t} = 0.
\end{aligned} \tag{5.2.10}$$

Rearranging terms yields

$$\begin{aligned}
&\frac{1}{2}\|c_\epsilon\|_\Omega^2 + \epsilon^4\lambda\|\Delta c_\epsilon\|_{\Omega,t}^2 \\
&= \frac{1}{2}\|c_\epsilon(0)\|_\Omega^2 + \epsilon^2\big(f''(c_{n,\epsilon})c_\epsilon\,,\Delta c_\epsilon\big)_{\Omega,t} \\
&\quad - \epsilon^2\big(e'(c_{n,\epsilon})\operatorname{tr}(\mathcal{S}_\epsilon)\,,\Delta c_\epsilon\big)_{\Omega,t} - \epsilon^2\big(e''(c_{n,\epsilon})c_\epsilon\operatorname{tr}(\mathcal{S}_{n,\epsilon})\,,\Delta c_\epsilon\big)_{\Omega,t} \\
&\quad + \epsilon^2\big((\mathcal{E}(u_{n,\epsilon}) - e(c_{n,\epsilon})\mathbb{1}) : \mathcal{A}'(c_{n,\epsilon})(\mathcal{E}(u_\epsilon) - e'(c_{n,\epsilon})c_\epsilon\mathbb{1})\,,\Delta c_\epsilon\big)_{\Omega,t} \\
&\quad + \epsilon^2\frac{1}{2}\big((\mathcal{E}(u_{n,\epsilon}) - e(c_{n,\epsilon})\mathbb{1}) : \mathcal{A}''(c_{n,\epsilon})c_\epsilon\,(\mathcal{E}(u_{n,\epsilon}) - e(c_{n,\epsilon})\mathbb{1})\,,\Delta c_\epsilon\big)_{\Omega,t}.
\end{aligned} \tag{5.2.11}$$

We estimate the scalar product terms on the right-hand side of (5.2.11) successively, using Hölder's and Young's inequalities. The first one gives

$$\epsilon^2\big(f''(c_{n,\epsilon})c_\epsilon\,,\Delta c_\epsilon\big)_{\Omega,t} \le \frac{1}{2\delta}\|f''(c_{n,\epsilon})\|_{L^\infty(\Omega),t}^2\|c_\epsilon\|_{\Omega,t}^2 + \frac{\delta}{2}\epsilon^4\|\Delta c_\epsilon\|_{\Omega,t}^2\,. \tag{5.2.12}$$

Similar to (5.1.10), we treat the terms including the traces of the stress tensors. With (5.1.9) and Young's inequality, we get

$$\begin{aligned}
\epsilon^2\big(e'(c_{n,\epsilon})\operatorname{tr}(\mathcal{S}_\epsilon)\,,\Delta c_\epsilon\big)_{\Omega,t} &\le \epsilon^2\|e'(c_{n,\epsilon})\mathcal{S}_\epsilon\|_{F,\Omega,t}\,\|\mathbb{1}\Delta c_\epsilon\|_{F,\Omega,t} \\
&\le \frac{1}{2\delta}\|e'(c_{n,\epsilon})\|_{\infty,t}^2\|\mathcal{S}_\epsilon\|_{F,\Omega,t}^2 + \epsilon^4\frac{\delta}{2}N\|\Delta c_\epsilon\|_{\Omega,t}^2 \\
&\le \frac{1}{2\delta}C\big(\|\mathcal{E}(u_\epsilon)\|_{\Omega,t}^2 + \|c_\epsilon\|_{\Omega,t}^2\big) + \epsilon^4\frac{\delta}{2}N\|\Delta c_\epsilon\|_{\Omega,t}^2
\end{aligned} \tag{5.2.13}$$

and

$$\begin{aligned}
\epsilon^2\big(e''(c_{n,\epsilon})c_\epsilon\operatorname{tr}(\mathcal{S}_{n,\epsilon})\,,\Delta c_\epsilon\big)_{\Omega,t} &\le \epsilon^2\|e''(c_{n,\epsilon})c_\epsilon\mathcal{S}_{n,\epsilon}\|_{F,\Omega,t}\,\|\mathbb{1}\Delta c_\epsilon\|_{F,\Omega,t} \\
&\le \frac{2}{\delta}\|e''(c_{n,\epsilon})\|_{L^\infty(\Omega),t}^2\|c_\epsilon\|_{\Omega,t}^2\|\mathcal{S}_{n,\epsilon}\|_{M,\Omega,t}^2 + \epsilon^4\frac{\delta}{2}N\|\Delta c_\epsilon\|_{\Omega,t}^2\,.
\end{aligned}$$

For the last two terms from the right-hand side of (5.2.11) we obtain

$$\begin{aligned}
&\epsilon^2\big((\mathcal{E}(u_{n,\epsilon}) - e(c_{n,\epsilon})\mathbb{1}) : \mathcal{A}'(c_{n,\epsilon})(\mathcal{E}(u_\epsilon) - e'(c_{n,\epsilon})c_\epsilon\mathbb{1})\,,\Delta c_\epsilon\big)_{\Omega,t} \\
&\quad\le \|\mathcal{E}(u_{n,\epsilon}) - e(c_{n,\epsilon})\mathbb{1}\|_{M,\Omega,t}\,\beta'\big(\|\mathcal{E}(u_\epsilon)\|_{F,\Omega,t} + N\|e'(c_{n,\epsilon})\|_{L^\infty(\Omega),t}\|c_\epsilon\|_{\Omega,t}\big)\epsilon^2\|\Delta c_\epsilon\|_{\Omega,t} \\
&\quad\le \frac{1}{2\delta}\|\mathcal{E}(u_{n,\epsilon}) - e(c_{n,\epsilon})\mathbb{1}\|_{M,\Omega,t}^2(\beta')^2\,2\big(\|\mathcal{E}(u_\epsilon)\|_{\Omega,t}^2 + N^2\|e'(c_{n,\epsilon})\|_{L^\infty(\Omega),t}^2\|c_\epsilon\|_{\Omega,t}^2\big) \\
&\qquad + \frac{\delta}{2}\epsilon^4\|\Delta c_\epsilon\|_{\Omega,t}^2
\end{aligned}$$

and

$$\epsilon^2 \frac{1}{2}\big((\mathcal{E}(u_{n,\epsilon}) - e(c_{n,\epsilon})\mathbb{1}) : \mathcal{A}''(c_{n,\epsilon})c_\epsilon\,(\mathcal{E}(u_{n,\epsilon}) - e(c_{n,\epsilon})\mathbb{1}), \Delta c_\epsilon\big)_{\Omega,t}$$
$$\leq \frac{1}{2\delta}(\beta'')^2 \|c_\epsilon\|^2_{\Omega,t} \|(\mathcal{E}(u_{n,\epsilon}) - e(c_{n,\epsilon})\mathbb{1})\|^4_{M,\Omega,t} + \frac{1}{4}\frac{\delta}{2}\epsilon^4 \|\Delta c_\epsilon\|^2_{\Omega,t}\,.$$

Now we can absorb the $\epsilon^4 \|\Delta c_\epsilon\|_{\Omega,t}$-terms and get

$$\begin{aligned}
&\frac{1}{2}\|c_\epsilon(t)\|^2_\Omega + (\lambda - (9/8+N)\delta)\left\|\epsilon^2\Delta c_\epsilon\right\|^2_{\Omega,t} \\
&\quad\leq \frac{1}{2}\|c_\epsilon(0)\|^2_\Omega + \frac{2}{\delta}\|f''(c_{n,\epsilon})\|^2_{L^\infty(\Omega),t}\|c_\epsilon\|^2_{\Omega,t} \\
&\qquad + \frac{2}{\delta}\|e'(c_{n,\epsilon})\|^2_{L^\infty(\Omega),t}\Big(2\beta^2\big(\|\mathcal{E}(u_\epsilon)\|^2_{\Omega,t} + N^2\|e'(c_{n,\epsilon}\|^2_{L^\infty(\Omega),t}\|c_\epsilon\|^2_{\Omega,t}\big) \\
&\qquad\qquad + (\beta')^2\|\mathcal{E}(u_{n,\epsilon}) - e(c_{n,\epsilon})\mathbb{1}\|^2_{M,\Omega,t}\|c_\epsilon\|^2_{\Omega,t}\Big) \qquad (5.2.14)\\
&\qquad + \frac{2}{\delta}\|e''(c_{n,\epsilon})\|^2_{L^\infty(\Omega),t}\|c_\epsilon\|^2_{\Omega,t}\|\mathcal{S}_{n,\epsilon}\|^2_{M,\Omega,t} \\
&\qquad + \frac{1}{2\delta}\|\mathcal{E}(u_{n,\epsilon}) - e(c_{n,\epsilon})\mathbb{1}\|^2_{M,\Omega,t}\,2(\beta')^2\big(\|\mathcal{E}(u_\epsilon)\|^2_{\Omega,t} + \|e'(c_{n,\epsilon})\|^2_{L^\infty(\Omega),t}N^2\|c_\epsilon\|^2_{\Omega,t}\big) \\
&\qquad + \frac{1}{4\delta}(\beta'')^2\|c_\epsilon\|^2_{\Omega,t}\|(\mathcal{E}(u_{n,\epsilon}) - e(c_{n,\epsilon})\mathbb{1})\|^4_{M,\Omega,t}\,.
\end{aligned}$$

For δ small enough, the left-hand side of (5.2.14) is positive and with the estimate (5.2.9) for $\|\mathcal{E}(u_\epsilon)\|^2_{\Omega,t}$ we get

$$\|c_\epsilon(t)\|^2_\Omega + \left\|\epsilon^2\Delta c_\epsilon\right\|^2_{\Omega,t} \leq C\|c_\epsilon\|^2_{\Omega,t} + \tilde{C}\left(\|c_\epsilon(0)\|^2_\Omega + \|g\|^2_{H^{-1/2}(\Gamma_g),t}\right) \qquad (5.2.15)$$

for some constants $C, \tilde{C} > 0$, which do not depend on ϵ. Now, we can now apply Gronwall's inequality and receive

$$\|c_\epsilon(t)\|^2_\Omega + \left\|\epsilon^2\Delta c_\epsilon\right\|^2_{\Omega,t} \leq C\left(\left\|c^{\text{in}}\right\|^2_\Omega + \|g\|^2_{H^{-1/2}(\Gamma_g),t}\right) \qquad (5.2.16)$$

for a constant $C > 0$ independent of ϵ. Due to the regularity assumptions on g and the initial data c^{in}, the right-hand side is bounded.

Since $c_\epsilon(t)$ and $\epsilon^2\Delta c_\epsilon(t)$ are bounded in $L^2(\Omega)$ for a.e. $t \in S$, the scaled gradient $\epsilon\nabla c_\epsilon(t)$ is bounded in $[L^2(\Omega)]^N$, for a.e. $t \in S$, since

$$-\int_\Omega c_\epsilon\,\epsilon^2\Delta c_\epsilon\,dx=\int_\Omega \epsilon^2\,(\nabla c_\epsilon)^2\,dx-\int_{\partial\Omega} c_\epsilon\,\epsilon^2\,\nabla c_\epsilon\cdot n\,d\sigma=\int_\Omega(\epsilon\nabla c_\epsilon)^2\,dx=\|\epsilon\nabla c_\epsilon\|_\Omega^2\geq 0, \tag{5.2.17}$$

whereby the boundary integral vanishes because of the no-flux condition $\nabla c_\epsilon\cdot n=0$ on $\partial\Omega$. With

$$|\int_\Omega c_\epsilon\,\epsilon^2\Delta c_\epsilon\,dx|\;\leq\;\|c_\epsilon\|_\Omega\,\left\|\epsilon^2\Delta c_\epsilon\right\|_\Omega\leq C, \tag{5.2.18}$$

it follows

$$\|\epsilon\nabla c_\epsilon\|_\Omega\leq\|c_\epsilon\|_\Omega\,\left\|\epsilon^2\Delta c_\epsilon\right\|_\Omega. \tag{5.2.19}$$

Integration with respect to time then gives the desired result. Estimates (5.2.9) and (5.2.16) now finally yield the boundedness of u_ϵ in $\mathcal{W}(\Omega)$,

$$\|u_\epsilon\|_{H^1(\Omega),t}^2\leq C\left(\|c_\epsilon(0)\|_\Omega^2+\|g\|_{H^{-1/2}(\Gamma_g),t}^2\right). \tag{5.2.20}$$

Alltogether we finally obtain

$$\|c_\epsilon\|_\Omega^2+\|\epsilon\nabla c_\epsilon\|_{\Omega,t}^2+\left\|\epsilon^2\Delta c_\epsilon\right\|_{\Omega,t}^2 \tag{5.2.21}$$

$$+\|\mathcal{E}(u_\epsilon)\|_{\Omega,t}^2+\|u_\epsilon\|_{H^1(\Omega),t}^2\leq C\left(\left\|c^{\mathrm{in}}\right\|_\Omega^2+\|g\|_{H^{-1/2}(\Gamma_g),t}^2\right) \tag{5.2.22}$$

for a constant $C>0$, which does not dependent on ϵ. □

Remark 5.2.7 (Equivalence of norms)**.**
In $V(\Omega)\subset H^2(\Omega)$ the norm $\|\cdot\|_{V(\Omega)}$ is equivalent to the standard norm on $H^2(\Omega)$,

$$\|v\|_{H^2(\Omega)}=\left(\|v\|_\Omega^2+\|\nabla v\|_\Omega^2+\|\Delta v\|_\Omega^2\right)^{1/2},\quad v\in H^2(\Omega),$$

since

$$\|v\|_{V(\Omega)}^2\leq\|v\|_{H^2(\Omega)}^2\leq c\,\|v\|_{V(\Omega)}^2, \tag{5.2.23}$$

with $c>0$. The first inequality in (5.2.23) *is obvious, the second one can be achieved by using* (5.2.19) *and Young's inequality.*

5.3 Existence of a weak solution

In this subsection we want to show the existence and uniqueness of a weak solution of the considered linear system. The proof is provided by a Galerkin approximation. Since the finite-dimensional system that is created in the course of this represents a linear differential–algebaic equation (DAE), we will first introduce some aspects of general theory about solvability of linear DAEs in a weak setting.

5.3.1 Existence of weak solutions of linear DAEs

In many applications, it occurs that partial differential equations must satisfy certain constraints and one has to deal with coupled systems, as for example in fluid dynamics or continuum mechanics. Think of the Navier–Stokes equation, for example, which is considered for the mathematical description of incompressible fluids under the constraint of a divergence-free velocity field. A semidiscretisation in space, in the course of numerical considerations or a proof of existence, then leads to a system of equations, which can be interpreted as a DAE in a weak functional analytical setting. Since the examined linear Cahn–Larché system represents a coupled system of partial differential equations of elliptic and parabolic type, we use the framework of linear differential–algebraic equations in a weak setting to proof the existence of a solution of the corresponding Galerkin equations.

We consider now differential–algebraic equations of the form

$$A(t)(D(t)u(t))' + B(t)u(t) = q(t), \tag{5.3.1}$$

with continuous matrices

$$A \in C([t_0, T], \mathbb{R}^{n\times m}), \quad D \in C([t_0, T], \mathbb{R}^{m\times n}), \quad B \in C([t_0, T], \mathbb{R}^{n\times n})$$

and a right-hand side $q \in L^2((t_0, T), \mathbb{R}^n)$. The matrix D specifies the differentiable part of u.

In [Tis03], the author studies coupled systems of partial differential and differential–algebraic equations in Hilbert spaces, so-called abstract differential–algebraic systems. Among other things, the unique solvability of such a system was proven there by use of a Galerkin method. In the following, we summarise some results of the theory of linear differential–algebraic equations concerning existence and uniqueness of solutions of linear DAEs of the form (5.3.1) according to [Tis03], which we refer to. The concept is based on decoupling the DAE into a dynamic part, which represents an ordinary differential equation and an algebraic part. The first definition tells us when the matrices $A(t)$ and $D(t)$ are well matched in a certain way. This is important when decoupling a system as stated above into a dynamic and an algebraic part.

Definition 5.3.1 (Properly stated leading term)**.**
A DAE of the form (5.3.1) *is said to have a properly stated leading term if*

(i) the coefficient matrices $A(t)$ *and* $D(t)$ *fulfil*

$$\ker A(t) \oplus \operatorname{im} D(t) = \mathbb{R}^m \tag{5.3.2}$$

for all $t \in [t_0, T]$ *and*

(ii) there exists a continuously differentiable projector

$$R\colon [t_0, T] \to L(\mathbb{R}^m, \mathbb{R}^m)$$

such that

$$\operatorname{im} R(t) = \operatorname{im} D(t), \quad \ker R(t) = \ker A(t), \tag{5.3.3}$$

for all $t \in [t_0, T]$.

Remark 5.3.2. *The projector function* $R(t)$ *from the definition above realises the decomposition* (5.3.2)*. It holds*

$$\begin{aligned} \operatorname{im} A(t)D(t) &= \operatorname{im} A(t)R(t) = \operatorname{im} A(t), \\ \ker A(t)D(t) &= \ker R(t)D(t) = \ker D(t). \end{aligned}$$

Moreover, on the subspace $\operatorname{im} D(t)$ *the projector acts like the identity, i.e.*

$$R(t)D(t)x = D(t)x, \quad x \in \mathbb{R}^n, \tag{5.3.4}$$

and further, it holds that

$$A(t)R(t)x = A(t)x, \quad x \in \mathbb{R}^m, \tag{5.3.5}$$

since $0 = A(t)x_k = A(t)R(t)x_k$ *for all* $x_k \in \ker A(t) = \ker R(t)$ *and* $A(t)R(t)x_i = A(t)x_i$ *for all* $x_i \in \operatorname{im} D(t)$ *due to* (5.3.4)*.*

Next, we present a index concept for the considered linear DAE. Laxly spoken, the index of a DAE indicates how much it differs from an ordinary differential equation. Following [Tis03], we introduce a projector-based index, which is compatible when working in a weak setting. As we will see later, the decoupling of the linear DAE, which is based on this index concept, is based on the decomposition of $\mathbb{R}^n$ realised by projectors. For the sake of notational simplicity, from now on we drop the time argument t from the matrices.

Definition 5.3.3 (Index, [Mär02])**.**
A DAE of the form (5.3.1) *with properly stated leading term has the index* $\mu \in \mathbb{N}$ *if there exists a continuous matrix-valued function sequence* $(G_i)_{i\geq 0}$ *and a continuous projector sequence* $(Q_i)_{i\geq 0}$ *such that*

(i) Q_i *is a projector onto* $\ker G_i$ *for all* $t \in [t_0, T]$ *and* $i \geq 0$,

(ii) G_i *has constant rank* $r_i > 0$ *on* $[t_0, T]$ *and all* $i \geq 0$,

(iii) $r_{\mu-1} < r_\mu = n$,

(iv) $Q_i\, Q_j = 0$, *for* $0 \leq j \leq i-1$, $i > 0$, $t \in [t_0, T]$,

(v) $D\, P_0 \dots P_i\, D^- \in C^1([t_0, T], L(\mathbb{R}^m, \mathbb{R}^m))$,

with

$$\begin{aligned} G_0 &= AD \quad \text{and} \quad G_{i+1} = G_i + B_i Q_i, \\ B_0 &= B \quad \text{and} \quad B_{i+1} = B_i P_i - G_{i+1} D^- (D\, P_0 \dots P_i\, D^-)' D\, P_0 \dots P_i, \\ P_i &= I - Q_i, \end{aligned}$$

for $i \geq 0$. *Here,* D^- *denotes the reflexive generalised inverse of* D, *i.e.*

$$D^- D D^- = D^-, \quad D D^- D = D$$

such that

$$D D^- = R, \quad D^- D = P_0, \tag{5.3.6}$$

where R *is the projector from definition 5.3.1.*

Remark 5.3.4. *For any matrix* $M \in \mathbb{R}^{m\times n}$ *with a reflexive generalised inverse* $M^- \in \mathbb{R}^{n\times m}$, *the matrices* MM^- *and* M^-M *are projectors, since*

$$(MM^-)^2 = MM^-MM^- = MM^- \quad \text{and} \quad (M^-M)^2 = M^-MM^-M = M^-M.$$

Uniqueness of the reflexive generalised inverse can be achieved by setting the products MM^- *and* M^-M *equal to certain projectors. Hence, by the identities* (5.3.6), *the reflexive generalised inverse* D^- *from the definition above is uniquely determined [Dok11].*

Now we can state the existence result we want to work with.

Theorem 5.3.5 (Existence of a unique solution, [Tis03])**.**
An initial value problem of the form

$$A(t)(D(t)x(t))' + B(t)x(t) = q(t), \tag{5.3.7}$$

$$D(t_0)x(t_0) = z_0 \in \operatorname{im} D(t_0), \tag{5.3.8}$$

with $q \in L^2((t_0,T),\mathbb{R}^n)$ and index $\mu = 1$ has a unique solution $x \in L^2((t_0,T),\mathbb{R}^n)$ such that $Dx \in C([t_0,T],\mathbb{R}^m)$ and Dx is differentiable for almost all $t \in [t_0,T]$. The equation (5.3.7) holds for almost all $t \in [t_0,T]$ and there exists a constant $C > 0$ such that

$$\|x\|_{L^2((t_0,T),\mathbb{R}^n)} + \|Dx\|_{C([t_0,T],\mathbb{R})} + \|(Dx)'\|_{L^2((t_0,T),\mathbb{R}^m)} \leq C\big(\|z_0\| + \|q\|_{L^2((t_0,T),\mathbb{R}^n)}\big). \tag{5.3.9}$$

Here, for the first time, the initial-value condition appears and with it the requirement, $z_0 \in \operatorname{im} D(t_0)$, to get a well-defined problem. We proof the existence result following the ideas of [Tis03]. For the decoupling of the DAE into its dynamic and its algebraic part we refer to [Dok11].

Proof. Due to the index 1 property of (5.3.7), the matrix

$$G_1 = AD + BQ_0$$

has constant rank for all $t \in [t_0,T]$ and, hence, its inverse G_1^{-1} exists. For any $x \in \mathbb{R}^m$, it holds that

$$\begin{aligned} G_1P_0x =& (AD + BQ_0)\,P_0x = (AD + BQ_0)\,(I - Q_0)\,x \\ =& ADx + BQ_0x - ADQ_0x - BQ_0^2x = ADx, \end{aligned} \tag{5.3.10}$$

since Q_0 is a projection onto $\ker AD = \ker D$ and thus $ADQ_0x = 0$ and $Q_0^2 = Q_0$. With (5.3.5) and (5.3.10), we write the leading term of (5.3.7) as follows

$$A(Dx)' = AR(Dx)' = ADD^-(Dx)' = G_1P_0D^-(Dx)'. \tag{5.3.11}$$

Next, we write

$$Bx = BIx = BP_0x + BQ_0x = BP_0x + (AD + BQ_0)\,Q_0x = BP_0x + G_1Q_0x, \tag{5.3.12}$$

for any $x \in \mathbb{R}^m$, since Q_0 is a projection onto $\ker AD$. Hence, using (5.3.11) and (5.3.12), we write the DAE (5.3.7) as

$$G_1P_0D^-(Dx)' + BP_0x + G_1Q_0x = q. \tag{5.3.13}$$

Multiplying (5.3.13) by G_1^{-1} from the left, we obtain

$$P_0 D^-(Dx)' + G_1^{-1} B P_0 x + Q_0 x = G_1^{-1} q. \tag{5.3.14}$$

Now, we multiply (5.3.14) with D from the left and get

$$D P_0 D^-(Dx)' + D G_1^{-1} B P_0 x = D G_1^{-1} q \tag{5.3.15}$$

since Q_0 is a projection onto $\ker D$. Due to the identities $P_0 = D^- D$ and $R = DD^-$, we get $DP_0D^- = DD^-DD^- = R^2 = R$, and equation (5.3.15) becomes

$$R(Dx)' + D G_1^{-1} B D^- Dx = D G_1^{-1} q. \tag{5.3.16}$$

Using $(Dx)' = (RDx)' = R'Dx + R(Dx)'$, from (5.3.16) it follows

$$(Dx)' - R'Dx + D G_1^{-1} B D^- Dx = D G_1^{-1} q. \tag{5.3.17}$$

We consider again equation (5.3.14) and multiply it now with Q_0 from the left and get

$$Q_0 P_0 D^-(Dx)' + Q_0 G_1^{-1} B D^- Dx + Q_0 x = Q_0 G_1^{-1} q. \tag{5.3.18}$$

Since $Q_0 P_0 = Q_0(I - Q_0) = 0$, we obtain

$$Q_0 x + Q_0 G_1^{-1} B D^- Dx = Q_0 G_1^{-1} q. \tag{5.3.19}$$

With this, we have split the DAE (5.3.7) into a dynamic part (5.3.17) and an algebraic part (5.3.19).

Equation (5.3.17), together with the initial condition (5.3.8), represents an ordinary differential equation for $y \coloneqq Dx$ of the form

$$\begin{aligned} y'(t) &= My(t) + b, \quad t \in (t_0, T), \\ y(t_0) &= y_0, \end{aligned} \tag{5.3.20}$$

with $M = R' + DG_1^{-1}BD^-$, $M \in C([t_0, T], \mathbb{R}^{m\times m})$ and $b = DG_1^{-1}q$, $b \in L^2((t_0, T), \mathbb{R}^m)$.

The above system satisfies the Carathéodory conditions, the map $x \mapsto Mx$ is Lipschitz-continuous and we can apply the existence theory of Carathéodory. Therefore, the initial-value problem (5.3.20) has a unique solution $y \in C([t_0, T], \mathbb{R}^m)$ with $y' \in L^2((t_0, T), \mathbb{R}^m)$ such that

$$y(t) = y(t_0) + \int_{t_0}^{T} y'(\tau)\,\mathrm{d}\tau.$$

Furthermore, there exists a constant $C > 0$, such that

$$\|y\|_{C([t_0,T],\mathbb{R}^m)} + \|y'\|_{L^2((t_0,T),\mathbb{R}^m)} \leq C\left(\|y_0\| + \|b\|_{L^2((t_0,T),\mathbb{R}^m)}\right). \tag{5.3.21}$$

Considering the algebraic part, due to the identities $I = Q_0 + P_0$ and $P_0 = D^- D$, from (5.3.19) we obtain a representation of a solution of the initial-value problem (5.3.7), (5.3.8), namely

$$x(t) = D^- y(t) - (Q_0 G_1^{-1} B D^-) y(t) + Q_0 G_1^{-1} q(t), \tag{5.3.22}$$

where y ist the unique solution of (5.3.20). All matrices appearing here are continuous on $[t_0, T]$ and, since $q \in L^2((t_0,T),\mathbb{R}^n)$, we deduce $x \in L^2((t_0,T),\mathbb{R}^n)$. Further, the estimate (5.3.9) follows directly from the representation (5.3.22) of x and the estimate (5.3.21). □

5.3.2 Existence of weak solutions of the linear Cahn–Larché system

To proof the existence of a weak solution of the scaled linear Cahn–Larché system, we consider the system in a form, where we separate the influence of the unknowns c_ϵ and u_ϵ in both equations. Therefore we write the equations (5.1.5), (5.1.6) in the following form:

$$\big(\partial_t c_\epsilon\,,\varphi\big)_\Omega + a_{\mathrm{ch}}(c_\epsilon\,,\varphi) + b_{\mathrm{ch}}(u_\epsilon\,,\varphi) = 0, \tag{5.3.23}$$

$$a_{\mathrm{m}}(c_\epsilon\,,\psi) + b_{\mathrm{m}}(u_\epsilon\,,\psi) = \langle g,\psi\rangle_{\Gamma_{\mathrm{g}}}, \tag{5.3.24}$$

$$c_\epsilon(\,\cdot\,,0) = c^{\mathrm{in}}, \tag{5.3.25}$$

with

$$\begin{aligned} a_{\mathrm{ch}}(v\,,\varphi) \coloneqq & -\epsilon^2\big(f''v\,,\Delta\varphi\big)_\Omega + \epsilon^4\lambda\big(\Delta v\,,\Delta\varphi\big)_\Omega \\ & - \epsilon^2\big(v\,e'\,\mathrm{tr}[\mathcal{A}e'\mathbb{1} - \mathcal{A}'(\mathcal{E}(u_{n,\epsilon}) - e(c_{n,\epsilon})\mathbb{1})]\,,\Delta\varphi\big)_\Omega \\ & + \epsilon^2\big(v\,e''\,\mathrm{tr}\,\mathcal{S}_{n,\epsilon}\,,\Delta\varphi\big)_\Omega + \epsilon^2\big((\mathcal{E}(u_{n,\epsilon}) - e(c_{n,\epsilon})\mathbb{1}) : \mathcal{A}'\mathbb{1}e'v\,,\Delta\varphi\big)_\Omega \\ & - \frac{1}{2}\epsilon^2\big((\mathcal{E}(u_{n,\epsilon}) - e(c_{n,\epsilon})\mathbb{1}) : \mathcal{A}''v\,(\mathcal{E}(u_{n,\epsilon}) - e(c_{n,\epsilon})\mathbb{1})\,,\Delta\varphi\big)_\Omega, \end{aligned} \tag{5.3.26}$$

$$b_{\mathrm{ch}}(w\,,\varphi) \coloneqq \epsilon^2\big(e'\,\mathrm{tr}[\mathcal{A}\,\mathcal{E}(w)],\,\Delta\varphi\big)_\Omega - \epsilon^2\big((\mathcal{E}(u_{n,\epsilon}) - e(c_{n,\epsilon})\mathbb{1}) : \mathcal{A}'\mathcal{E}(w),\,\Delta\varphi\big)_\Omega, \tag{5.3.27}$$

$$a_{\mathrm{m}}(v\,,\psi) \coloneqq -\big(\mathcal{A}\,e'v\mathbb{1}\,,\mathcal{E}(\psi)\big)_{F,\Omega} + \big(\mathcal{A}'\,v\,(\mathcal{E}(u_{n,\epsilon}) - e(c_{n,\epsilon})\mathbb{1})\,,\mathcal{E}(\psi)\big)_{F,\Omega}, \tag{5.3.28}$$

$$b_{\mathrm{m}}(w\,,\psi) \coloneqq \big(\mathcal{A}\,\mathcal{E}(w)\,,\mathcal{E}(\psi)\big)_{F,\Omega}, \tag{5.3.29}$$

for $v \in \mathcal{V}(\Omega)$, $w \in \mathcal{W}(\Omega)$ and $\varphi \in V(\Omega)$, $\psi \in W(\Omega)$. Here we have used the abbreviation $f'' \coloneqq f''(c_{n,\epsilon})$ and $\mathcal{A} \coloneqq \mathcal{A}(c_{n,\epsilon})$ and analogously to this, $\mathcal{A}'$ and $\mathcal{A}''$ as well as e, e' and e''.

In addition to the assumption of regularity to the nonlinear solutions, (5.1.1), we now further

require continuity with respect to time.

Theorem 5.3.6. *For every fixed $\epsilon > 0$, there exists a unique weak solution*

$$(c_\epsilon, u_\epsilon) \in \left(L^\infty(S, L^2(\Omega)) \cap L^2(S, V(\Omega))\right) \times L^2(S, W(\Omega))$$

of (5.1.5), (5.1.6), *with* $\partial_t c_\epsilon \in L^2(0, T; V(\Omega)')$.

In the following, we proof this result in four steps using a Galerkin approach and the theory on linear differential–algebraic equations in a weak setting introduced in the previous part of this chapter.

Step 1: Galerkin equations

We consider the finite dimensional spaces $V_n \subset V$ and $W_m \subset W$, each spanned by linearly independent functions v_i, $1 \le i \le n$, and w_j, $1 \le j \le m$, i.e.

$$V_n = \operatorname{span}\{v_1, \dots, v_n\} \quad \text{and} \quad W_m = \operatorname{span}\{w_1, \dots, w_m\}$$

such that $\bigcup_{i\in\mathbb{N}} V_i$ and $\bigcup_{j\in\mathbb{N}} W_j$ are dense in V and W, respectively. Further, we choose a sequence c_n^{in} in V_n, which converges strongly to c^{in} in $L^2(\Omega)$. Then, we consider the following basis representations

$$c_n : [0, T] \to V_n, \quad c_n(t) = \sum_{i=1}^{n} c_{ni}(t)\, v_i, \tag{5.3.30}$$

and

$$u_m : [0, T] \to W_m, \quad u_m(t) = \sum_{j=1}^{m} u_{mj}(t)\, w_j, \tag{5.3.31}$$

with $v_i \in V_n$, $w_j \in W_m$ for $i \in \{1, \dots, N\}$, $j \in \{1, \dots, M\}$ and coefficient functions c_{ni} and u_{mj}, $1 \le i \le n, 1 \le j \le m$, to be determined. Using these representations, we consider now the Galerkin approximation of the system (5.3.23), (5.3.24),

$$\begin{aligned} (c_n'(t)\,, v)_\Omega + a_{\mathrm{ch}}(c_n(t)\,, v) + b_{\mathrm{ch}}(u_m(t)\,, v) &= 0, \\ a_{\mathrm{m}}(c_n(t)\,, w) + b_{\mathrm{m}}(u_m(t)\,, w) &= \langle g\,, w\rangle_{\Gamma_{\mathrm{g}}}, \end{aligned} \tag{5.3.32}$$

which holds for every $v \in V_n, w \in W_m$ and

$$c_n(0) = c_n^{\mathrm{in}} \tag{5.3.33}$$

with

$$(c_n^{\mathrm{in}}\,, v)_\Omega = (c^{\mathrm{in}}\,, v)_\Omega$$

for all $v \in V_n$. Let

$$c_n^{\mathrm{in}} = \sum_{i=1}^{n} \alpha_{ni} v_i.$$

An equivalent formulation to this is

$$\begin{aligned} \sum_{i=1}^{n} c_{ni}'(t)\big(v_i\,, v_k\big)_\Omega + \sum_{i=1}^{n} c_{ni}(t)\, a_{\mathrm{ch}}(v_i\,, v_k) + \sum_{j=1}^{m} u_{mj}(t)\, b_{\mathrm{ch}}(w_j\,, v_k) = 0, \\ \sum_{i=1}^{n} c_{ni}(t)\, a_{\mathrm{m}}(v_i\,, w_l) + \sum_{j=1}^{m} u_{mj}(t)\, b_{\mathrm{m}}(w_j\,, w_l) = \langle g\,, w_l\rangle_{\Gamma_{\mathrm{g}}}, \end{aligned} \tag{5.3.34}$$

for $1 \le k \le n$, $1 \le l \le m$ and

$$c_{ni}(0) = \alpha_{ni}, \tag{5.3.35}$$

for $1 \le i \le n$.

Proposition 5.3.7. *The Galerkin equations* (5.3.32), (5.3.33) *have a unique solution* (c_n, u_m),

$$c_n \colon [0,T] \to V_n, \quad u_m \colon [0,T] \to W_m,$$

with

$$c_n' \in L^2(S, V_n) \quad \text{and} \quad c_n(t) = c_n^{\mathrm{in}} + \int_0^T c_n'(s)\,\mathrm{d}s. \tag{5.3.36}$$

Proof. The system (5.3.34), (5.3.35) represents a linear differential–algebraic equation of the form (5.3.7) with an initial condition (5.3.8). According to the previously presented theory about linear DAEs, there exists a unique solution, if the differential–algebraic equation has a properly stated leading term and if it has index 1. To show this, we first identify the setting and write the Galerkin equations in the form of an initial-value differential–algebraic system:

$$A(t)(D(t)x(t))' + B(t)x(t) = q(t), \tag{5.3.37}$$

$$D(0)\,x(0) = z_0, \tag{5.3.38}$$

with

$$x \in \mathbb{R}^{n+m}, \quad q \in \mathbb{R}^{n+m},$$

and

$$\begin{aligned} A &\in C\big([0,T],\mathbb{R}^{(n+m)\times n)}\big),\\ D &\in C\big([0,T],\mathbb{R}^{n\times(n+m)}\big),\\ B &\in C\big([0,T],\mathbb{R}^{(n+m)\times(n+m)}\big). \end{aligned}$$

We identify

$$x \coloneqq (c_{n1}(t),\dots,c_{nn}(t),u_{m1}(t),\dots,u_{mm}(t))^{\mathrm{T}} \in \mathbb{R}^{n+m},$$

and the right-hand side

$$q \coloneqq (0,\dots 0,q_1(t),\dots,q_m(t))^{\mathrm{T}} \in \mathbb{R}^{n+m},$$

where the non-zero components are defined by

$$q_l \coloneqq \langle g\,,w_l\rangle_{\Gamma_{\mathrm{g}}}, \quad \text{for } 1\le l\le m.$$

We further identify the matrices

$$A = \left(\begin{array}{c} \big((v_j\,,v_i)_\Omega\big)_{1\le i,j\le n} \\ \hline 0_{m\times n} \end{array}\right)$$

and

$$D = \left(\begin{array}{c|c} I_n & 0_{n\times m} \end{array}\right),$$

both constant and with $I_n \in \mathbb{R}^{n\times n}$ being the identity matrix and $0_{n\times m} \in \mathbb{R}^{n\times m}$ a matrix only having entries equal to zero. The matrix B corresponds to the elliptic part of the equations and is given by

$$B = \left(\begin{array}{c|c} (a_{ij}^{\mathrm{ch}})_{1\le i,j\le n} & (b_{ij}^{\mathrm{ch}})_{1\le i\le n,1\le j\le m} \\ \hline (a_{ij}^{\mathrm{m}})_{1\le i\le m,1\le j\le n} & (b_{ij}^{\mathrm{m}})_{1\le i,j\le m} \end{array}\right),$$

with $a_{ij}^{\mathrm{ch}} \coloneqq a_{\mathrm{ch}}(v_j\,,v_i)$, $b_{ij}^{\mathrm{ch}} \coloneqq b_{\mathrm{ch}}(w_j\,,v_i)$, $a_{ij}^{\mathrm{m}} \coloneqq a_{\mathrm{m}}(v_j\,,w_i)$ and $b_{ij}^{\mathrm{m}} \coloneqq b_{\mathrm{m}}(w_j\,,w_i)$. Notice that B is continuous with respect to time, due to the regularity assumptions on the nonlinear solutions. Finally, we specify the initial value in (5.3.38) as

$$z_0 = (\alpha_{n1},\dots,\alpha_{nn},0,\dots,0) \in \mathbb{R}^{n+m}, \tag{5.3.39}$$

Next, we check if the conditions of theorem 5.3.5 are satisfied. Equation (5.3.37) has a properly stated leading term. It is $\ker A = \{\emptyset\}$, since the matrix $\big((v_j\,, v_i)_\Omega\big)_{1\le i,j\le n}$ is regular and $\operatorname{im} D = \mathbb{R}^n$. Hence,

$$\ker A \oplus \operatorname{im} D = \mathbb{R}^n.$$

Further, we can simply choose $R = I_n$ as constant projector onto $\operatorname{im} D$ along $\ker A$. Notice that the matrix

$$G_0 = AD = \left(\begin{array}{c|c} \big((v_j, v_i)_\Omega\big)_{1\le i,j\le n} & 0_{n\times m} \\ \hline 0_{m\times n} & 0_{m\times m} \end{array}\right).$$

is singular. Now let Q_0 be the projection onto the kernel of $G_0 = AD$. If the matrix $G_1 = AD + BQ_0$ is regular the equation (5.3.37) has index $\mu = 1$ and hence, there exists a unique solution. We have

$$G_1 = \left(\begin{array}{c|c} \big((v_j, v_i)_\Omega\big)_{1\le i,j\le n} & (b^{\mathrm{ch}}_{ij})_{1\le i\le n, 1\le j\le m} \\ \hline 0_{m\times n} & (b^{\mathrm{m}}_{ij})_{1\le i,j\le m} \end{array}\right).$$

Due to the property of the basis functions v_i, $1 \le i \le n$, the matrix $\big((v_j, v_i)_\Omega\big)_{1\le i,j\le n}$ is regular. Hence, it is sufficient to show that the matrix $(b^{\mathrm{m}}_{ij})_{1\le i,j\le m}$, which corresponds to the mechanical equation, is regular. This is equivalent to the well-known fact that there exists a unique solution of the Galerkin scheme for the equation of linear elasticity with the applied boundary conditions. Therefore, the differential–algebraic system (5.3.37), (5.3.38) has index $\mu = 1$ and consequently, according to theorem 5.3.5, there exist a unique solution of the Galerkin equations (5.3.34), (5.3.35). Thus, there exists a unique solution (c_n, u_m) of the equivalent equations (5.3.32), (5.3.33), which fulfil (5.3.36). □

Step 2: Estimates for approximate solutions

Proposition 5.3.8. *There exists a constant $C > 0$, independent of n and m, such that*

$$\begin{aligned} \|c_n\|_{L^\infty(S,L^2(\Omega))} + \|c_n\|_{L^2(S,V(\Omega))} + \|c_n'\|_{L^2(S,V(\Omega)')} \\ + \|u_m\|_{L^2(S,H^1(\Omega))} \le C. \end{aligned} \tag{5.3.40}$$

Proof. For fixed $n, m \in \mathbb{N}$ we set $v = c_n$ and $w = u_m$ in (5.3.32). Then the result follows directly from the estimates in § 5.2. Since ϵ is fixed, from (5.2.16), we get

$$\|c_n(t)\|^2_\Omega + \|\Delta c_n\|^2_{\Omega,t} \le C\big(\,\|c_n(0)\|^2_\Omega + \|g\|^2_{H^{-1/2}(\Gamma_{\mathrm{g}}),t}\big), \tag{5.3.41}$$

for $t \in [0,T]$ and a constant $C > 0$, independent of n and m. This implies that

$$\|c_n\|_{L^\infty(S,L^2(\Omega))} \leq C \quad \text{and} \quad \|c_n\|_{L^2(S,V(\Omega))} \leq C.$$

Further, from (5.2.9), we obtain

$$\|u_m\|_{L^2(S,H^1(\Omega))} \leq C$$

for a constant $C > 0$, which does not depend on n and m. Finally, we get the boundedness of c_n' in $L^2(S, V(\Omega)')$ completely analogously to (5.1.7). □

Step 3: Convergence of approximate solutions

Proposition 5.3.9. *There exists a subsequence of the approximated solutions, which converges weakly to a weak solution*

$$(c,u) \in L^2(S,V(\Omega)) \times L^2(S,W(\Omega))$$

of (5.3.23) – (5.3.25) *with* $\partial_t c \in L^2(S,(V(\Omega))')$.

Proof. Since the sequences of the approximate solutions c_n and u_m are bounded in $L^2(S,V(\Omega))$ and $L^2(S,W(\Omega))$, respectivley, one can extract subsequences, still denoted by c_n and u_m, and there exist functions $c \in L^2(S,V(\Omega))$ and $u \in L^2(S,W(\Omega))$ such that

$$\begin{aligned} c_n &\rightharpoonup c \qquad \text{in } L^2(S,V(\Omega)), \\ u_m &\rightharpoonup u \qquad \text{in } L^2(S,W(\Omega)). \end{aligned}$$

For $\varphi \in C^1[0,T]$ with $\varphi(T) = 0$ and some fixed $n_1, m_1 \in \mathbb{N}$ we consider now $v \in V_{n_1}$ and $w \in W_{m_1}$ and choose $\tilde{v} := \varphi v$ as test function in (5.3.23) and $\tilde{w} := \varphi w$ in (5.3.24). Integration of the resulting equations with respect to t from 0 to T yields

$$\int_0^T (c_n'(t)\,,v)_\Omega\,\varphi(t)\,\mathrm{d}t + \int_0^T a_{\mathrm{ch}}(c_n\,,v)\,\varphi(t)\,\mathrm{d}t + \int_0^T b_{\mathrm{ch}}(u_m\,,v)\,\varphi(t)\,\mathrm{d}t = 0 \tag{5.3.42}$$

$$\int_0^T a_{\mathrm{m}}(c_n\,,w)\,\varphi(t)\,\mathrm{d}t + \int_0^T b_{\mathrm{m}}(u_m\,,w)\,\varphi(t)\,\mathrm{d}t = \int_0^T \langle g\,,w\rangle_{\Gamma_{\mathrm{g}}}\,\varphi(t)\,\mathrm{d}t \tag{5.3.43}$$

for $n \geq n_1, m \geq m_1$. Intergrating by parts in the first term in (5.3.42) yields

$$\begin{aligned} -(c_n(0),\, v)_\Omega\, \varphi(0) - \int_0^T \langle c_n(t),\, v\rangle_{V(\Omega)}\, \varphi'(t)\,\mathrm{d}t \\ + \int_0^T a_{\mathrm{ch}}(c_n, v)\, \varphi(t)\,\mathrm{d}t + \int_0^T b_{\mathrm{ch}}(u_m, v)\, \varphi(t)\,\mathrm{d}t = 0. \end{aligned} \tag{5.3.44}$$

Since

$$x \mapsto \int_0^T \langle x(t),\, v\rangle_{V(\Omega)}\, \varphi'(t)\,\mathrm{d}t, \tag{5.3.45}$$

$$x \mapsto \int_0^T a_{\mathrm{ch}}(x(t), v)\, \varphi(t)\,\mathrm{d}t, \quad x \mapsto \int_0^T a_{\mathrm{m}}(x(t), w)\, \varphi(t)\,\mathrm{d}t, \tag{5.3.46}$$

define linear and continuous functionals on $L^2(S, V(\Omega))$ and

$$z \mapsto \int_0^T b_{\mathrm{ch}}(z(t), v)\, \varphi(t)\,\mathrm{d}t, \quad z \mapsto \int_0^T b_{\mathrm{m}}(z(t), w)\, \varphi(t)\,\mathrm{d}t, \tag{5.3.47}$$

define linear and continuous functionals on $L^2(S, W(\Omega))$, we can now pass to the limit in the corresponding terms of (5.3.43) and (5.3.44) as $n, m \to \infty$. We get

$$\begin{aligned} -(c^{\mathrm{in}},\, v)_\Omega\, \varphi(0) - \int_0^T \langle c(t),\, v\rangle_{V(\Omega)}\, \varphi'(t)\,\mathrm{d}t \\ + \int_0^T a_{\mathrm{ch}}(c(t), v)\, \varphi(t)\,\mathrm{d}t + \int_0^T b_{\mathrm{ch}}(u(t), v)\, \varphi(t)\,\mathrm{d}t = 0, \end{aligned} \tag{5.3.48}$$

$$\int_0^T a_{\mathrm{m}}(c(t), w)\, \varphi(t)\,\mathrm{d}t + \int_0^T b_{\mathrm{m}}(u(t), w)\, \varphi(t)\,\mathrm{d}t = \int_0^T \langle g\,, w\rangle_{\Gamma_{\mathrm{g}}}\, \varphi(t)\,\mathrm{d}t. \tag{5.3.49}$$

Since $\bigcup_{k\in\mathbb{N}} V_k$ is dense in $V(\Omega)$ and $\bigcup_{l\in\mathbb{N}} W_l$ is dense in $W(\Omega)$ the above equations are valid for all $v \in V(\Omega), w \in W(\Omega)$. It remains to prove that c has a weak time derivative $c' \in L^2(S, V(\Omega)')$ and that c satisfies the initial condition $c(0) = c^{\mathrm{in}}$. Since

$$|\, a_{\mathrm{ch}}(c(t)\,, v)\,| \leq C\, \|c(t)\|_{V(\Omega)}\, \|v\|_{V(\Omega)}$$

and

$$|\, b_{\mathrm{ch}}(u(t)\,, v)\,| \leq C\, \|u(t)\|_{H^1(\Omega)}\, \|v\|_{V(\Omega)}\,,$$

(which follows from the estimates stated in § 5.2, since ϵ is fixed) the relations

$$\langle a^*(t)\,,v\rangle_{V(\Omega)} = a_{\mathrm{ch}}(c(t)\,,v), \quad \langle b^*(t)\,,v\rangle_{V(\Omega)} = b_{\mathrm{ch}}(u(t)\,,v),$$

for $v \in V(\Omega)$, $t \in S$, define elements $a^*, b^* \in L^2(S, V(\Omega)')$. Then, from (5.3.48), we get

$$-\int_0^T \langle c(t)\,,v\rangle_{V(\Omega)}\,\varphi'(t)\,\mathrm{d}t = -\int_0^T \langle a^*(t)\,,v\rangle_{V(\Omega)}\,\varphi(t)\,\mathrm{d}t - \int_0^T \langle b^*(t)\,,v\rangle_{V(\Omega)}\,\varphi(t)\,\mathrm{d}t, \tag{5.3.50}$$

for all $\varphi \in C_0^\infty(S)$. Hence, c has a weak derivative $c' \in L^2(S, V(\Omega)')$ with

$$c'(t) = -a^*(t) - b^*(t) \tag{5.3.51}$$

Moreover, we can conclude $c \in C([0,T], L^2(\Omega))$. We insert (5.3.51) into (5.3.48) and get

$$-(c^{\mathrm{in}}\,,v)_\Omega\,\varphi(0) - \int_0^T \langle c(t)\,,v\rangle_{V(\Omega)}\,\varphi'(t)\,\mathrm{d}t = \int_0^T \langle c'(t)\,,v\rangle_{V(\Omega)}\,\varphi(t)\,\mathrm{d}t,$$

which holds for all $\varphi \in C^1[0,T]$ with $\varphi(T) = 0$. Integrating by parts applied to $t \mapsto \varphi(t)v$ now yields

$$-(c^{\mathrm{in}}\,,v)_\Omega\,\varphi(0) + \int_0^T \langle c'(t)\,,v\rangle_{V(\Omega)}\,\varphi(t)\,\mathrm{d}t + (c(0)\,,v)_\Omega\,\varphi(0) = \int_0^T \langle c'(t)\,,v\rangle_{V(\Omega)}\,\varphi(t)\,\mathrm{d}t.$$

Choosing a test function that additionally fulfils $\varphi(0) = 1$, we get

$$(c^{\mathrm{in}}\,,v)_\Omega = (c(0)\,,v)_\Omega, \quad \text{for all } v \in V(\Omega). \tag{5.3.52}$$

In summary, we have shown that the functions $c \in L^2(S, V(\Omega))$ with weak derivative $c' \in L^2(S, V'(\Omega))$ and $u \in L^2(S, W(\Omega))$ fulfil the system (5.3.23) – (5.3.25). □

Step 4: Uniqueness of the solution

Proposition 5.3.10 (Uniqueness)**.**
There exists at most one solution (c_ϵ, u_ϵ) *of the system* (5.3.23) – (5.3.25).

Proof. The proof is standard. For two supposedly different pairs of solutions $c_\epsilon^{(1)}$, $u_\epsilon^{(1)}$ and $c_\epsilon^{(2)}$, $u_\epsilon^{(2)}$, due to linearity of the equations the differences $c_\epsilon^{(1)} - c_\epsilon^{(2)}$ and $u_\epsilon^{(1)} - u_\epsilon^{(2)}$ fulfil the equations (5.3.23) – (5.3.25) with $g \equiv 0$ and $c^{\mathrm{in}} \equiv 0$. Since ϵ is fixed, from (5.2.16), we get

$$\left\|c_\epsilon^{(1)}(t) - c_\epsilon^{(2)}(t)\right\|_\Omega^2 + \left\|\Delta c_\epsilon^{(1)} - \Delta c_\epsilon^{(2)}\right\|_{\Omega,t}^2 \leq 0.$$

Therefore, we can conclude $\|c_\epsilon^{(1)} - c_\epsilon^{(2)}\|_{V(\Omega),t} = 0$ and hence $c_\epsilon^{(1)} = c_\epsilon^{(2)}$. This, together with (5.2.9) implies, that

$$\|u_\epsilon^{(1)} - u_\epsilon^{(2)}\|^2_{H^1(\Omega),t} \leq 0, \tag{5.3.53}$$

which provides $u_\epsilon^{(1)} = u_\epsilon^{(2)}$ and which finishes our proof. □

6 Rigorous homogenisation of the linear Cahn–Larché system

This part is devoted to homogenise the linear Cahn–Larché system in a mathematically rigorous way using the concept of two-scale convergence introduced in section 3.2. First, we specify further assumptions, then, we state the homogenisation result, which we proof afterwards in several steps. Finally, we state some properties of the homogenised system and provide a relation to the formally homogenised systems from section 4.2.

6.1 Two-scale limit system

Before we turn to the derivation of the two-scale limit system, we need to make further assumptions. In § 2.5 we have linearised about general solutions $c_{n,\epsilon}$ and $u_{n,\epsilon}$ of (2.4.15), (2.4.16), for each $\epsilon > 0$. In order to pass to the limit in each term of the linear system (5.1.5), (5.1.6), we have to deal with the convergence behaviour of the sequences of the solutions of the nonlinear system. Considering the linearised Cahn–Larché system, there are several products of sequences we have to be aware of. We recall the choices we made concerning the local free energy density,

$$f(c) = \varphi\, c^2(1-c)^2, \tag{6.1.1}$$

and the interpolation of the component elasticity tensors

$$\mathcal{A}(c) = \mathcal{A}^{\mathrm{E}} + d(c)\big(\mathcal{A}^{\mathrm{C}} - \mathcal{A}^{\mathrm{E}}\big), \tag{6.1.2}$$

with cubic interpolation function d. Regarding the eigenstrain, we restrict from now on to a linear interpolation, i.e.

$$\bar{\mathcal{E}}(c) = e(c)\mathbb{1} \quad \text{with} \quad e(c) = e_{\mathrm{E}} + c\,(e_{\mathrm{C}} - e_{\mathrm{E}}). \tag{6.1.3}$$

Note, that the derivative $e' = e_{\mathrm{C}} - e_{\mathrm{E}}$ is now only a constant and hence, from now on, we just write e' instead of $e'(c_{n,\epsilon})$. With regard to (6.1.1), (6.1.2) and (6.1.3), we require the following convergences concerning the sequences of the solutions of the nonlinear system:

- There exists a function $c_{n,0} \in L^\infty(\Omega \times Y \times S)$ such that at least a subsequence of $c_{n,\epsilon}$, two-scale converges strongly to $c_{n,0}$ in $L^6(\Omega \times S)$, i.e.

$$c_{n,\epsilon} \overset{\text{2s.}}{\rightharpoonup} c_{n,0} \tag{6.1.4}$$

and

$$\lim_{\epsilon \to 0} \|c_{n,\epsilon}\|_{L^6(\Omega \times S)} = \|c_0\|_{L^6(\Omega \times Y \times S)} . \tag{6.1.5}$$

- There exist functions $u_{n,0} \in (L^\infty(\Omega \times S))^N$ and $u_{n,1} \in (L^\infty(\Omega \times Y \times S))^N$ with $\mathcal{E}_x(u_{n,0}) \in (L^\infty(\Omega \times S))^{N \times N}$ and $\mathcal{E}_y(u_{n,1}) \in (L^\infty(\Omega \times Y \times S))^{N \times N}$, such that, up to a subsequence, $(u_{n,\epsilon})_i$ (the i-th component of $u_{n,\epsilon}$) two-scale converges strongly to $(u_{n,0})_i$ in $L^6(\Omega \times S)$ and $\partial_{x_j}(u_{n,\epsilon})_i$ two-scale converges strongly to $\partial_{x_j}(u_{n,0})_i + \partial_{y_j}(u_{n,1})_i$ in $L^6(\Omega \times S)$, i.e.

$$(u_{n,\epsilon})_i \overset{\text{2s.}}{\rightharpoonup} (u_{n,0})_i, \tag{6.1.6}$$

$$\partial_{x_j}(u_{n,\epsilon})_i \overset{\text{2s.}}{\rightharpoonup} \partial_{x_j}(u_{n,0})_i + \partial_{y_j}(u_{n,1})_i \tag{6.1.7}$$

and

$$\lim_{\epsilon \to 0} \|(u_{n,\epsilon})_i\|_{L^6(\Omega \times S)} = \|(u_{n,0})_i\|_{L^6(\Omega \times S)} , \tag{6.1.8}$$

$$\lim_{\epsilon \to 0} \left\|\partial_{x_j}(u_{n,\epsilon})_i\right\|_{L^6(\Omega \times S)} = \left\|\partial_{x_j}(u_{n,0})_i + \partial_{y_j}(u_{n,1})_i\right\|_{L^6(\Omega \times Y \times S)} , \tag{6.1.9}$$

for $1 \leq i, j \leq N$.

The following theorem now gives the homogenisation result.

Theorem 6.1.1. *There exist functions $c_0 \in L^2(\Omega \times S; H^2_{\#}(Y))$, $u_0 \in L^2(S; W(\Omega))$ and $u_1 \in L^2(\Omega \times S; [H^1_{\#}(Y)]^N)$ such that the sequences c_ϵ and u_ϵ of the solutions of (2.5.5) and (2.5.6) two-scale converge to c_0 and u_0, respectively. Furthermore, the sequence $\mathcal{E}(u_\epsilon)$ two-scale converges to $\mathcal{E}_x(u_0) + \mathcal{E}_y(u_1)$ and the sequence $\epsilon^2 \Delta c_\epsilon$ two-scale converges to $\Delta_{yy} c_0$. The triple of the limit functions $\big(c_0, u_0, u_1\big)$ is the unique solution of the following homogenised system:*

$$
\begin{aligned}
\partial_t c_0 = \Delta_{yy} \Big(& f''(c_{n,0}) c_0 - \lambda \Delta_{yy} c_0 - e' \operatorname{tr}(\mathcal{S}_0) \\
& + \big(\mathcal{E}_x(u_{n,0}) + \mathcal{E}_y(u_{n,1}) - e(c_{n,0}) \mathbb{1}\big) \\
& \quad : \mathcal{A}'(c_{n,0}) \big(\mathcal{E}_x(u_0) + \mathcal{E}_y(u_1) - e' c_0 \mathbb{1}\big) \\
& + \frac{1}{2} \big(\mathcal{E}_x(u_{n,0}) + \mathcal{E}_y(u_{n,1}) - e(c_{n,0}) \mathbb{1}\big) \\
& \quad : \mathcal{A}''(c_{n,0}) c_0 \left(\mathcal{E}_x(u_{n,0}) + \mathcal{E}_y(u_{n,1}) - e(c_{n,0}) \mathbb{1}\right) \Big) \qquad \text{in } \Omega \times Y \times S,
\end{aligned}
\tag{6.1.10}
$$

$$
\begin{aligned}
0 = -\nabla_y \cdot \Big(& \mathcal{A}(c_{n,0}) \big(\mathcal{E}_x(u_0) + \mathcal{E}_y(u_1) - e' c_0 \mathbb{1}\big) \\
& + \mathcal{A}'(c_{n,0}) c_0 \big(\mathcal{E}_x(u_{n,0}) + \mathcal{E}_y(u_{n,1}) - e(c_{n,0}) \mathbb{1}\big) \Big) \qquad \text{in } \Omega \times Y \times S,
\end{aligned}
\tag{6.1.11}
$$

$$
\begin{aligned}
0 = -\sum_{j=1}^{N} \partial_{x_j} \int_Y \sum_{k,h=1}^{N} \Big(& a_{ijkh}(c_{n,0}) \big(e_{khx}(u_0) + e_{khy}(u_1) - e' c_0 \delta_{kh}\big) \\
& + a'_{ijkh}(c_{n,0}) c_0 \big(e_{khx}(u_{n,0}) + e_{khy}(u_{n,1}) - e(c_{n,0}) \delta_{kh}\big) \Big) \, \mathrm{d}y
\end{aligned}
\tag{6.1.12}
$$

in $\Omega \times Y \times S$, for $1 \le i \le N$, where

$$
\mathcal{S}_0 = \mathcal{A}(c_{n,0}) \big(\mathcal{E}_x(u_0) + \mathcal{E}_y(u_1) - e' c_0 \mathbb{1}\big) \tag{6.1.13}
$$

$$
+ \mathcal{A}'(c_{n,0}) c_0 \big(\mathcal{E}_x(u_{n,0}) + \mathcal{E}_y(u_{n,1}) - e(c_{n,0}) \mathbb{1}\big), \tag{6.1.14}
$$

and with

$$
\begin{aligned}
u_0 &= 0 \quad \text{on } \Gamma_0 \times S, \\
\mathcal{S}_0 \, n &= g \quad \text{on } \Gamma_g \times S, \\
u_0 \cdot n &= 0 \quad \text{on } \Gamma_s \times S, \\
\tau \cdot \mathcal{S}_0 \, n &= 0 \quad \text{on } \Gamma_s \times S, \\
c_0, u_1 &\quad Y\text{-periodic in } y,
\end{aligned}
$$

and $c_0(\,\cdot\,, \,\cdot\,, 0) = c^{\mathrm{in}}$ being Y-periodic with respect to y.

Proof. The proof consists of several steps. First, we pass to the limit in the weak form of the linear scaled Cahn–Larché system. Afterwards, we proof the uniquness of the solutions of the resulting weak homogenised system and, in a third step, we derive the strong formulation of the homogenised system.

Homogenisation process

We start by identifying the precise form of the two-scale limits of the sequences of the unknowns. We have already proven that c_ϵ and $\epsilon^2\Delta c_\epsilon$ are bounded in $L^2(S, L^2(\Omega))$, ∇c_ϵ is bounded in $L^2(S, [L^2(\Omega)]^N)$ and the sequence u_ϵ is bounded in $L^2(S; W(\Omega))$, cf. proposition 5.2.6. Then, from theorem 3.2.5, we know that there exists a function $c_0 \in L^2(\Omega \times S; H^2_\#(Y))$ such that, up to a subsequence,

$$\begin{aligned} c_\epsilon &\overset{2s.}{\rightharpoonup} c_0, \\ \epsilon^2\Delta c_\epsilon &\overset{2s.}{\rightharpoonup} \Delta_y c_0. \end{aligned} \tag{6.1.15}$$

Furthermore, according to theorem 3.2.4, there exists two functions, $u_0 \in L^2(S; W(\Omega))$ and $u_1 \in L^2(S \times \Omega; [H^1_\#(Y)/\mathbb{R}]^2)$ such that, up to a subsequence,

$$\begin{aligned} u_\epsilon &\overset{2s.}{\rightharpoonup} u_0, \\ \mathcal{E}(u_\epsilon) &\overset{2s.}{\rightharpoonup} \mathcal{E}_x(u_0) + \mathcal{E}_y(u_1). \end{aligned} \tag{6.1.16}$$

We start the limit process with the mechanical equation (5.1.6). Considering the two-scale limit of u_ϵ, the sequence is expected to behave as $u_0 + \epsilon u_1$. Therefore we choose a test function $\psi \in [C^\infty(\Omega; C^\infty_\#(Y))]^N$ with the same structure, namely

$$\psi(x, \frac{x}{\epsilon}) = \psi_0(x) + \epsilon\psi_1(x, \frac{x}{\epsilon}),$$

with $\psi_0 \in [C^\infty(\Omega)]^N$ and $\psi_1 \in [C^\infty(\Omega; C^\infty_\#(Y))]^N$ for the mechanical equation. Note that according to definition 3.2.2, ψ is an admissible test function for two-scale convergence. We obtain

$$\begin{aligned} &\int_\Omega \mathcal{A}(c_{n,\epsilon})\big(\mathcal{E}(u_\epsilon(x,t)) - e'c_\epsilon(x,t)\mathbb{1}\big) : \big(\mathcal{E}(\psi_0(x)) + \epsilon\,\mathcal{E}(\psi_1(x, \frac{x}{\epsilon}))\big)\,\mathrm{d}x \\ &+ \int_\Omega \mathcal{A}'(c_{n,\epsilon})c_\epsilon(x,t)\big(\mathcal{E}(u_{n,\epsilon}) - e(c_{n,\epsilon})\mathbb{1}\big) : \big(\mathcal{E}(\psi_0(x)) + \epsilon\,\mathcal{E}(\psi_1(x, \frac{x}{\epsilon}))\big)\,\mathrm{d}x \\ &= \int_{\Gamma_g} g(x,t)\,\big(\psi_0(x) + \epsilon\,\psi_1(x, \frac{x}{\epsilon})\big)\,\mathrm{d}\sigma_x. \end{aligned} \tag{6.1.17}$$

Proposition 3.2.8 enables us to pass to the limit in (6.1.17). The proof shows that (3.2.5) also applies when choosing $\varphi = \varphi(x, x/\epsilon)$ from $C^\infty(\Omega, C^\infty_\#(Y))$ instead from $C^\infty(\Omega)$. Considering

(6.1.2), several terms of products of sequences appear here. The most critical terms include products of one weakly convergent sequence with three strongly convergent sequences. So the required convergences of the sequences $c_{n,\epsilon}$ and $u_{n,\epsilon}$ are sufficient to pass to the limit. Hence, for $\epsilon \to 0$, we get

$$\begin{aligned}
&\lim_{\epsilon\to 0} \int_\Omega \mathcal{A}(c_{n,\epsilon})\big(\mathcal{E}(u_\epsilon(x,t)) - e' c_\epsilon(x,t)\mathbb{1}\big) : \big(\mathcal{E}(\psi_0(x)) + \epsilon\, \mathcal{E}(\psi_1(x, \frac{x}{\epsilon}))\big)\, \mathrm{d}x \\
&= \int_\Omega \int_Y \mathcal{A}(c_{n,0})\big(\mathcal{E}_x(u_0(x,t)) + \mathcal{E}_y(u_1(x,y,t)) - e' c_0(x,y,t)\mathbb{1}\big) \\
&\qquad\qquad : \big(\mathcal{E}_x(\psi_0(x)) + \mathcal{E}_y(\psi_1(x,y))\big)\, \mathrm{d}y\, \mathrm{d}x
\end{aligned}$$

and

$$\begin{aligned}
&\lim_{\epsilon\to 0} \int_\Omega \mathcal{A}'(c_{n,\epsilon}) c_\epsilon(x,t)\big(\mathcal{E}(u_{n,\epsilon}) - e(c_{n,\epsilon})\mathbb{1}\big) : \big(\mathcal{E}(\psi_0(x)) + \epsilon\, \mathcal{E}(\psi_1(x, \frac{x}{\epsilon}))\big)\, \mathrm{d}x \\
&= \int_\Omega \int_Y \mathcal{A}'(c_{n,0}) c_0(x,y,t)\big(\mathcal{E}_x(u_{n,0}) + \mathcal{E}_y(u_{n,1}) - e(c_{n,0})\mathbb{1}\big) \\
&\qquad\qquad : \big(\mathcal{E}_x(\psi_0(x)) + \mathcal{E}_y(\psi_1(x,y))\big)\, \mathrm{d}y\, \mathrm{d}x
\end{aligned}$$

For the boundary term in (6.1.17), we get

$$\lim_{\epsilon\to 0} \int_{\Gamma_g} g(x,t)\, \big(\psi_0(x) + \epsilon\, \psi_1(x, \frac{x}{\epsilon})\big)\, \mathrm{d}\sigma_x = \int_{\Gamma_g} g(x,t)\, \psi_0(x)\, \mathrm{d}\sigma_x$$

since g is bounded and $\psi_0 + \epsilon\, \psi_1$ converges weakly to ψ_0. Altogether, for the mechanical equilibrium equation (6.1.25), we obtain

$$\begin{aligned}
&\int_\Omega \int_Y \mathcal{A}(c_{n,0})\big(\mathcal{E}_x(u_0(x,t)) + \mathcal{E}_y(u_1(x,y,t)) - e' c_0(x,y,t)\mathbb{1}\big) \\
&\qquad\qquad : \big(\mathcal{E}_x(\psi_0(x)) + \mathcal{E}_y(\psi_1(x,y))\big)\, \mathrm{d}y\, \mathrm{d}x \\
&+ \int_\Omega \int_Y \mathcal{A}'(c_{n,0}) c_0(x,y,t)\, \big(\mathcal{E}(u_{n,0}) + \mathcal{E}_y(u_{n,1}) - e(c_{n,0})\mathbb{1}\big) \\
&\qquad\qquad : \big(\mathcal{E}_x(\psi_0(x)) + \mathcal{E}_y(\psi_1(x,y))\big)\, \mathrm{d}y\, \mathrm{d}x \\
&= \int_{\Gamma_g} g(x,t)\, \psi_0(x)\, d\sigma.
\end{aligned} \tag{6.1.18}$$

Now, we want to pass to the limit of the extended Cahn–Hilliard equation. In view of the two-scale limit (6.1.15), we choose $\varphi \in C^\infty(\Omega; C^\infty_\#(Y))$ as test function, which reflects the

behaviour of c_ϵ. From (5.1.5), we get

$$\begin{aligned}
&\int_\Omega \partial_t c_\epsilon(x,t)\,\varphi(x,\frac{x}{\epsilon})\,\mathrm{d}x \\
&= \epsilon^2 \int_\Omega \big(f''(c_{n,\epsilon})c_\epsilon(x,t) - \epsilon^2\lambda\Delta c_\epsilon(x,t) - e'\,\mathrm{tr}(\mathcal{S}_\epsilon)\big)\,\Delta\varphi(x,\frac{x}{\epsilon})\,\mathrm{d}x \\
&\quad + \epsilon^2 \int_\Omega \big(\mathcal{E}(u_{n,\epsilon}) - e(c_{n,\epsilon})\mathbb{1}\big) : \mathcal{A}'(c_{n,\epsilon})\big(\mathcal{E}(u_\epsilon(x,t)) - e'(c_{n,\epsilon})c_\epsilon(x,t)\mathbb{1}\big)\,\Delta\varphi(x,\frac{x}{\epsilon})\,\mathrm{d}x \\
&\quad + \frac{1}{2}\epsilon^2 \int_\Omega \big(\mathcal{E}(u_{n,\epsilon}) - e(c_{n,\epsilon})\mathbb{1}\big) : \mathcal{A}''(c_{n,\epsilon})c_\epsilon(x,t)\big(\mathcal{E}(u_{n,\epsilon}) - e(c_{n,\epsilon})\mathbb{1}\big)\,\Delta\varphi(x,\frac{x}{\epsilon})\,\mathrm{d}x.
\end{aligned} \tag{6.1.19}$$

Now, we pass to the limit in each term as ϵ tends to zero. For the first term of the right-hand side of (6.1.19) we use theorem 3.2.8. Since f is a fourth-order polynomial, f'' is a quadratic function and the required convergence of $c_{n,\epsilon}$ is sufficient to pass to the limit. We get

$$\begin{aligned}
&\lim_{\epsilon\to 0}\epsilon^2 \int_\Omega f''(c_{n,\epsilon})c_\epsilon(x,t)\,\Delta\varphi(x,\frac{x}{\epsilon})\,\mathrm{d}x \\
&\qquad = \lim_{\epsilon\to 0}\int_\Omega f''(c_{n,\epsilon})c_\epsilon(x,t)\left[\epsilon^2\Delta_{xx} + \epsilon\nabla_x\cdot\nabla_y + \epsilon\nabla_y\cdot\nabla_x + \Delta_{yy}\right]\varphi(x,\frac{x}{\epsilon})\,\mathrm{d}x \\
&\qquad = \int_\Omega\int_Y f''(c_{n,0})c_0(x,y,t)\,\Delta_{yy}\varphi(x,y)\,\mathrm{d}y\,\mathrm{d}x
\end{aligned} \tag{6.1.20}$$

and

$$\begin{aligned}
&\lim_{\epsilon\to 0}\epsilon^2 \int_\Omega \epsilon^2\lambda\,\Delta c_\epsilon(x,t)\Delta\varphi(x,\frac{x}{\epsilon})\,\mathrm{d}x = \lim_{\epsilon\to 0}\int_\Omega \epsilon^2\lambda\Delta c_\epsilon(x,t)\,\epsilon^2\Delta\varphi(x,\frac{x}{\epsilon})\,\mathrm{d}x \\
&= \int_\Omega\int_Y \lambda\Delta_{yy}c_0(x,y,t)\,\Delta_{yy}\varphi(x,y)\,\mathrm{d}y\,\mathrm{d}x
\end{aligned} \tag{6.1.21}$$

as the two-scale limit of the Laplacian term. With regard to the limit of the mechanical equation (6.1.18), or more precisely to the limit of the sequence of the stress, we get

$$\epsilon^2\int_\Omega e'\,\mathrm{tr}(\mathcal{S}_\epsilon)\,\Delta\varphi(x,\frac{x}{\epsilon})\,\mathrm{d}x \to \int_\Omega\int_Y e'\,\mathrm{tr}(\mathcal{S}_0)\,\Delta_{yy}\varphi(x,y)\,\mathrm{d}y\,\mathrm{d}x, \tag{6.1.22}$$

where we denote the limit of the stress tensor by

$$\begin{aligned}
\mathcal{S}_0 = &\mathcal{A}(c_{n,0})\big(\mathcal{E}_x(u_0) + \mathcal{E}_y(u_1) - e'c_0\mathbb{1}\big) \\
&+ \mathcal{A}'(c_{n,0})c_0\big(\mathcal{E}_x(u_{n,0}) + \mathcal{E}_y(u_{n,1}) - e(c_{n,0})\mathbb{1}\big).
\end{aligned} \tag{6.1.23}$$

Similarly, we pass to the limit in the remaining terms using proposition 3.2.8. The most

critical parts appearing in the quadratic terms consist, as before, of products of three strongly converging sequences and one weakly converging sequence. We get

$$\begin{aligned}
&\lim_{\epsilon\to 0} \epsilon^2 \int_\Omega \big(\mathcal{E}(u_{n,\epsilon}) - e(c_{n,\epsilon})\mathbb{1}\big) : \mathcal{A}'(c_{n,\epsilon})\big(\mathcal{E}(u_\epsilon(x,t)) - e'(c_{n,\epsilon})c_\epsilon(x,t)\mathbb{1}\big)\,\Delta\varphi(x,\frac{x}{\epsilon})\,\mathrm{d}x \\
&= \int_\Omega \int_Y \big(\mathcal{E}_x(u_{n,0}) + \mathcal{E}_y(u_{n,1}) - e(c_{n,0})\mathbb{1}\big) \\
&\qquad : \mathcal{A}'(c_{n,0})\big(\mathcal{E}_x(u_0(x,t)) + \mathcal{E}_y(u_1(x,y,t)) - e'(c_{n,0})c_0(x,y,t)\mathbb{1}\big)\,\Delta_{yy}\varphi(x,y)\,\mathrm{d}y\,\mathrm{d}x
\end{aligned}$$

and

$$\begin{aligned}
&\lim_{\epsilon\to 0} \frac{1}{2}\epsilon^2 \int_\Omega \big(\mathcal{E}(u_{n,\epsilon}) - e(c_{n,\epsilon})\mathbb{1}\big) : \mathcal{A}''(c_{n,\epsilon})c_\epsilon(x,t)\big(\mathcal{E}(u_{n,\epsilon}) - e(c_{n,\epsilon})\mathbb{1}\big)\,\Delta\varphi(x,\frac{x}{\epsilon})\,\mathrm{d}x \\
&= \frac{1}{2}\int_\Omega \int_Y \big(\mathcal{E}_x(u_{n,0}) + \mathcal{E}_y(u_{n,1}) - e(c_{n,0})\mathbb{1}\big) \\
&\qquad : \mathcal{A}''(c_{n,0})c_0(x,y,t)\big(\mathcal{E}(u_{n,0}) + \mathcal{E}_y(u_{n,1}) - e(c_{n,0})\mathbb{1}\big)\,\Delta_{yy}\varphi(x,y)\,\mathrm{d}y\,\mathrm{d}x
\end{aligned}$$

Passing to the limit in the term with the time derivative first requires integration by parts with respect to time since $\partial_t c_\epsilon$ is only bounded in $L^2(S,(V(\Omega))')$. Re-integration then results in the limit of the time derivative corresponding to the time derivative of the limit function c_0.

In summary, we can now read off a variational formulation for the two-scale limit functions $(c_0, u_0, u_1) \in L^2(\Omega \times S, H^2_\#(Y)) \times L^2(S, W(\Omega)) \times [L^2(\Omega \times S, H^1_\#(Y)/\mathbb{R})]^N$:

$$
\begin{aligned}
&\int_\Omega \int_Y \partial_t c_0(x,y,t)\, \varphi(x,y)\, \mathrm{d}y\, \mathrm{d}x \\
&= \int_\Omega \int_Y \big(f''(c_{n,0}) c_0(x,y,t) - \lambda \Delta_{yy} c_0(x,y,t) - e' \operatorname{tr}(\mathcal{S}_0) \big)\, \Delta_{yy} \varphi(x,y)\, \mathrm{d}y\, \mathrm{d}x \\
&\quad + \int_\Omega \int_Y \big(\mathcal{E}_x(u_{n,0}) + \mathcal{E}_y(u_{n,1}) - e(c_{n,0})\mathbb{1} \big) \\
&\qquad\qquad : \mathcal{A}'(c_{n,0}) \big(\mathcal{E}_x(u_0(x,t)) + \mathcal{E}_y(u_1(x,y,t)) - e' c_0(x,y,t)\mathbb{1} \big)\, \Delta_{yy} \varphi(x,y)\, \mathrm{d}y\, \mathrm{d}x \\
&\quad + \frac{1}{2} \int_\Omega \int_Y \big(\mathcal{E}(u_{n,0}) + \mathcal{E}_y(u_{n,1}) - e(c_{n,0})\mathbb{1} \big) \\
&\qquad\qquad : \mathcal{A}''(c_{n,0}) c_0(x,y,t) \big(\mathcal{E}_x(u_{n,0}) + \mathcal{E}_y(u_{n,1}) - e(c_{n,0})\mathbb{1} \big)\, \Delta_{yy} \varphi(x,y)\, \mathrm{d}y\, \mathrm{d}x,
\end{aligned}
\tag{6.1.24}
$$

$$
\begin{aligned}
&\int_\Omega \int_Y \mathcal{A}(c_{n,0}) \big(\mathcal{E}_x(u_0(x,t)) + \mathcal{E}_y(u_1(x,y,t)) - e' c_0(x,y,t)\mathbb{1} \big) \\
&\qquad\qquad : \big(\mathcal{E}_x(\psi_0(x)) + \mathcal{E}_y(\psi_1(x,y)) \big)\, \mathrm{d}y\, \mathrm{d}x \\
&+ \int_\Omega \int_Y \mathcal{A}'(c_{n,0}) c_0(x,y,t) \big(\mathcal{E}(u_{n,0}) + \mathcal{E}_y(u_{n,1}) - e(c_{n,0})\mathbb{1} \big) \\
&\qquad\qquad : \big(\mathcal{E}_x(\psi_0(x)) + \mathcal{E}_y(\psi_1(x,y)) \big)\, \mathrm{d}y\, \mathrm{d}x \\
&= \int_{\Gamma_g} g(x,t)\, \psi_0(x)\, \mathrm{d}\sigma_x,
\end{aligned}
\tag{6.1.25}
$$

which holds for all $(\varphi, \psi_0, \psi_1) \in C^\infty(\Omega; C^\infty_\#(Y)) \times [C^\infty(\Omega)]^N \times [C^\infty(\Omega; C^\infty_\#(Y))]^N$. By density, the above equations still hold for all $(\varphi, \psi_0, \psi_1) \in L^2(\Omega, H^2_\#(Y)) \times W(\Omega) \times [L^2(\Omega, H^1_\#(Y)/\mathbb{R})]^N$ and since the limits $c_{n,0}$, $u_{n,0}$ and $u_{n,1}$ are essentially bounded with respect to space and time, the integrals are well-defined.

Uniqueness of the limit solutions:

It remains to prove that the solution triple (c_0, u_0, u_1) of (6.1.24) and (6.1.25) is unique in $L^2(\Omega \times S, H^2_\#(Y)) \times L^2(S, W(\Omega)) \times [L^2(\Omega \times S, H^1_\#(Y)/\mathbb{R})]^N$. To do so, we consider two supposedly different solution triples (c_0, u_0, u_1) and $(\tilde{c}_0, \tilde{u}_0, \tilde{u}_1)$. Their difference fulfils the equations (6.1.24) and (6.1.25) with $g \equiv 0$ and we also use these as test functions. Then, we decompose

the equation (6.1.25) and estimate

$$\int_\Omega \int_Y \mathcal{A}(c_{n,0})\big(\mathcal{E}_x(u_0-\tilde{u}_0)+\mathcal{E}_y(u_1-\tilde{u}_1)\big) : \big(\mathcal{E}_x(u_0-\tilde{u}_0)+\mathcal{E}_y(u_1-\tilde{u}_1)\big)\,\mathrm{d}y\,\mathrm{d}x$$
$$\geq \alpha \left\| \big(\mathcal{E}_x(u_0-\tilde{u}_0)+\mathcal{E}_y(u_1-\tilde{u}_1)\big)\right\|^2_{\Omega\times Y},$$

and

$$\Big|\int_\Omega \int_Y \mathcal{A}(c_{n,0})e'(c_0-\tilde{c}_0)\mathbb{1} : \big(\mathcal{E}_x(u_0-\tilde{u}_0)+\mathcal{E}_y(u_1-\tilde{u}_1)\big)\,\mathrm{d}y\,\mathrm{d}x\Big|$$
$$\leq \beta N|e'|\ \|\mathcal{E}_x(u_0-\tilde{u}_0)+\mathcal{E}_y(u_1-\tilde{u}_1)\|_{\Omega\times Y}\ \|c_0-\tilde{c}_0\|_{\Omega\times Y},$$

as well as

$$\Big|\int_\Omega \int_Y \mathcal{A}'(c_{n,0})(c_0-\tilde{c}_0)\left(\mathcal{E}(u_{n,0})+\mathcal{E}_y(u_{n,1})-e(c_{n,0})\mathbb{1}\right) : \big(\mathcal{E}_x(u_0-\tilde{u}_0)+\mathcal{E}_y(u_1-\tilde{u}_1)\big)\,\mathrm{d}y\,\mathrm{d}x\Big|$$
$$\leq \beta' \|\mathcal{E}_x(u_{n,0})+\mathcal{E}_y(u_{n,1})-e(c_{n,0})\mathbb{1}\|_{M,\Omega\times Y}\ \|\mathcal{E}_x(u_0-\tilde{u}_0)+\mathcal{E}_y(u_1-\tilde{u}_1)\|_{\Omega\times Y}\ \|c_0-\tilde{c}_0\|_{\Omega\times Y},$$

for a.e. $t\in S$. Hence, we obtain

$$\|\mathcal{E}_x(u_0-\tilde{u}_0)+\mathcal{E}_y(u_1-\tilde{u}_1)\|_{\Omega\times Y}\leq C\ \|c_0-\tilde{c}_0\|_{L^2(\Omega\times Y)}. \tag{6.1.26}$$

Completely analogous to the a-priori estimates from section 5.2, from (6.1.24), we get

$$\frac{1}{2}\frac{\mathrm{d}}{\mathrm{d}t}\|c_0-\tilde{c}_0\|^2_{\Omega\times Y}+\|\Delta_{yy}(c_0-\tilde{c}_0)\|^2_{\Omega\times Y}$$
$$\leq C\left(\|c_0-\tilde{c}_0\|_{\Omega\times Y}+\|\mathcal{E}_x(u_0-\tilde{u}_0)+\mathcal{E}_y(u_1-\tilde{u}_1)\|_{\Omega\times Y}\right)\|\Delta_{yy}(c_0-\tilde{c}_0)\|_{\Omega\times Y},$$

for a constant $C>0$ and a.e $t\in S$. With (6.1.26) and Young's inequality, we obtain

$$\begin{aligned}\frac{1}{2}\frac{\mathrm{d}}{\mathrm{d}t}\|c_0-\tilde{c}_0\|^2_{\Omega\times Y}&+\|\Delta_{yy}(c_0-\tilde{c}_0)\|^2_{\Omega\times Y}\\ &\leq C\,\|c_0-\tilde{c}_0\|_{\Omega\times Y}\,\|(\Delta_{yy}c_0-\tilde{c}_0)\|_{\Omega\times Y}\\ &\leq \frac{1}{2}C\left(\frac{1}{\delta}\|c_0-\tilde{c}_0\|^2_{\Omega\times Y}+\delta\,\|\Delta_{yy}(c_0-\tilde{c}_0)\|^2_{\Omega\times Y}\right),\end{aligned}$$

with $0<\delta<1$. Absorbing the Laplacian term, integrating with respect to time from 0 to T and applying Gronwall's inequality then yields

$$\|c_0(t)-\tilde{c}_0(t)\|^2_{\Omega\times Y}+\int_0^T\|\Delta_{yy}c_0(t)-\Delta_{yy}\tilde{c}_0(t)\|^2_{\Omega\times Y}\,\mathrm{d}t\ \leq\ 0. \tag{6.1.27}$$

Thus, $c_0 = \tilde{c}_0$ and $\Delta_{yy} c_0 = \Delta_{yy} \tilde{c}_0$, and since

$$\|\nabla_y v\|_{\Omega\times Y} \leq \|v\|_{\Omega\times Y} \|\Delta_{yy} v\|_{\Omega\times Y}, \quad \forall v \in L^2(\Omega, H^2_{\#}(Y)),$$

we also get $\nabla_y c_0 = \nabla_y \tilde{c}_0$ and hence, the uniqueness of c_0 in $L^2(\Omega \times S, H^2_{\#}(Y))$. From (6.1.26), it follows

$$0 \geq \|\mathcal{E}_x(u_0 - \tilde{u}_0) + \mathcal{E}_y(u_1 - \tilde{u}_1)\|^2_{\Omega\times Y}.$$

It holds

$$\begin{aligned}
&\|\mathcal{E}_x(u_0 - \tilde{u}_0) + \mathcal{E}_y(u_1 - \tilde{u}_1)\|^2_{\Omega\times Y} \\
&= \|\mathcal{E}_x(u_0 - \tilde{u}_0)\|^2_{\Omega} + \|\mathcal{E}_y(u_1 - \tilde{u}_1)\|^2_{\Omega\times Y} + 2\int_\Omega \int_Y \mathcal{E}_x(u_0 - \tilde{u}_0) : \mathcal{E}_y(u_1 - \tilde{u}_1)\,\mathrm{d}y\,\mathrm{d}x \\
&\geq C\,\|u_0 - \tilde{u}_0\|^2_{H^1(\Omega)} + \|\nabla_y(u_1 - \tilde{u}_1)\|^2_{\Omega\times Y},
\end{aligned}$$

where we have applied Korn's inequalities 5.2.1 and 5.2.2. The integral term vanishes, since

$$\begin{aligned}
&2\int_\Omega \int_Y \mathcal{E}_x(u_0 - \tilde{u}_0) : \mathcal{E}_y(u_1 - \tilde{u}_1)\,\mathrm{d}y\,\mathrm{d}x \\
&= 2\int_\Omega \int_Y \nabla_y \cdot \big[\mathcal{E}_x(u_0 - \tilde{u}_0)\,(u_1(x,y) - \tilde{u}_1(x,y))\big]\,\mathrm{d}y\,\mathrm{d}x \\
&= 2\int_\Omega \int_{\partial Y} \mathcal{E}_x(u_0 - \tilde{u}_0)\,(u_1(x,y) - \tilde{u}_1(x,y)) \cdot n\,\mathrm{d}\sigma_y\,\mathrm{d}x = 0.
\end{aligned}$$

Therefore, we get the uniqueness of u_0 in $L^2(S, W(\Omega))$ and u_1 in $[L^2(S\times\Omega; H^1_{\#}(Y)/\mathbb{R})]^N$. This proves that the entire sequences converge to the respective specified limit.

Strong form of the homogenised system

To finish the proof of theorem 6.1.1, we now derive the strong form of the homogenised system above. This will be accomplished by choosing special test functions and integrating by parts. First, we choose $\psi_0 \equiv 0$ in (6.1.25), which yields

$$\begin{aligned}
-\nabla_y \cdot \Big(&\mathcal{A}(c_{n,0})\big(\mathcal{E}_x(u_0) + \mathcal{E}_y(u_1) - e'(c_{n,0})c_0\mathbb{1}\big) \\
&+ \mathcal{A}'(c_{n,0})c_0\big(\mathcal{E}_x(u_{n,0}) + \mathcal{E}_y(u_{n,1}) - e(c_{n,0})\mathbb{1}\big)\Big) = 0.
\end{aligned} \tag{6.1.28}$$

This is the local equation (4.2.25) that we also already know from § 4.2.2 where we applied the method of asymptotic expansions to the linear system. Then, choosing $\psi_1 \equiv 0$ in (6.1.25)

and integrating by parts, we obtain

$$0 = -\sum_{j=1}^{N} \partial_{x_j} \int_Y \sum_{k,h=1}^{N} \Big(a_{ijkh}(c_{n,0}) \big(e_{khx}(u_0) + e_{khy}(u_1) - e' c_0 \delta_{kh} \big) + a'_{ijkh}(c_{n,0}) c_0 \big(e_{khx}(u_{n,0}) + e_{khy}(u_{n,1}) - e(c_{n,0}) \delta_{kh} \big) \Big) \, \mathrm{d}y \tag{6.1.29}$$

for $1 \leq i \leq N$, which is a macroscopic averaged equation. At this step, we have applied the following boundary conditions

$$\begin{aligned} u_0 &= 0 \quad \text{on } \Gamma_0 \times S, \\ \mathcal{S}_0 \, n &= g \quad \text{on } \Gamma_g \times S, \\ u_0 \cdot n &= 0 \quad \text{on } \Gamma_s \times S, \\ \tau \cdot \mathcal{S}_0 \, n &= 0 \quad \text{on } \Gamma_s \times S. \end{aligned}$$

Twofold integration by parts of the equation (6.1.24) finally gives us the *homogenised system* in a strong form:

$$\begin{aligned} \partial_t c_0 = \Delta_{yy} \Big(& f''(c_{n,0}) c_0 - \lambda \Delta_{yy} c_0 - e' \operatorname{tr} \mathcal{S}_0 \\ & + \big(\mathcal{E}(u_{n,0}) + \mathcal{E}_y(u_{n,1}) - e(c_{n,0}) \mathbb{1} \big) \\ & \quad : \mathcal{A}'(c_{n,0}) \big(\mathcal{E}_x(u_0) + \mathcal{E}_y(u_1) - e' c_0 \mathbb{1} \big) \\ & + \frac{1}{2} \big(\mathcal{E}(u_{n,0}) + \mathcal{E}_y(u_{n,1}) - e(c_{n,0}) \mathbb{1} \big) \\ & \quad : \mathcal{A}''(c_{n,0}) c_0 \big(\mathcal{E}(u_{n,0}) + \mathcal{E}_y(u_{n,1}) - e(c_{n,0}) \mathbb{1} \big) \Big) \quad \text{in } \Omega \times Y \times S, \end{aligned} \tag{6.1.30}$$

$$\begin{aligned} 0 = \nabla_y \cdot \Big(& \mathcal{A}(c_{n,0}) \big(\mathcal{E}_x(u_0) + \mathcal{E}_y(u_1) - e' c_0 \mathbb{1} \big) \\ & + \mathcal{A}'(c_{n,0}) c_0 \big(\mathcal{E}_x(u_{n,0}) + \mathcal{E}_y(u_{n,1}) - e(c_{n,0}) \mathbb{1} \big) \Big) \qquad \text{in } \Omega \times Y \times S, \end{aligned} \tag{6.1.31}$$

$$0 = -\sum_{j=1}^{N} \partial_{x_j} \int_Y \sum_{k,h=1}^{N} \Big(a_{ijkh}(c_{n,0}) \big(e_{khx}(u_0) + e_{khy}(u_1) - e' c_0 \delta_{kh} \big) + a'_{ijkh}(c_{n,0}) c_0 \big(e_{khx}(u_{n,0}) + e_{khy}(u_{n,1}) - e(c_{n,0}) \delta_{kh} \big) \Big) \, \mathrm{d}y \tag{6.1.32}$$

$$\text{in } \Omega \times Y \times S, \text{ for } i = 1, \ldots, N.$$

This system is equivalent to the equations (4.2.31), (4.2.33) and (4.2.25) of the formally homogenised linear system derived in § 4.2.2 when setting $c_{n,\epsilon} = c_{n,0}$ and $\mathcal{E}(u_{n,\epsilon}) = \mathcal{E}_x(u_{n,0}) + \mathcal{E}_y(u_{n,1})$, which is the limit of $c_{n,\epsilon}$ and $\mathcal{E}(u_{n,\epsilon})$ from § 4.2.1. From equations (6.1.30) and (6.1.32), we can eliminate the unknown u_1 and therefore the homogenised two-scale system can be decoupled in a macroscopic and a microscopic equation. For this, from equation (6.1.31)

together with the cell problems 4.1.1, we gain a representation for u_1 in terms of u_0 and the solutions of the cell problems. This representation is the same as the one we received in the previous chapter in the course of the procedure of asymptotic expansions. Therefore, the homogenised system above is equivalent to (4.2.35), (4.2.36) through the relation

$$\begin{aligned}\mathcal{A}(c_{n,0})\,\mathcal{E}_y(u_1) = \mathcal{A}(c_{n,0})\big(\mathcal{E}_\omega\,\mathcal{E}_x(u_0) + e'c_0\,\mathbb{1}\big)\\ - \mathcal{A}'(c_{n,0})\big(\mathcal{E}_x(u_{n,0}) + \mathcal{E}_y(u_{n,1}) - e(c_{n,0})\mathbb{1}\big)c_0\end{aligned} \tag{6.1.33}$$

or by

$$\mathcal{E}_y(u_1) = \mathcal{E}_\omega\,\mathcal{E}_x(u_0) + e'c_0\mathbb{1} - \mathcal{A}^{-1}(c_{n,0})\,\mathcal{A}'(c_{n,0})(\mathcal{E}_x(u_{n,0}) + \mathcal{E}_y(u_{n,1}) - e(c_{n,0})\mathbb{1})c_0. \tag{6.1.34}$$

Using the notation (4.2.20) and (4.2.21) introduced in § 4.2.1 in the course of the method of asymptotic expansions, we write the system (6.1.30)–(6.1.32) in the usual decoupled form:

$$\begin{aligned}\partial_t c_0 = \Delta_{yy}\Big(&f''(c_{n,0})c_0 - \lambda\Delta_{yy}c_0 - e'(c_{n,0})\,\mathrm{tr}\left[\mathcal{A}(c_{n,0})\left(\mathcal{E}_\omega + \mathcal{I}\right)\mathcal{E}_x(u_0)\right]\\ &- \big(\mathcal{E}_x(u_{n,0}) + \mathcal{E}_y(u_{n,1}) - e(c_{n,0})\mathbb{1}\big)\\ &\quad : \mathcal{A}'(c_{n,0})\mathcal{A}^{-1}(c_{n,0})\mathcal{A}'(c_{n,0})\big(\mathcal{E}_x(u_{n,0}) + \mathcal{E}_y(u_{n,1}) - e(c_{n,0})\mathbb{1}\big)c_0\big)\\ &+ \big(\mathcal{E}_x(u_{n,0}) + \mathcal{E}_y(u_{n,1}) - e(c_{n,0})\mathbb{1}\big) : \mathcal{A}'(c_{n,0})\big(\mathcal{E}_\omega + \mathcal{I}\big)\mathcal{E}_x(u_0)\\ &+ \frac{1}{2}\big(\mathcal{E}_x(u_{n,0}) + \mathcal{E}_y(u_{n,1}) - e(c_{n,0})\mathbb{1}\big)\\ &\quad : \mathcal{A}''(c_{n,0})c_0\left(\mathcal{E}_x(u_{n,0}) + \mathcal{E}_y(u_{n,1}) - e(c_{n,0})\mathbb{1}\right)\Big) \quad \text{in } \Omega\times Y\times S,\end{aligned} \tag{6.1.35}$$

$$0 = \nabla_x\cdot\left(\mathcal{A}^{\mathrm{hom}}\,\mathcal{E}_x(u_0)\right) \quad \text{in } \Omega\times Y\times S. \tag{6.1.36}$$

In this form of the homogenised system, we now find the effective or homogenised elasticity tensor $\mathcal{A}^{\mathrm{hom}}$ definied through its components

$$a^{\mathrm{hom}}_{ijkh} = \int\limits_Y \sum_{l,m=1}^{N} a_{ijlm}(c_{n,0})\left(\delta_{kl}\delta_{hm} + e_{lmy}(\omega^{kh})\right)\,\mathrm{d}y, \quad 1\le i,j,k,h\le N. \tag{6.1.37}$$

The only unknowns left in this system are c_0, the unknown of the microscopic equation (6.1.35), and the purely macroscopic displacement u_0.

6.2 Properties of the limit systems

In the following we want to state and recall properties of the two formally homogenised systems derived in section 4.2 and the two-scale limit system.

Note, that the rigorous homogenised system is also of the distributed-microstructure type, cf. § 4.2.1. Further, in the presented homogenised systems – formally and analytically rigorous – the effective elasticity tensor $\mathcal{A}^{\mathrm{hom}}$ is of the same form and it has the same properties as the oscillating tensor:

Corollary 6.2.1. *For $\mathcal{A}^{\mathrm{hom}}$ defined by (6.1.37), there exist positive numbers α^0, β^0, with $0 < \alpha^0 < \beta^0$, such that*

$$\mathcal{A}^{\mathrm{hom}}(\,\cdot\,, t) \in \mathcal{M}(\alpha^0, \beta^0, \Omega), \quad t \in S. \tag{6.2.1}$$

See [CD99] for the proof. Although the definition of the tensor class stated in [CD99] differs slightly from ours (cf. definition 4.1.1), because the additional symmetry condition (2.2.30) is not included there and the homogenised tensor stated there is constant on Ω, this does not affect the proof given there, since $a_{ijkh}(c_{n,0}) \in L^\infty(\Omega \times Y \times S)$.

Furthermore, the macroscopic equations of the three systems have the same structure and in particular the eigenstrain is macroscopically not present. However, the eigenstrain is still indirectly included in the microscopic equations via the cell solutions.

Linearisation and homogenisation

We have already seen that for the linearised system, the formally homogenised system and the two-scale limit system are equivalent. Now we would like to examine whether there is a connection between the linear homogenised system and the nonlinear formally homogenised system. To be able to make a comparison, we consider the nonlinear formally homogenised system (4.2.15), (4.2.16) completed by the local equation (4.2.7),

$$\begin{aligned}
\partial_t c_0 = {} & \Delta_{yy}\big(f'(c_0) - \lambda\Delta_y c_0 - e'(c_0)\operatorname{tr}\mathcal{S}_0 \\
& \qquad + \frac{1}{2}(\mathcal{E}_x(u_0) + \mathcal{E}_y(u_1) - e(c_0)\mathbb{1}) : \mathcal{A}'(c_0)\,(\mathcal{E}_x(u_0) + \mathcal{E}_y(u_1) - e(c_0)\mathbb{1})\big), \\
0 = {} & -\nabla_y \cdot \big(\mathcal{A}(c_0)\,(\mathcal{E}_x(u_0) + \mathcal{E}_y(u_1) - e(c_0)\mathbb{1})\big), \\
0 = {} & \sum_{j=1}^{N} \partial_{x_j} \int\limits_Y \sum_{k,h=1}^{N} a_{ijkh}(c_0)\big(e_{khx}(u_0) + e_{khy}(u_1) - e(c_0)\delta_{kh}\big)\,\mathrm{d}y, \quad 1 \le i \le N.
\end{aligned} \tag{6.2.2}$$

We linearise the above system about general solutions $c_{0,n}$, $u_{0,n}$ and $u_{1,n}$, i.e. we consider

$$c_0 = c_{0,n} + h\tilde{c}_0, \quad u_0 = u_{0,n} + h\tilde{u}_0, \quad \text{and} \quad u_1 = u_{1,n} + h\tilde{u}_1,$$

for some $\tilde{c}_0, \tilde{u}_0, \tilde{u}_1$ and a small $h > 0$. To enable a comparison, we restrict ourselves to a linear

eigenstrain as defined by (6.1.3). Then, $\tilde{c}_0, \tilde{u}_0, \tilde{u}_1$ fulfil the linearised system:

$$\begin{aligned}\partial_t \tilde{c}_0 = \Delta_y \Big(& f''(c_{0,n})\tilde{c}_0 - \lambda \Delta_y \tilde{c}_0 - e' \operatorname{tr}\left[\mathcal{A}(c_{0,n})\left(\mathcal{E}_x(\tilde{u}_0) + \mathcal{E}_y(\tilde{u}_1) - e'(c_{0,n})\tilde{c}_0 \mathbb{1}\right)\right] \\ & - e' \operatorname{tr}\left[\mathcal{A}'(c_{0,n})\tilde{c}_0 \left(\mathcal{E}_x(u_{0,n}) + \mathcal{E}_y(u_{1,n}) - e(c_{0,n})\mathbb{1}\right)\right] \\ & + \left(\mathcal{E}_x(u_{0,n}) + \mathcal{E}_y(u_{1,n}) - e(c_{0,n})\mathbb{1}\right) : \mathcal{A}'(c_{0,n})\left(\mathcal{E}_x(\tilde{u}_0) + \mathcal{E}_y(\tilde{u}_1) - e'\tilde{c}_0 \mathbb{1}\right) \\ & + \frac{1}{2}\left(\mathcal{E}_x(u_{0,n}) + \mathcal{E}_y(u_{1,n}) - e(c_{0,n})\mathbb{1}\right) : \mathcal{A}''(c_{0,n})\tilde{c}_0 \left(\mathcal{E}_x(u_{0,n}) + \mathcal{E}_y(u_{1,n}) - e(c_{0,n})\mathbb{1}\right)\Big),\end{aligned} \tag{6.2.3}$$

$$\begin{aligned}0 = \nabla_y \cdot \Big(& \mathcal{A}'(c_{0,n})\tilde{c}_0\big(\mathcal{E}_x(u_{0,n}) + \mathcal{E}_y(u_{1,n}) - e(c_{0,n})\mathbb{1}\big) \\ & + \mathcal{A}(c_{0,n})\big(\mathcal{E}_x(\tilde{u}_0) + \mathcal{E}_y(\tilde{u}_1) - e'(c_{0,n})\tilde{c}_0 \mathbb{1}\big)\Big),\end{aligned} \tag{6.2.4}$$

$$\begin{aligned}0 = \sum_{j,k,h=1}^{N} \partial_{x_j} \int_Y & a_{ijkh}(c_{0,n})(e_{khx}(\tilde{u}_0) + e_{khy}(\tilde{u}_1) - e'(c_{0,n})\tilde{c}_0\delta_{kh}) \\ & + a'_{ijkh}(c_{0,n})\tilde{c}_0 \left(e_{khx}(u_{0,n}) + e_{khy}(u_{1,n}) - e(c_{0,n})\delta_{kh}\right) \mathrm{d}y, \quad 1 \le i \le N,\end{aligned} \tag{6.2.5}$$

These equations correspond to the two-scale homogenised system (6.1.30), (6.1.31) and (6.1.32). Homogenisation and linearisation therefore commutate here. This relation is illustrated in figure 6.1. We were able to homogenise the scaled nonlinear system formally via asymptotic expansions. A linearisation of this nonlinear formally homogenised system leads to the linear homogenised system, the convergence of which we could prove rigorously.

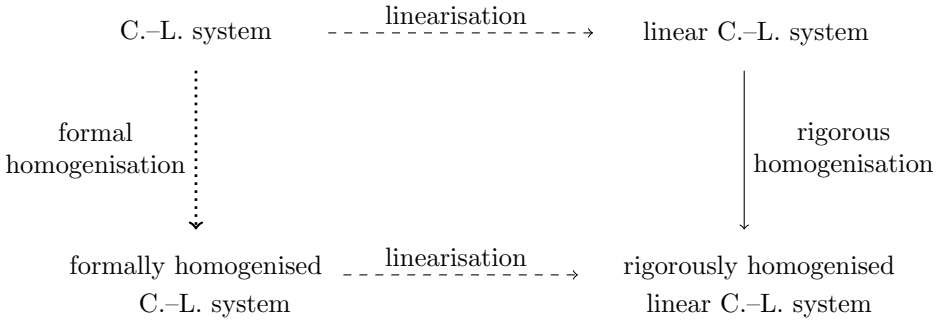

Figure 6.1: Relationship of the systems

7 Numerical simulations

In the following, we consider the nonlinear distributed-microstructure model resulting from the formal homogenisation process derived in § 4.2.1, where we focus on numerical simulations of this model. Numerical analysis for models of the distributed-microstructure type can be found for example in [Pes92] or in [Arb89].

As we have already noted in the course of the nondimensionalisation and scaling of the system, no complete measurement data from the experiments are available, so that we want to test the formally homogenised system phenomenologically numerically and demonstrate what can be realised with the model for $N = 2$.

For convenience, we repeat the essential equations. We consider the distributed-microstructure model resulting from the formal homogenisation process with the equation describing the phase separation on the microscale

$$\begin{aligned}\partial_t c_0 = 10^{-2}\,\Delta_y\Big(f'(c_0) - \lambda\Delta_y c_0 - e'(c_0)\,\mathrm{tr}\left[\mathcal{A}(c_0)(\mathcal{I}+\mathcal{E}_\omega)\,\mathcal{E}_x(u_0)\right] \\ + \frac{1}{2}(\mathcal{I}+\mathcal{E}_\omega)\,\mathcal{E}_x(u_0) : \mathcal{A}'(c_0)\,(\mathcal{I}+\mathcal{E}_\omega)\,\mathcal{E}_x(u_0)\Big) \quad \text{in } \Omega\times Y\times S,\end{aligned} \tag{7.0.1}$$

the macroscopic equation for the mechanics

$$0 = \kappa\,\nabla_x\cdot\left(\mathcal{A}^{\mathrm{hom}}\,\mathcal{E}_x(u_0)\right) \quad \text{in } \Omega\times S, \tag{7.0.2}$$

and the cell problems

$$-\nabla_y\cdot\left(\mathcal{A}(y)\,\mathcal{E}_y(\omega^{lm})\right) = \nabla_y\cdot\left(\mathcal{A}(y)\,\mathcal{E}_y(\lambda^{lm})\right) \quad \text{in } Y, \tag{7.0.3}$$

for $l, m = 1, 2$. We have now supplemented equations (7.0.1) and (7.0.2) again with the constants 10^{-2} and κ from section 2.4.

We choose $\Omega = (0,1)^2$ as macroscopic domain provided with the boundary parts as specified in § 2.2.2 and a standard unit cell $Y_{x_i} = Y = (0,1)^2$ at each macroscopic point. Since we do not rely on experiments for our simulations anyway, we choose slightly different boundary conditions than those we motivated in § 2.2.2. We choose these in order to obtain a non-uniform macroscopic strain and thus have a different local influence on the separation process. For the displacement, we now choose a zero Dirichlet boundary condition also on the lateral

parts of the boundary,

$$u = 0 \quad \text{on } (\Gamma_0 \cup \Gamma_s) \times S. \tag{7.0.4}$$

To realise the process of compression, we use a path-controlled approach and set

$$u \cdot n = u_g \quad \text{on } \Gamma_g \times S, \tag{7.0.5}$$

as well as free slip in tangential direction on $\Gamma_g \times S$ instead of the force-controlled approach which we used for the modelling an the analysis. This choice is practically motivated, because the advantage of (7.0.5) is that the magnitude of the deformation can be easily controlled in the course of numerical simulations. For c_0, we have periodic boundary conditions and as initial condition we use a locally randomly disturbed constant function c_{m}, which is Y-periodic in y. More precisely,

$$c_{\mathrm{in}}(y) = c_{\mathrm{m}} + \xi(y), \quad y \in Y,$$

where ξ is function drawing random numbers from a uniform distribution in the interval $[-0.005, 0.005)$ for each argument and c_{in} is Y-periodic.

Numerical scheme

To solve the above equations numerically, we use finite element methods. To solve the equation describing the phase separation numerically, we use a mixed finite element method. For this purpose, we write the microscopic fourth-order equation (7.0.1) as a system of equations of second-order by using the chemical potential μ_0 as an auxiliary variable as described in § 2.2.2. This allows us to use globally continuous, piecewise affine trial functions for c_0 and μ_0 with respect to a given conformal triangulation $S_h(Y)$ of Y. We use periodic boundary conditions for c_0 and μ_0. For discretisation in time, we use the backward Euler method. The same numerical methods were used in [Wei02] for solving the Cahn–Larché system numerically in a single-scale setting. Further, we use the same finite element test and trial functions for solving each cell problem numerically, a standard choice for a classical finite element approach of second-order problems. For the numerical treatment of the macroscopic equation (7.0.2), we choose globally continuous, piecewise linear vector-valued trial functions for u_0 with respect to a conformal triangulation $S_{h_c}(\Omega)$ of Ω.

The micro–macro coupling

Let N_Ω denote the number of nodes associated to the macroscopic mesh $S_{h_c}(\Omega)$. At each node x_i, $i = 1, \ldots, N_\Omega$, of the macroscopic mesh, there is an associated unit cell $Y_{x_i} = Y$ provided with a finer mesh compared with the macroscopic one, as illustrated in figure 7.1. Owing to the fact that the system is the result of a process-adapted homogenisation procedure, it is sufficient to take the macroscopic mesh quite coarse.

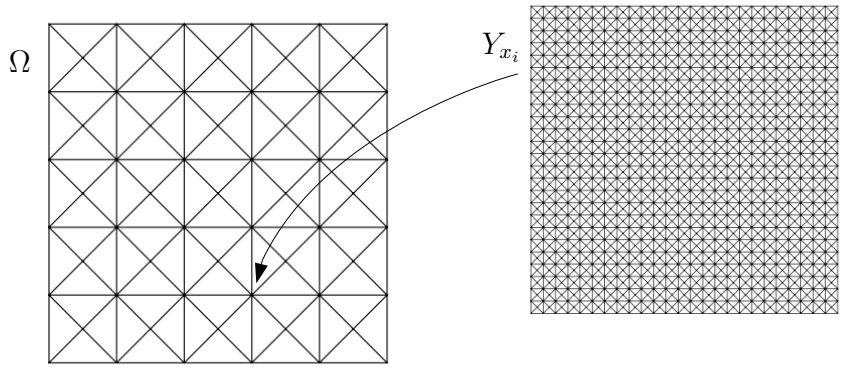

Figure 7.1: Visualisation of the macroscopic domain Ω provided with an exemplary coarse macroscopic mesh and a unit cell Y_{x_i} provided with a fine mesh attached in a node of the macroscopic mesh.

For a fixed timestep size $\tau > 0$ we consider the discrete timesteps $t_k = t_{k-1} + \tau$ or $t_k = k\,\tau$, for $k = 1, \ldots, k_{\max}$ for one $k_{\max} \in \mathbb{N}$ and we set $T_{\max} \coloneqq \tau k_{\max}$. Then, the solution procedure at each discrete timestep t_k works as follows:

$t_k \coloneqq 0$
while $t_k < T_{\max}$ **do**

  for $i = 1, \ldots, N_\Omega$ **do**
    for $l, m = 1, 2$ **do**
      solve the cell problem (7.0.3) on Y_{x_i}
    end for
    assemble $\mathcal{A}^{\hom}$ in each x_i
  end for

  interpolate $\mathcal{A}^{\hom}$ on Ω
  solve macroscopic problem (7.0.2), (7.0.4), (7.0.5)

  for $i = 1, \ldots, N_\Omega$ **do**
    evaluate $\mathcal{E}_x(u_0)$ at each macroscopic point x_i
    solve microscopic evolution equation (7.0.1) in Y_i
  end for

  $t_k = t_{k+1}$
end while

So first, in each time step, we solve the cell problems in each unit cell Y_{x_i} associated to each macroscopic node x_i of the macroscopic mesh. With these cell solutions, we can assemble and solve the macroscopic equation. Then, with the calculated macroscopic displacement, iterating over each macroscopic node x_i, we solve the evolution equation in every microscopic cell Y_{x_i}. In fact, since $\mathcal{E}_y(\lambda^{ij}) = \mathcal{E}_y(\lambda^{ji})$, for $i, j = 1, 2$, only three cell problems have to be solved on each Y_{x_i} in every time step.

The implementation was realised by using the programming language Python and the finite element library FEniCS [AL12]. Although this platform provides a wide range of implemented finite elements and nonlinear and linear solvers, there is no pre-implemented tool for a micro–macro coupling in a homogenisation setting. The resulting data was visualised using ParaView [Aya19].

We examine four cases: we consider isotropic as well as anisotropic elasticity and binodal as well as spinodal phase separation. In the following simulations, we choose $c_\mathrm{m} = 0.3$ when we consider binodal phase separation and $c_\mathrm{m} = 0.5$ in the case of spinodal phase separation. In each of these two cases, i.e. binodal and spinodal phase separation, we always take the exact same initial value for all simulations and for c_0 in each Y_{x_i}. In addition, we compare all four case studies with numerical simulations of the Cahn–Hilliard equation, non-dimensionalised corresponding to section 2.4, to compare the respective separation process with a separation process without the influence of mechanical stress. In each of the following cases, this is done by using the same values for the parameters λ and φ, the scaling parameter of the local free energy, as well as exactly the same initial value for c. We then solve the Cahn–Hilliard equation numerically on $(0, 1)^2$ with the same numerical methods and using periodic boundary conditions.

According to [BFL$^+$13] and noting that we have already taken care of the factor ϵ^2, we choose $\lambda = 10^{-4}$ in all following simulations and the timestep size $\tau = 5 \times 10^{-2}$. Figure 7.2 shows the magnitude of the displacement with some marked points of the macroscopic domain in which we consider the separation processes in all following simulations, where we have compressed the macroscopic domain by 5 % in horizontal direction.

As can be seen in figure 7.2, we have chosen a rather coarse macroscopic mesh. With the selected boundary conditions, this should actually be finer near the two right corner points of Ω. However, since we are primarily interested in the microscopic processes and we do not make any comparisons to experiments, we have chosen a coarse mesh for reasons of computing effort. The microscopic mesh is chosen in such a way that an alignment of the pattern of the evolving microstructure caused by structures of the mesh is avoided and we refer to [Fra14] for studies on such mesh effects. Unless stated otherwise, for the following simulations of the phase-separation processes, we use the colour bar given by figure 7.3 for the representation of the order parameter c. Of course, due to the numerical solution methods and modelling

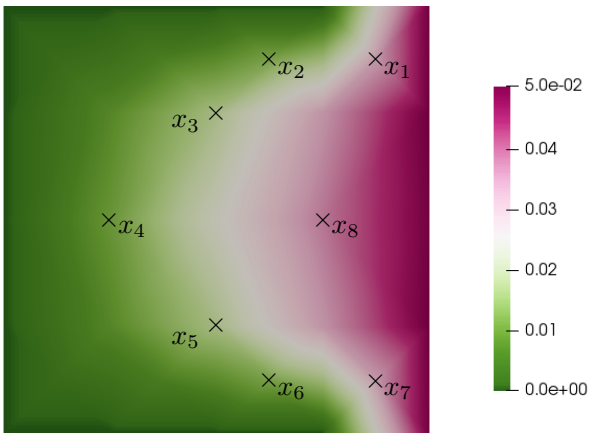

Figure 7.2: Typical magnitude of the macroscopic displacement u_0 and eight marked macroscopic points $x_1, \ldots, x_8$.

aspects, such as the choice of the local free energy, there may be a deviation beyond the limits 0 and 1 for values of the order parameter. However, these are minimal and for standardisation we always use the colour bar given below.

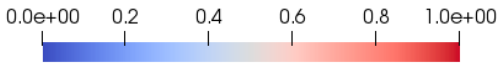

Figure 7.3: Colour bar giving values from 0 to 1 for the visualisation of the order parameter c.

As one can see, the macroscopic strain $\mathcal{E}(u_0)$ enters in the evolution equation (7.0.1) describing the evolving microstructure and, as it may be different in each macroscopic point, the microstructure may be different in each macroscopic point. For the numerical simulations, we have chosen the boundary conditions for the displacement in such a way that the strain tensor varies locally and, in particular, includes shear. In the following simulations, we therefore expect that the phase separations in the different macroscopic points differ from each other and that possibly an influence on the resulting patterns can be detected.

7.1 The case of isotropic elasticity

First, we consider the isotropic case with an elasticity tensor defined in § 2.2.2, where we choose

$$\lambda^{\mathrm{E}} = 0.1, \quad \mu^{\mathrm{E}} = 0.1 \tag{7.1.1}$$

for the elastically softer phase and

$$\lambda^{\mathrm{C}} = 0.3, \quad \mu^{\mathrm{C}} = 0.2 \tag{7.1.2}$$

for the elastically slightly harder phase. Further, we use $\varphi = 0.7$ and $e'(c) = 0.6$.

7.1.1 Binodal phase separation

In the case of isotropic binodal phase separation, we first compare the evolution in time of the separation process in the macroscopic point x_7 of the distributed-microsctructure model with the separation process without elasticity of the corresponding Cahn–Hilliard simulation. Figure 7.4 shows the results of the Cahn–Hilliard simulation in the left column and the results of the simulation of the distributed-microsctructure model in the right column. Plots in one row are at the same time t_k specified underneith. The results of the Cahn–Hilliard simulation first show the separation process, which is quite far advanced already at time t_{40}.

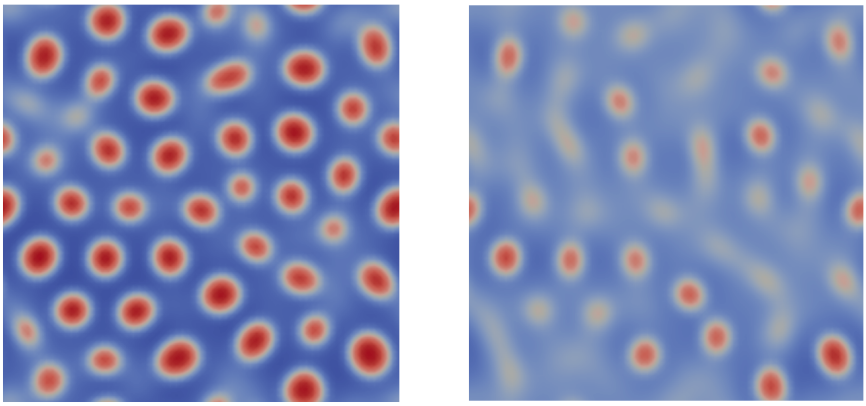

(a) $t_{35} = 1.75$

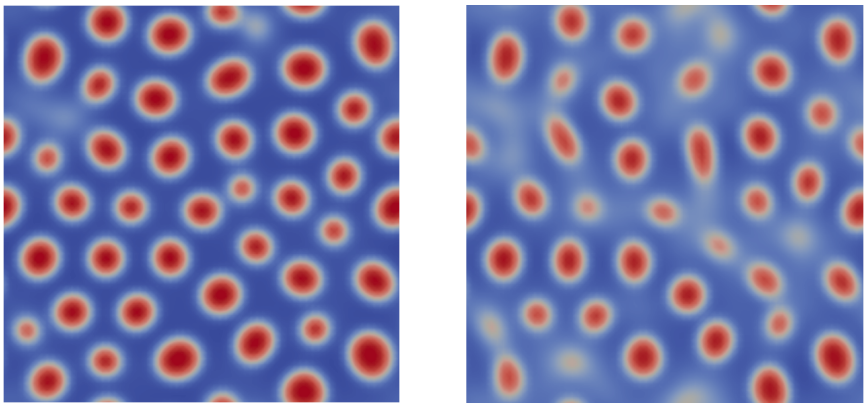

(b) $t_{40} = 2$

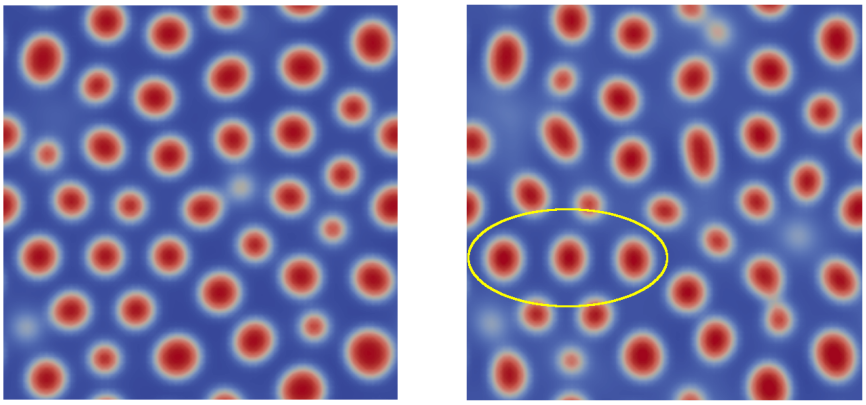

(c) $t_{45} = 2.25$

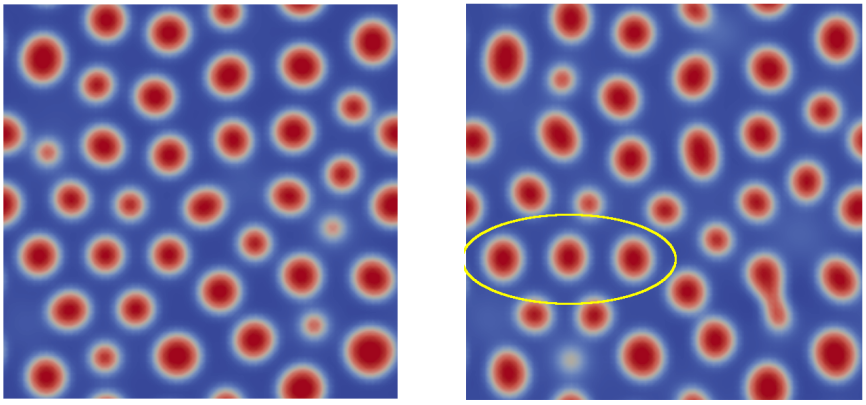

(d) $t_{50} = 2.5$

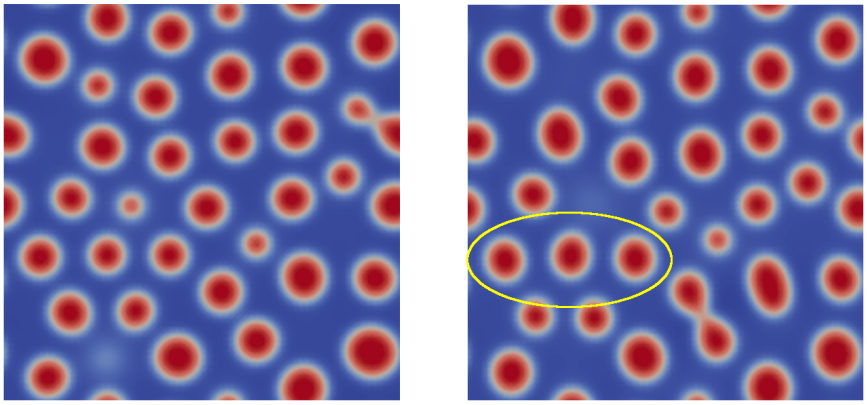

(e) $t_{65} = 3.25$

Figure 7.4: Pattern of two separation processes at different times t_k; left: results of the Cahn–Hilliard model simulation; right: results of the distributed-microstructure model simulation in the point x_7.

This results in regions of pure phases and domains of one component (corresponding to $c = 1$) are formed in the other contiguous phase (corresponding to $c = 0$). As time progresses further, the fusion and growth of the domains can be observed, which corresponds to a reduction of the phase boundaries. The shape of the domains corresponds to the energetically favourable circular shape. During the fusion of two domains, ellipsoidal structures also occur temporarily, as can be seen particularly well in figures 7.4a and 7.4b, but these quickly relax again into circular-shaped domains. Considering the results of the DM simulation (we use this abbreviation in what follows for the simulation of the distributed-microstructure model), one can see that the process is roughly the same as in the Cahn–Hilliard simulation. The initially homogeneous mixture separates, regions of pure phases are formed and the resulting domains of the elastically harder phase merge and grow together. A comparison of the two separation processes shows first of all that the separation of the phases is slower in the DM-simulation in x_7 than in the Cahn–Hilliard simulation. This seems to be generally the case in macroscopic points close to the compression boundary Γ_{g}. Even more significantly, the domains in the DM simulation are not only ellipsoidal during fusion. This can be clearly seen especially when looking at the emerging microstructure, i.e. at times t_{30} and t_{35}. This ellipsoidal structure is retained for at least a certain period of time as time progresses, which can be seen in particular, for example, in the domains marked yellow at times t_{45}, t_{50} and t_{65} and in comparison to the corresponding domains at the same times of the Cahn–Hilliard simulation. These marked domains do not grow and remain ellisoidal-shaped during the considered period. In the DM simulation, the ellipsoid structure is already recognisable from the beginning, i.e. immediately with the formation of the domains, see figures 7.4a and 7.4b. These plots also show particularly well that the ellipsoidal domains seem to be aligned in the direction from top to bottom. This circumstance is also observable in the other plots of the DM simulation.

Since the effect of the ellipsoid-shaped domains described above is more noticeable at an earlier stage of the process shown in figure 7.4, we take a closer look on it. In figure 7.5, we consider the evolution in time of the microstructure in the macroscopic points x_6 and x_2, where the corresponding results are shown in the left and the middle column of figure 7.5, respectively. In the right column of the figure, the colour bar is stated for the presented results in the corresponding row. To improve the resolution of the microstructure, it is scaled according to the plots in each row. For this reason we use here the only time a different colour scale than our standard colour scale given by figure 7.3. Figure 7.5a shows plots of the evolving micrcostructure at time $t_{20} = 1$. The mixture has not yet been separated far, but the patterns in the two points considered already show a different orientation, which can be seen well in comparison to each other. The pattern in x_6 is aligned more strongly along the diagonal from the upper left corner to the lower right corner, whereas the pattern in x_2 is aligned more closely along the diagonal from the upper right corner to the lower left corner. This alignment can also be observed with continued separation at time t_{25}, see figure 7.5b. At t_{37}, regions of pure phases are present. As can be seen in figure 7.5c, the orientation of the patterns remains unchanged.

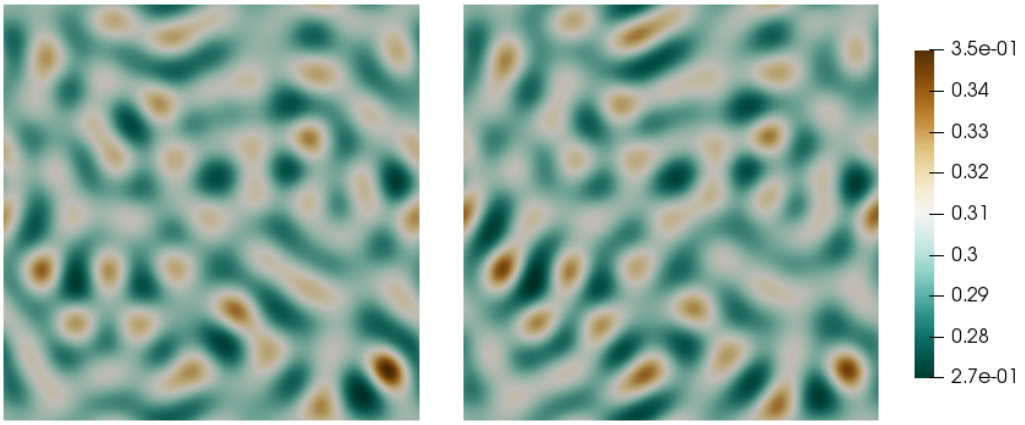

(a) Pattern at $t_{20} = 1$.

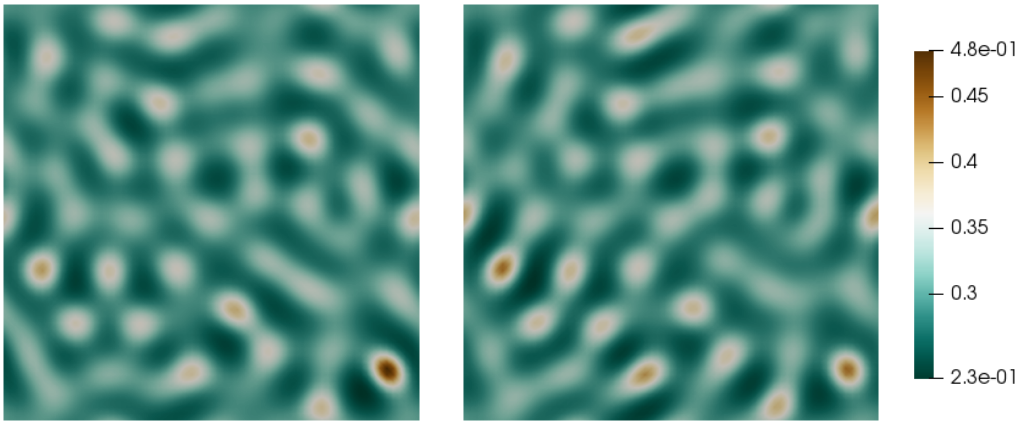

(b) Pattern at $t_{25} = 1.25$.

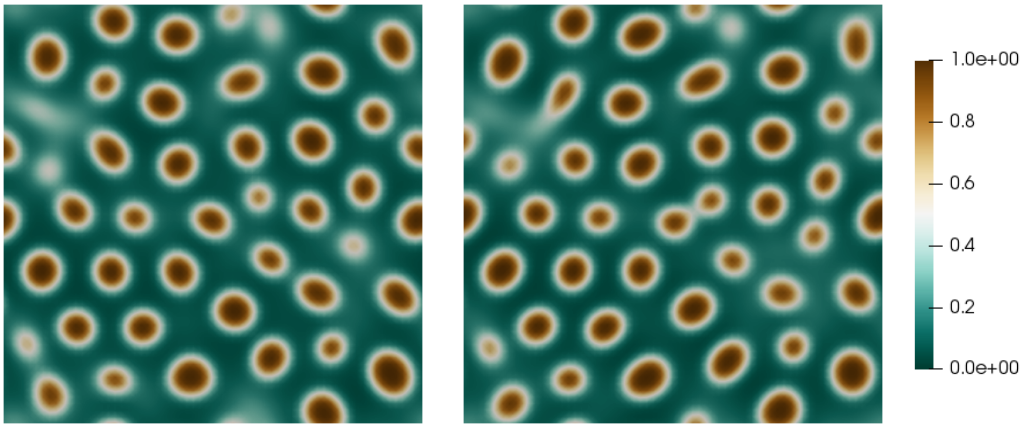

(c) Pattern at $t_{37} = 1.85$.

Figure 7.5: Pattern of the evolving microstructure showing different alignments; left: pattern in x_6; middle: pattern in x_2; right: corresponding colour bars.

Figure 7.6 shows patterns in different macroscopic points with different alignment of the domains. The arrangement of the single results corresponds approximately to the position of the macroscopic points in Ω to which the patterns belong, cf. figure 7.2.

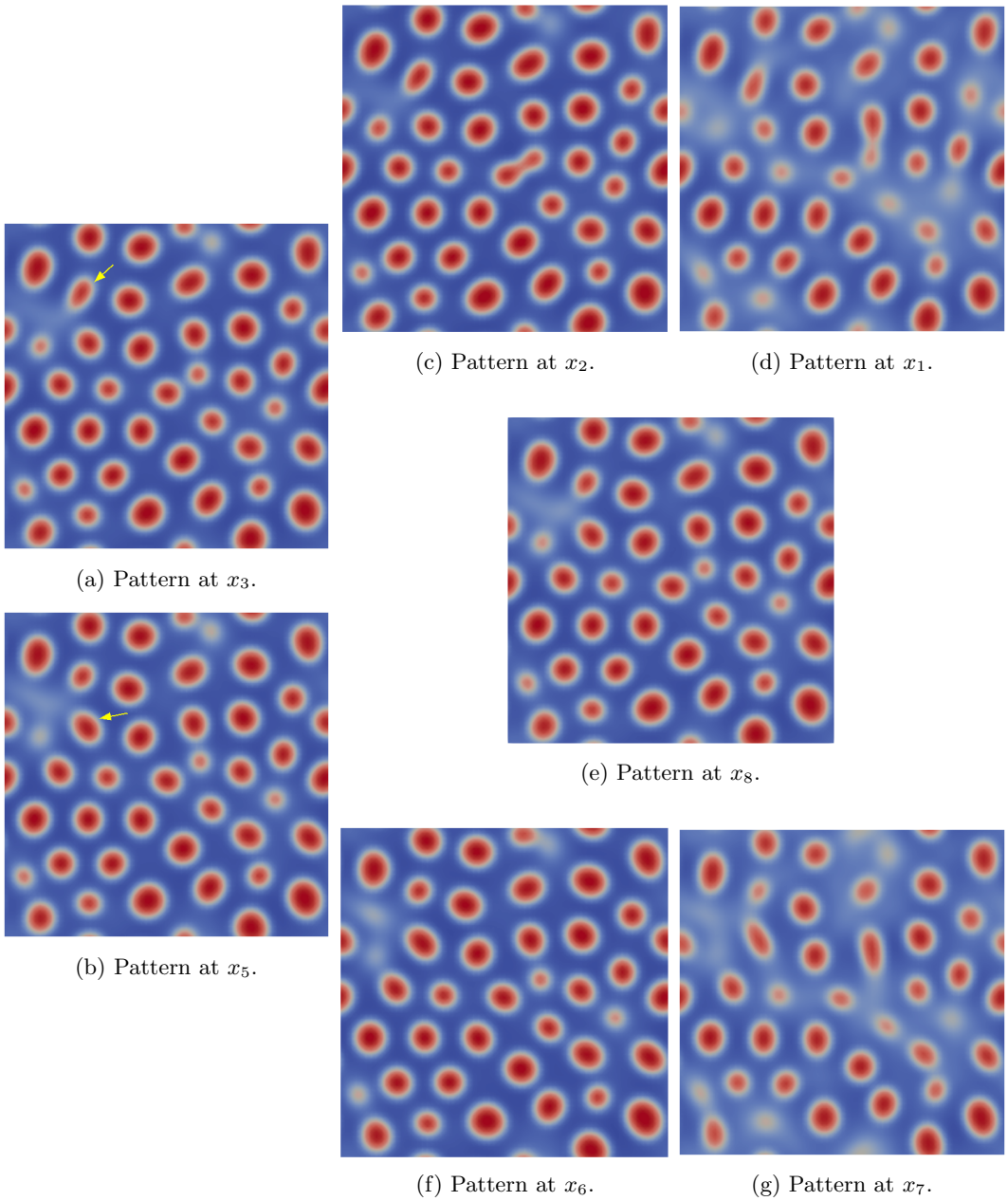

(a) Pattern at x_3.

(b) Pattern at x_5.

(c) Pattern at x_2.

(d) Pattern at x_1.

(e) Pattern at x_8.

(f) Pattern at x_6.

(g) Pattern at x_7.

Figure 7.6: Pattern of the evolving microstructure in different macroscopic points at time $t_{40} = 2$.

The orientation of ellipsoidal domains is most obvious in points x_1 and x_7, see figures 7.6d and 7.6g. The orientation here is roughly from top to bottom, whereas in point x_1 several domains show a slightly tilted inclination towards the lower left corner in comparison with those in point x_7. What can also be seen here, and what can be observed again and again in other simulations, is that there seems to be a preferred direction in which domains merge with other domains. This direction corresponds to the direction of the respective orientation angle of the ellipsoidal domains. If one compares the patterns in points x_1 and x_2 as well as x_6 and x_7 with each other, a fine difference of the orientation direction of some domains can be determined. If one looks from figure 7.6d to figure 7.6c the inclination of the domains seems to change slightly towards the lower left corner; if one goes from figure 7.6g to figure 7.6f the domains incline more towards the upper left corner. Accordingly, and as can be seen very well in a direct comparison, the difference in the orientation of the domains also increases between the patterns in the points x_2 and x_6. Generally, it can be observed that the orientation direction of the domains in macroscopic points in the upper half of Ω is rather towards the lower left corner and the upper right corner (which corresponds to the points x_1, x_2 and x_3), whereas the domains in the macroscopic points of the lower half of Ω are rather oriented towards the upper left corner and the lower right corner (which corresponds to the points x_5, x_6 and x_7). In the following, we often refer to these two occurring directions, the two diagonals just described, as orientation diagonals for the alignment of the patterns. The patterns shown by figures 7.6a and 7.6b hardly differ and the orientation behaviour described above is only slightly present here, consider the marked domains in figures 7.6a and 7.6b. The point x_8 lies exactly in the middle along the vertical coordinate of Ω. A difference of the pattern in this point compared to the patterns in x_3 or x_5 is hardly recognisable in this case.

These observations fully meet our initial expectations. The macroscopic strain influences the phase separation. It has an effect on the shape and orientation of the domains and the dynamics of the separation process, e.g. merging of domains.

7.1.2 Spinodal phase separation

The influence of the locally different macroscopic strain becomes more pronounced in the case of spinodal separation. First, we compare the Cahn–Hilliard simulation with the simulation of the separation process in the macroscopic point x_7. The patterns at different times can be seen in figure 7.7. In the left column of the figure, there are the results of the Cahn–Hilliard simulation, in the right column the plots of the solution of the DM simulation. Results next to each other are at the same time specified underneith. For the following comparison of the results from the two simulations, we have chosen different points in times than for the corresponding comparison in the case of binodal separation. The only reason for this is that the phase separation is faster here and the selected points in time are adjusted accordingly.

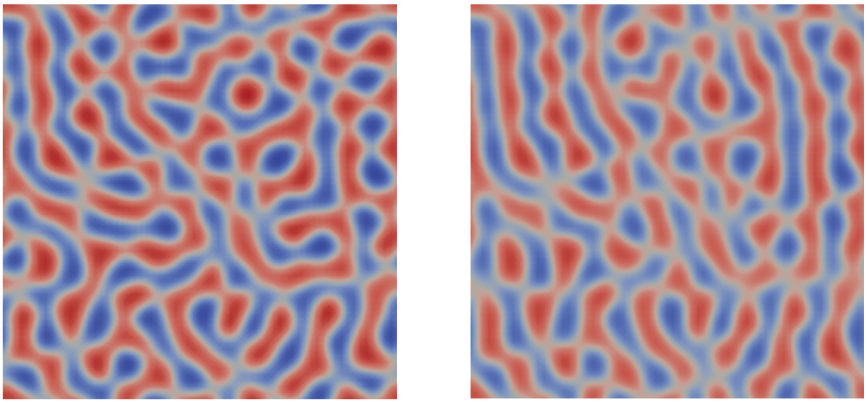

(a) $t_{10} = 6 \times 10^{-1}$

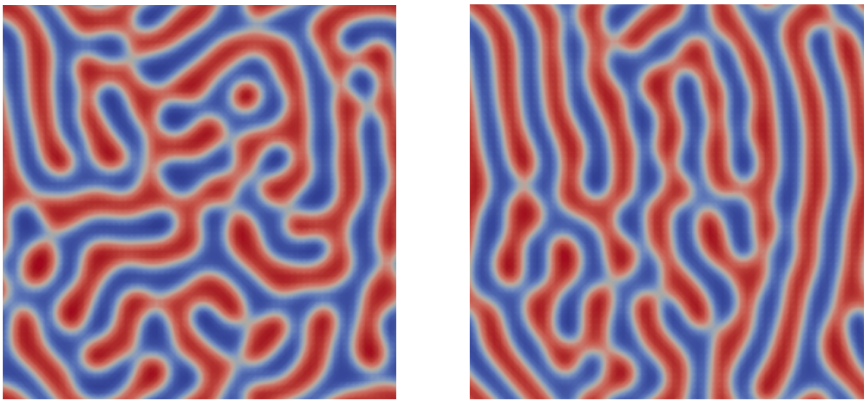

(b) $t_{20} = 1$

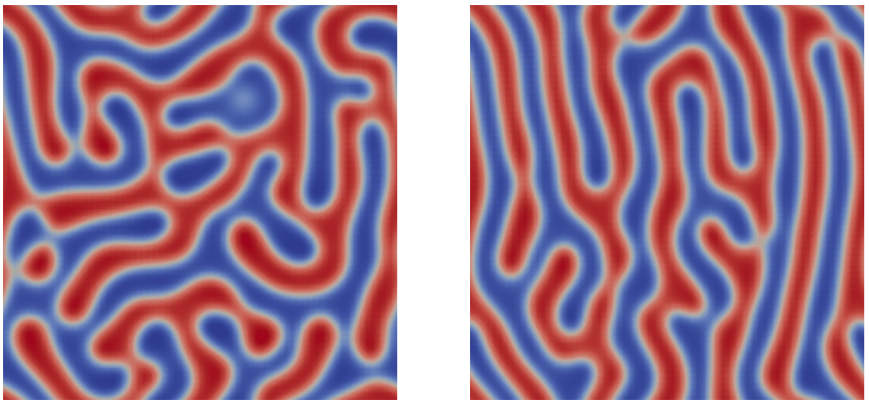

(c) $t_{30} = 1.5$

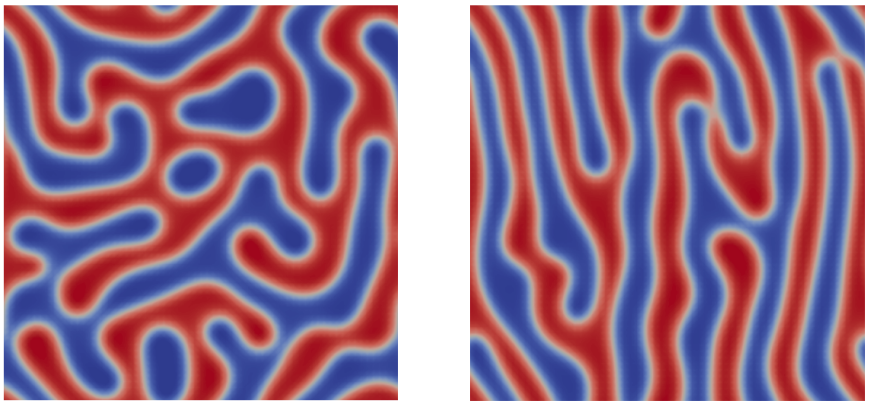

(d) $t_{45} = 2.25$

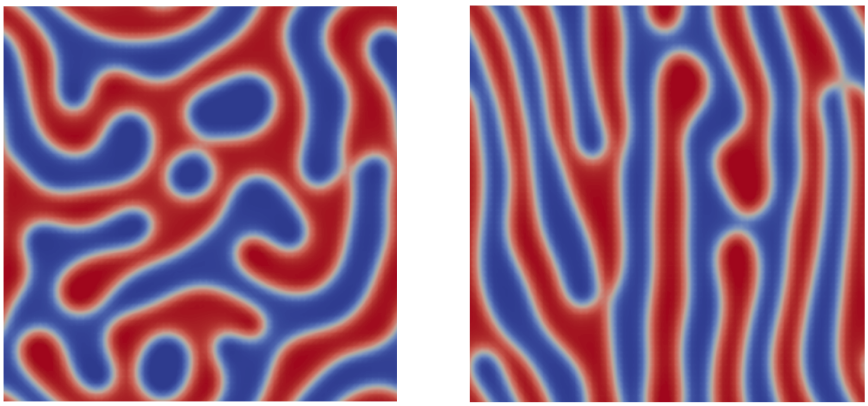

(e) $t_{65} = 3.25$

Figure 7.7: Pattern of two separation processes at different times t_k; left: results of the Cahn–Hilliard model simulation; right: results of the distributed-microstructure model simulation in the macroscopic point x_7.

The process of both simulations is roughly the same. In the beginning, the homogeneous mixture seperates and regions of pure phases are formed, but in comparison to binodal phase separation, no circular or ellipsoidal domains are formed. It is rather a pattern of confused snakes that emerges. As time progresses, the regions of the pure phases grow, which corresponds to a reduction of the phase boundaries. At time t_{10}, the phase separation has not completed yet in both cases. At this time, in contrast to the Cahn–Hilliard simulation, in the DM simulation a vertical orientation of the microstructure is clearly visible. This difference becomes clearer at time t_{20}. The plots of the DM simulation show the vertical alignment of the pattern and there are structures which extend over the entire domain from top to bottom. As time progresses, this preferential alignment of the patterns also remains present during the growth of the pure phases as can be seen at times t_{35}, t_{45} and t_{65}. In a slight exaggeration, the structure of the pattern becomes more similar to vertical stripes as time proceeds. A comparison of figures 7.7d and 7.7e also shows that the phase boundaries smoothen over time. The patterns of the Cahn–Hilliard simulation, on the other hand, still appear disordered and do not show any orientation.

In figure 7.8, one can nicely distinguish a different orientation of the pattern in different macroscopic points. As in figure 7.6, the arrangement of the single macroscopic pictures corresponds approximately to the position of the macroscopic points to which the patterns belong. In spinodal separation, the characteristics of the different orientations of the patterns are more pronounced. At first glance, it can be said that in all patterns shown by figure 7.8 a certain orientation is noticeable in comparison to the pattern of the Cahn–Hilliard simulation, cf. figure 7.7e. As before, we first look at the patterns in the two points on the right, i.e. in x_1 and x_7. The pattern shown by figures 7.8g and figure 7.8d show more or less an orientation from top to bottom, whereby this alignment is more significant in the pattern in x_7. In x_1, the pattern already shows a more oblique inclination. The observation that we made in the binodal case during the discussion of figure 7.6 also applies here, that is that the microstructure in those macroscopic points that are located in the upper half of Ω is oriented along the diagonals between the lower left corner and the upper right corner, whereas the resulting patterns in those points from the lower half of Ω are oriented along the opposite diagonals, i.e. from the upper left corner to the lower left corner. In the spinodal case, it is wonderful to see an orientation of the patterns when looking at figures 7.8d, 7.8c and 7.8a as well as figures 7.8g, 7.8f and 7.8b, which deviates differently from the corresponding orientation diagonal. Thus, as already mentioned, the pattern in x_1 has only a very slight inclination along the corresponding diagonals, whereas the orientation of the pattern in x_2 is strongly oriented to the diagonal. The pattern belonging to point x_3 is rather vertical; nevertheless, there are diagonal structures present, although less or with slight deviation to the orientation diagonal compared to the pattern in point x_2. In x_7, the pattern extends rather from top to bottom, whereby in the left half an orientation can be seen to the upper corner and thus according to the orientation diagonals. The pattern in x_6 is clearly oriented to the diagonal and thus opposed to the orientation of the pattern shown by figure 7.8c. Like the pattern in x_3, the pattern in x_5 has a certain vertical orientation; however, some structures are orientated towards the corresponding orientation diagonal. The

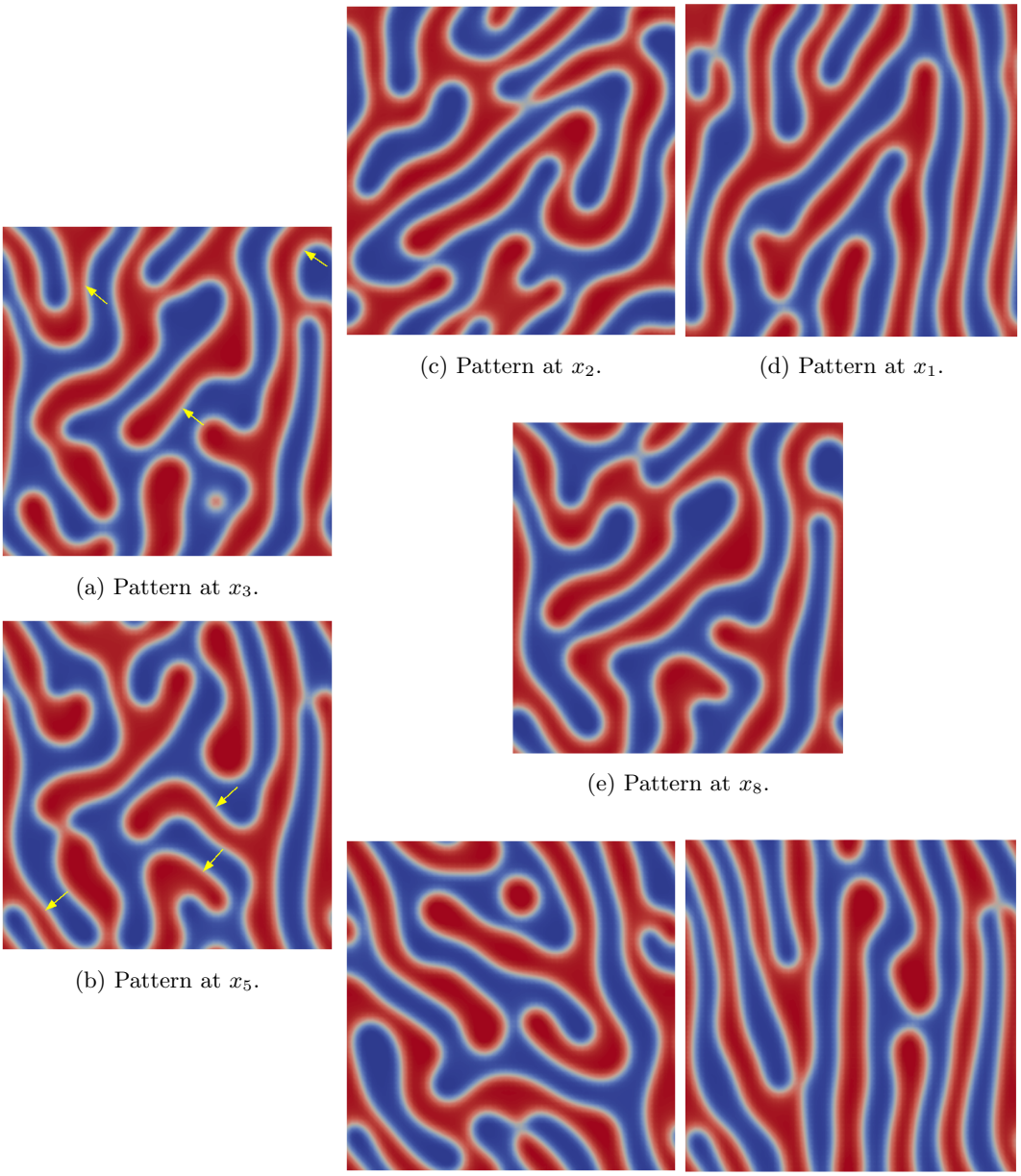

(a) Pattern at x_3.

(b) Pattern at x_5.

(c) Pattern at x_2.

(d) Pattern at x_1.

(e) Pattern at x_8.

(f) Pattern at x_6.

(g) Pattern at x_7.

Figure 7.8: Pattern of the evolving microstructure at different macroscopic points at time $t_{65} = 3.25$.

yellow markings in figures 7.8a and 7.8b indicate structures that are arranged more in the direction of the orientation of the patterns shown by figures 7.8c and 7.8f, respectively. Located vertically centred in Ω, the formation of the pattern presented by figure 7.8e can be observed. In comparison to the pattern of the Cahn–Hilliard simulation, cf. figure 7.7, the pattern is also

rather vertically aligned, but also a diagonal alignment of the structure can be detected.

Results for increased stiffness

Finally, we investigate which effects occur when we make the material elastically stiffer. We increase the Lamé constants to

$$\lambda^{\mathrm{C}} = 2.4, \quad \mu^{\mathrm{C}} = 1.6, \quad \lambda^{\mathrm{E}} = 0.8, \quad \mu^{\mathrm{E}} = 0.8. \tag{7.1.3}$$

which means to enlarge the stiffness. The first row in figure 7.9 shows the resulting DM simulation patterns at selected macroscopic points with the Lamé constants given by (7.1.3). In the second row, the respective results of the DM simulation with the previously used Lamé constants given by (7.1.1) and (7.1.2) at the same point in time can be seen. Figures 7.9a and

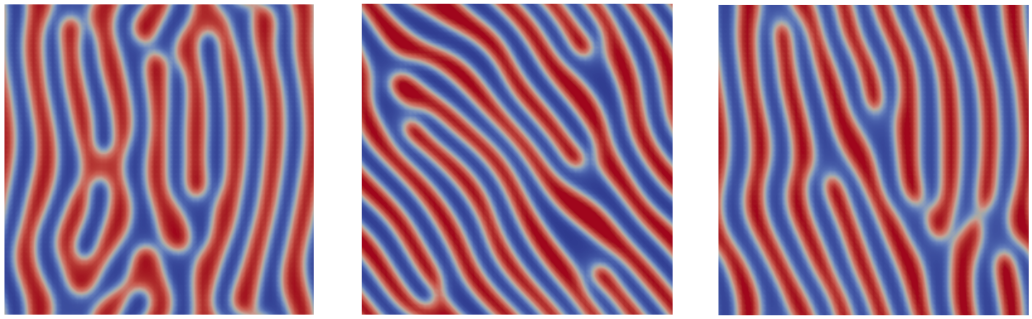

(a) Pattern at x_4 (b) Pattern at x_6 (c) Pattern at x_7

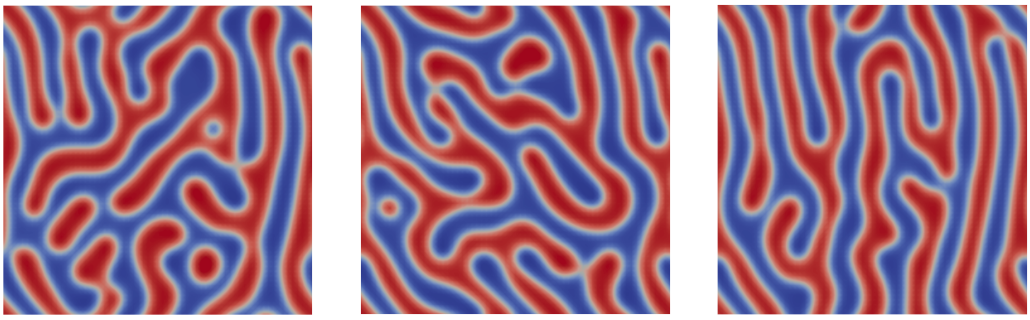

(d) Pattern at x_4 (e) Pattern at x_6 (f) Pattern at x_7

Figure 7.9: Pattern at different macroscopic points at time $t_{35} = 1.75$.

7.9d show patterns in the in the vertically centred macroscopic point x_4 at time $t_{35} = 1.75$. In the case of higher Lamé constants, the vertical alignment of the pattern is much more pronounced at this time and corresponds to the expectations concerning the orientation of the pattern in a macroscopic vertically central point. Figures 7.9b and 7.9e show patterns in x_6, which is located in the lower half of Ω. In the plot of the simulation with the values for elastically harder components, the orientation of the patterns is also much more stringent here

than in the case of elastically softer components. In figur 7.9b, the pattern has hardly any intertwined structures, it looks more like diagonal stripes. This also applies when comparing the patterns in figures 7.9c and 7.9f. The orientation of the stripe-like pattern which can be seen in figure 7.9c corresponds to that orientation which we already know from the previously considered patterns in the point x_7; it is only much more pronounced here than in the previously observed cases or than in the pattern shown by figure 7.9f.

7.1.3 Brief summary of the results for isotropic elasticity

In both cases shown above, we presented typical simulation results for the distributed-microstructure model. As in a single-scale setting, where the separation process is described by the standard Cahn–Larché system, the influence of the mechanics on the patterns can be clearly seen during phase separation. In the DM model, this effect arises on the microscale and it is particularly evident in the spinodal case.

In all simulations shown, in the binodal case ellipsoidal shapes were seen particularly clearly during the early stage of phase separation. Over time, it could be observed that the ellipsoidal shape relaxes into a more circular shape. In contrast, in the case of spinodal separation, we found that the alignment of the patterns due to elastic stresses becomes clearer and stricter as time progresses. As we have also seen, these effects can appear more strongly with elastically harder material parameters. Nevetheless, in all cases, a certain alignment of the microstructure can be seen, which varies locally macroscopically and which is in-line with our expectations regarding the model.

7.2 The case of anisotropic elasticity

Inspired by the work and the simulations of Garcke and Weikard [Wei02], [GW05], we also briefly consider the case of an anisotropic elasticity with cubic symmetry, in which there are three parameters determining the elasticity tensor. For the general N-dimensional case, the components of the elasticity tensor are defined by

$$\begin{aligned} a^i_{kkkk} &= a^i_{11}, \quad \text{for } k = 1, \dots, N, \\ a^i_{kkhh} &= a^i_{12}, \quad \text{for } k \neq h, \\ a^i_{khkh} &= a^i_{44}, \quad \text{for } k \neq h, \\ a^i_{khlm} &= 0, \qquad \text{otherwise,} \end{aligned}$$

for $i \in \{\mathrm{E}, \mathrm{C}\}$, where $a^i_{11}, a^i_{12}, a^i_{44}$ are constants. We present the anisotropic case without going into details and without making quantitative comparisons to the isotropic case. We choose only a mild anisotropy and we use $\varphi = 0.75$ for all following simulations to accelerate the separation process slightly. It turns out that the results of this anisotropic case are quite similar to the isotropic case and analogous conclusions apply. At the end of this section, we discuss some further observations of the mechanical influence on the separation process.

7.2.1 Binodal phase separation

In the case of anisotropic binodal phase separation, we choose

$$a^{\mathrm{C}}_{11} = 2.4, \quad a^{\mathrm{C}}_{12} = 0.3, \quad a^{\mathrm{C}}_{44} = 0.3$$

and 20% smaller values for the elastically softer phase. We first compare the separation process in the macroscopic point x_7 of the distributed-microstructure model with the separation process without elasticity of the corresponding Cahn–Hilliard simulation. Figure 7.10 shows the results of the Cahn–Hilliard simulation in the left column and the results of the simulation of the distributed-microstructure model in the right column. As before, the plots in one row are at the same time t_k specified underneith. The results of the Cahn–Hilliard simulation show the separation process, which has already advanced quite far at time t_{35}. The process is analogous to the Cahn–Hilliard simulation in the previous case of binodal phase separation, as shown in figure 7.4e, where $\varphi = 0.7$. Domains of one phase are formed and with further proceeding in time, the fusion and growth of the domains can be observed. For a short time, ellipsoidal forms occur during the fusion, but these quickly relax into circular shaped domains.

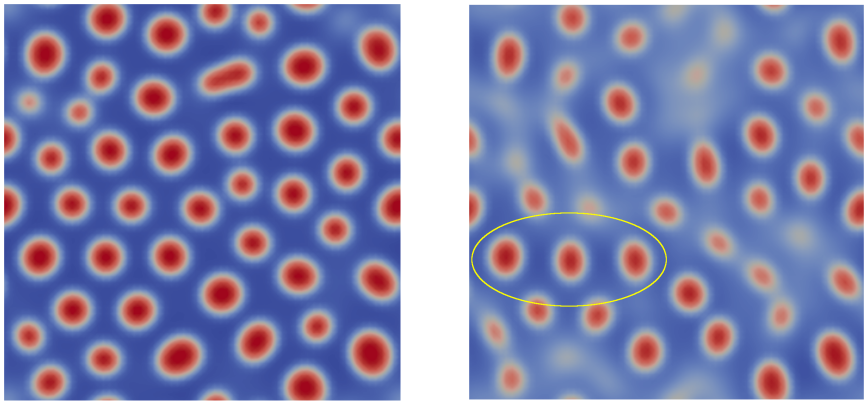

(a) $t_{35} = 1.75$

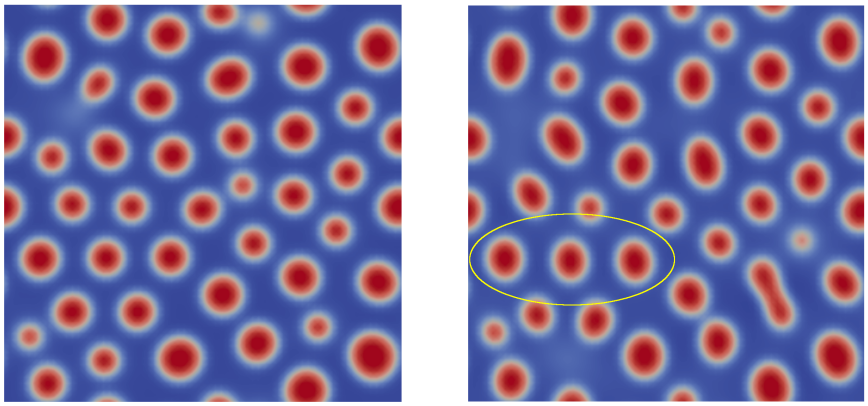

(b) $t_{45} = 2.25$

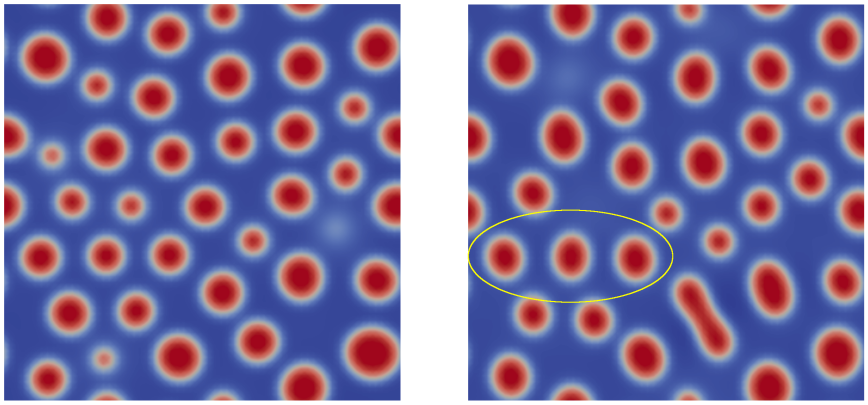

(c) $t_{65} = 3.25$

Figure 7.10: Pattern of two separation processes at different times t_k; left: results of the Cahn–Hilliard simulation; right: results of the DM simulation in the point x_7.

Considering the results of the DM simulation, one can see that the process is roughly the same as in the Cahn–Hilliard simulation. The initially homogeneous mixture separates, regions of pure phases are formed and the resulting domains merge and grow together. As in the case of binodal phase separation with isotropic elasticity, a comparison of the two separation processes shows that the separation of the initial mixture is slower in the DM simulation than in the Cahn–Hilliard simulation and the ellipsoidal-shaped domains do not only occur during fusion of domains in the DM simulation. This can be clearly seen especially when looking at the emerging microstructure, i.e. at time t_{35}, where numerous ellipsoid-shaped domains are present. As in the isotropic case, this ellipsoidal structure is retained for at least a certain period of time, which can be seen, for example, in the three domains marked yellow at times t_{35}, t_{45} and t_{65}. In comparison, consider the circular shapes of the corresponding domains at the same times of the Cahn–Hilliard simulation.

Figure 7.11 presents patterns of the evolving microstructure at selected macroscopic points at time $t_{40} = 2$. The arrangement of the single plots corresponds approximately to the position of the macroscopic points in Ω. Because of the similarity to the isotropic case we have limited the selection of the macroscopic points. The characteristics of the ellipsoid-shaped domains as well as their different orientation, which is analogous to the orientation in the isotropic elastic case, are clearly visible, see figure 7.6. The patterns in the points x_1 and x_2, which are from the upper half of Ω, show an orientation of the domains along the orientation diagonal from the lower left corner to the upper right corner; the domains in x_6 and x_7, which are from the lower half of Ω, are more closely oriented along the diagonal between the upper left corner and the lower right corner. This direction of alignment seems to be accompanied by a preferred direction for merging with other domains. In contrast to the previous case, here we have chosen point x_4 instead of x_8, which is also vertically centered in Ω, but further away from the compression boundary Γ_{g}. However, there is no difference in the characteristics of the patterns appearing in x_4 and x_8, which is also the case in all other cases considered here. We want to mention here that in comparison to figure 7.6, the separation in the points x_1 and x_7 has already progressed further at the same time, but this is simply due to a higher local free energy parameter φ.

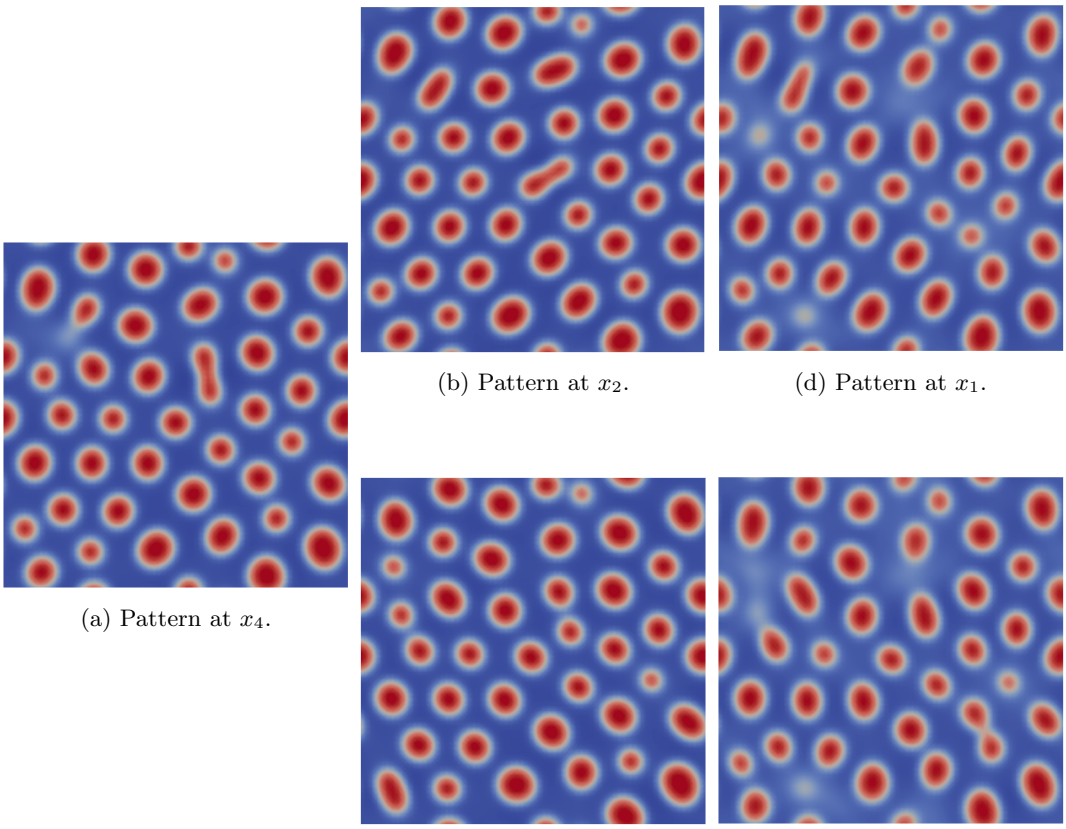

(a) Pattern at x_4.

(b) Pattern at x_2.

(d) Pattern at x_1.

(c) Pattern at x_6.

(e) Pattern at x_7.

Figure 7.11: Pattern of the evolving microstructure at different macroscopic points at time $t_{40} = 2$.

7.2.2 Spinodal phase separation

For the following simulations of spinodal phase separation with anisotropic elasticity with cubic symmetry, we have increased the values for $a_{11}^{\mathrm{C}}, a_{12}^{\mathrm{C}}, a_{44}^{\mathrm{C}}$ by a factor 1/15 and, again, we use 20% smaller values for the elastically softer phase. As before, we first compare the Cahn–Hilliard simulation with the DM simulation in the macroscopic point x_7. In figure 7.12, plots of the solution of both simulations are compared at three points in time, where the results of the Cahn–Hilliard simulation are located in the left column and the results of the DM simulation in x_1 are in the right column. At t_{20}, the microstructure in both simulations is already clearly formed and regions of pure phases exist. Already at this point in time the vertical alignment of the patterns is clearly visible in the DM simulation. At points in time t_{45} and t_{65}, the results of both simulations show the growth of the pure phases and a smoothing of the phase boundary, which corresponds to their minimisation. While in the Cahn–Hilliard simulation the pattern seems to be disordered, in the DM simulation one can see a vertical alignment of the pattern. This can be seen in figure 7.12b on the yellow marked structure and in figure 7.12c. In figure 7.12b, there are two horizontal creases marked yellow, but as shown in figure 7.12c these are reduced with time and the structure is vertically aligned.

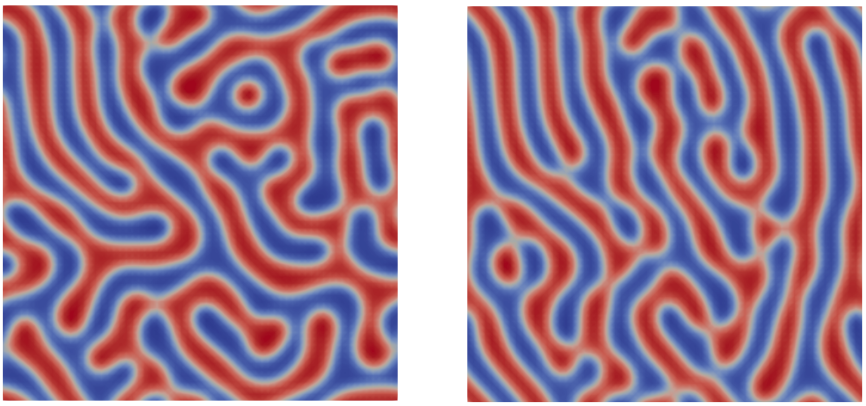

(a) $t_{20} = 1$

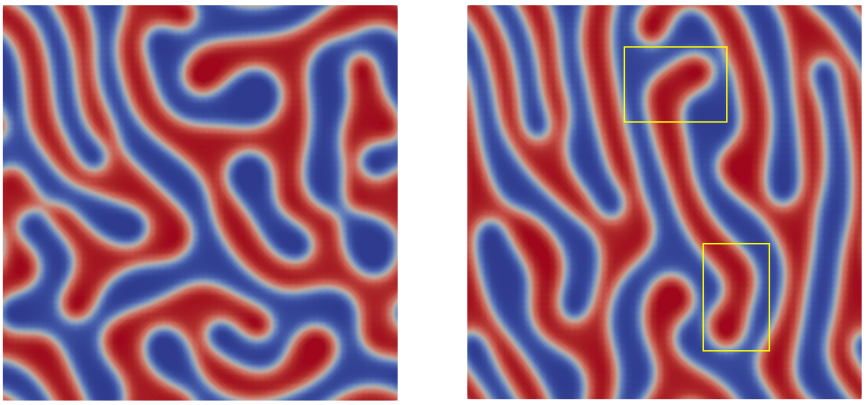

(b) $t_{45} = 2.25$

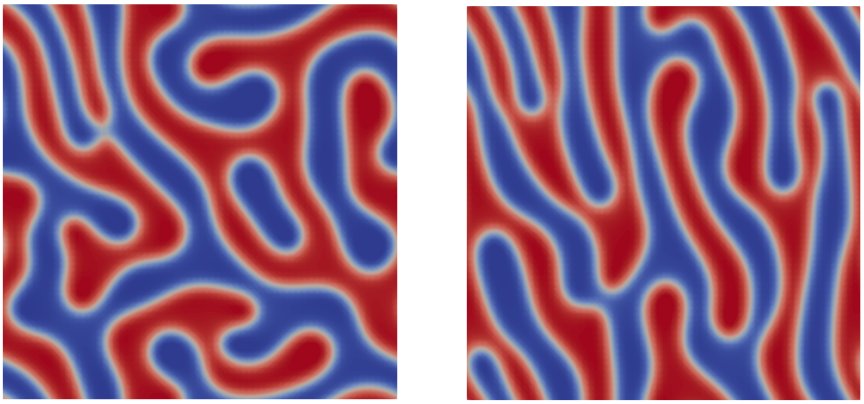

(c) $t_{65} = 3.25$

Figure 7.12: Pattern of two separation processes at different times t_k; left: results of the Cahn–Hilliard model simulation; right: results of the distributed-microstructure model simulation in the point x_7.

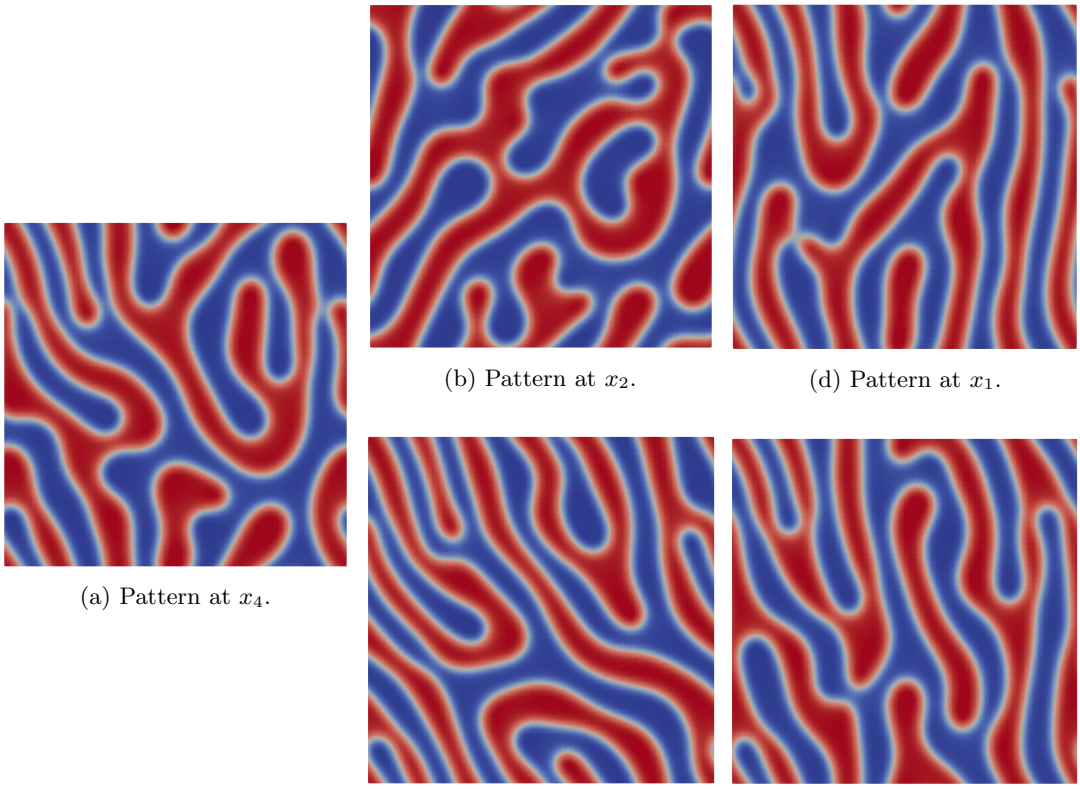

(a) Pattern at x_4.

(b) Pattern at x_2.

(d) Pattern at x_1.

(c) Pattern at x_6.

(e) Pattern at x_7.

Figure 7.13: Pattern of the evolving microstructure at different macroscopic points at time $t_{65} = 3.25$.

As in the previous cases, we also consider and compare the pattern in different macroscopic points. Therefore, figure 7.13 shows patterns at time $t_{65} = 3.25$. As before, one can see a clear orientation of the patterns. The patterns shown by figures 7.13c and 7.13b show an alignment of the patterns along the respective orientation diagonals. This is also the case with the patterns in x_1 and x_7, although here the orientation of the patterns, as in the cases considered above, is rather vertical with a slight inclination in the direction of the respective orientation diagonals. As in figure 7.11, we also consider the patterns in the vertically centred point x_4. Again, a more vertical orientation of the pattern appears to be present, although not as strongly as in the other patterns.

7.2.3 Further effects of elasticity

Finally we compare the DM simulation in the vertically centered point x_8 with the Cahn–Hilliard simulation. We want to compare separation processes with and without elasticity and focus on the fusion of the phases. Figure 7.14 shows the results, where as before, the plots of the solution of the Cahn–Hilliard simulation are located in the left column and the plots of the

solution of the DM simulation are located in the right column. Up to time t_{10}, the patterns of the simulations are approximately the same, but small differences can already be seen here. In the yellow marked part of the pattern of the DM simulation, a direct comparison of the same part of the pattern of the Cahn–Hilliard simulation shows that red coloured structures are still separated and not growing together as they do in the Cahn–Hilliard simulation. In figure 7.14b, at time t_{20}, one can see the different development of the pattern in the yellow marked parts. In the DM simulation the affected structures are still separated, the pattern here has rather been oriented upwards. In the corresponding part of the Cahn–Hilliard simulation, the structures horizontally grow together at the described position. The fact can also be observed in the second yellow marked part of the plot of the DM simulation in figure 7.14b. In the corresponding part of the plot of the Cahn–Hilliard simulation, the red coloured structures of the pattern grow together in horizontal direction. This can also be observed in other parts of the results. A comparison of the pattern in figure 7.14c confirms the general observation that the pattern of the DM simulation seems to be rather vertical orientated, whereas the pattern of the Cahn–Hilliard simulation does not seem to have a clearly recognisable preferred direction of alignment. At this time, in the upper left part of the plots, one can see parts with almost identical characteristics of the patterns, but in the right half and also in the lower half, the described difference in alignment is clearly visible.

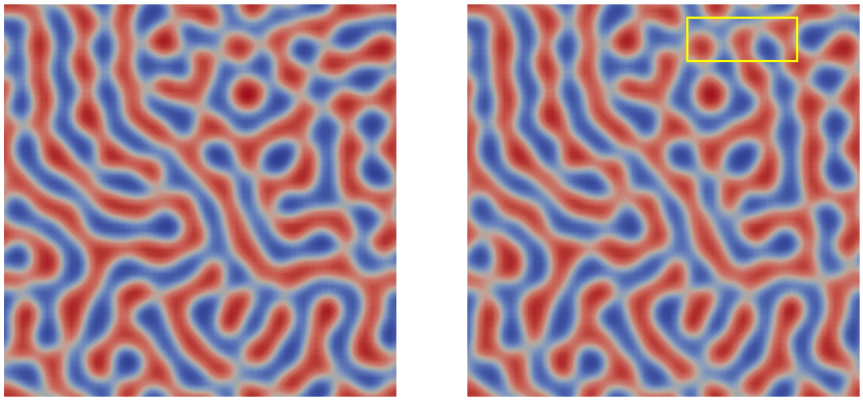

(a) $t_{10} = 0.5$

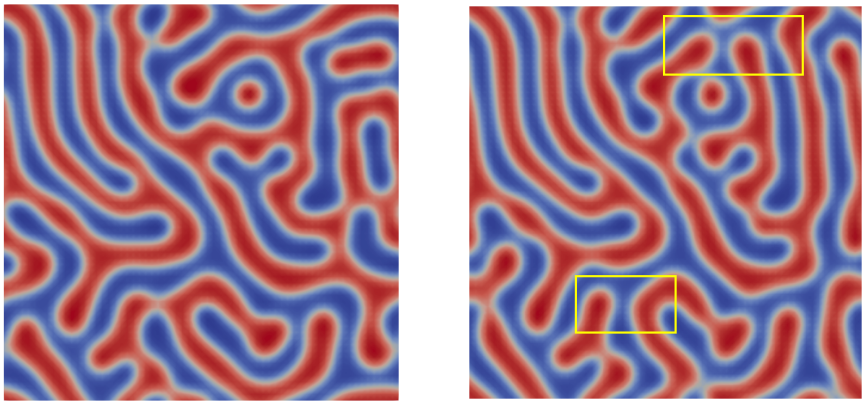

(b) $t_{20} = 1$

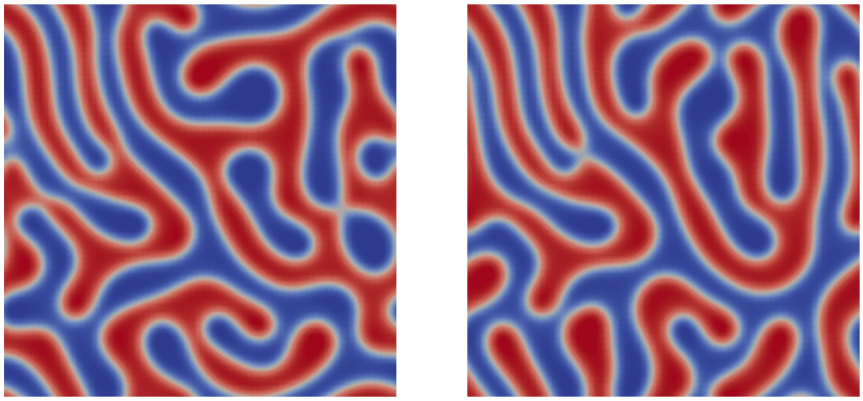

(c) $t_{40} = 2$

Figure 7.14: Pattern of two separation processes at different times t_k; left: results of the Cahn–Hilliard model simulation; right: results of the distributed-microstructure model simulation in the point x_8.

8 Conclusion and outlook

This thesis has been concerned with the Cahn–Larché system, a coupled system of a parabolic fourth-order equation and a second-order elliptic equation. Film-balance experiments motivated considering this classical problem in a multiscale context. By a non-dimensionalisation, we transferred this system into a model in which the physical processes, described in section 2.1, are accounted for on the correct scales. In doing so, we prepared the system for the application of homogenisation techniques to obtain a process-adapted model in the limit. We proceeded with the homogenisation process formally for the nonlinear system and also for the linearised system. This lead to models of distributed-microstructure type, which is a reasonable model structure to describe the physical context of the film-balance experiments. Furthermore, we showed the well-posedness of the linear system in chapter 5, where we proved the existence and uniqueness of a weak solution. Further, we gave an a-priori estimate, which enabled the homogenisation process carried out in chapter 6, where we proved the homogenisation result for the linear system via two-scale convergence. In particular, this has been achieved with two extended results of the concept of two-scale convergence, stated in section 3.2, with which we could pass to the limit in the term with second derivatives and in those consisting of several products of sequences. The convergence to the linear homogenised system could thus be proved rigorously and, further, it turned out that linearisation and homogenisation commute. The rigorous proof of an analogous convergence result for the nonlinear system from section 4.2.1 remains an open problem beyond the scope of this thesis. The finite element based numerical simulations presented in chapter 7 showed, in particular, that the nonlinear distributed-microstructure model indeed describes a separation process on the microscale influenced by the local macroscopic strain. As we have seen, the patterns of the resulting microstructure can have a different orientation and thus differ at each macroscopic point.

The film-balance experiments, which constitute a two-dimensional setting, were the motivation for this thesis and the basis for the modeling of the developed multiscale model. Even though a quantitative comparison to experiments was not possible due to missing data, we performed the numerical simulations in two dimensions to showcase the qualitative behaviour of the model. For future work, numerical simulations of film-balance experiments together with quantitative comparisons would be very interesting. Since the mathematics has been kept general, an application in three dimensions is also feasible, for example for modelling evolving microstructures in metal alloys under macroscopic mechanical stress.

Bibliography

[AJH90] T. Arbogast, J. Douglas Jr., and U. Hornung. Deriving the double porosity model of single phase flow via homogenization theory. *SIAM J. Math. Anal.*, 21(4):823–863, 1990.

[AL12] G. N. Wells A. Logg, K.-A. Mardal, editor. *Automated Solution of Differential Equations by the Finite Element Method*. Springer, 2012.

[All92] G. Allaire. Homogenization and two-scale convergence. *SIAM J. Math. Anal.*, 23(6):1482–1518, 1992.

[Arb89] T. Arbogast. Analysis of the simulation of single phase flow through a naturally fractured reservoir. *SIAM J. Num. Anal.*, 26(1):12–29, 1989.

[Aya19] U. Ayachit. The paraview guide, 2019.

[BBF+17] O. Boyarkin, S. Burger, T. Franke, T. Fraunholz, R. H. W. Hoppe, S. Kirschler, K. Lindner, M. A. Peter, F.G. Strobl, and A. Wixforth. Transport at interfaces in lipid membranes and enantiomer separation. In D. Bothe and A. Reusken, editors, *Transport Processes at Fluidic Interfaces*, chapter 17, pages 489–530. Springer International Publishing, 2017. `https://doi.org/10.1007/978-3-319-56602-3_17`.

[BFL+13] S. Burger, T. Fraunholz, C. Leirer, R. H. W. Hoppe, A. Wixforth, M. A. Peter, and T. Franke. Comparative study of the dynamics of lipid membrane phase decomposition in experiment and simulation. *Langmuir*, 29:7565–7570, 2013.

[BHS09] M. Burger, L. He, and C.-B. Schönlieb. Cahn–Hilliard inpainting and a generalization for grayvalue images. *SIAM J. Imaging Sciences*, 2:1129–1167, 01 2009.

[Bra02] A. Braides. Γ-*convergence for Beginners*. Oxford lecture series in mathematics and its applications. Oxford University Press, 2002.

[Bur11] S. Burger. *Akustisch induzierte 2D Strömung von chiralen Lipidmonolayerdomänen*. Bachelor thesis, Universität Augsburg, 2011.

[CCS03] N.D. Cristescu, E.M. Craciun, and E. Soós. *Mechanics of Elastic Composites*. CRC series–modern mechanics and mathematics. CRC Press, 2003.

[CD99] D. Cioranescu and P. Donato. *An Introduction to Homogenization*. Oxford lecture series in mathematics and its applications. Oxford University Press, 1999.

[CDG18] D. Cioranescu, A. Damlamian, and G. Griso. *The Periodic Unfolding Method: Theory and Applications to Partial Differential Problems*. Series in Contemporary Mathematics. Springer, 2018.

[CH58] J.W. Cahn and J.E. Hilliard. Free energy of a nonuniform system. i. interfacial free energy. *J. Chem. Phys.*, 28:258–267, 1958.

[CS99] G.W. Clark and R.E. Showalter. Two-scale convergence of a model for flow in a partially fissured medium. *Electronic Journal of Differential Equations (EJDE) [electronic only]*, 1999(2):1–20, 1999.

[DM93] G. Dal Maso. *An Introduction to Γ-Convergence*. Birkhäuser Basel, 1993.

[Dok11] R. Dokchan. *Numerical Integration of Differential–Algebraic Equations with Harmless Critical Points*. PhD thesis, Humboldt-Universität zu Berlin, 2011.

[Esh61] J. Eshelby. *Elastic inclusions and inhomogeneities, Vol. 2*. North Holland Publishing Company, Amsterdam, 1961.

[FPL99] P. Fratzl, O. Penrose, and J.L. Lebowitz. Modeling of phase separation in alloys with coherent elastic misfit. *Journal of Statistical Physics*, 95, 1999.

[Fra14] T. Fraunholz. *Transport at Interfaces in Lipid Membranes and Enantiomer Separation*. PhD thesis, Universität Augsburg, 2014.

[Gar00] H. Garcke. *On mathematical models for phase separation in elastically stressed solids*. Habilitation thesis, Universität Bonn, 2000.

[GFBH09] M. Gudmand, M. Fidorra, T. Bjrnholm, and T. Heimburg. Diffusion and partitioning of fluorescent lipid probes in phospholipid monolayers. *Biophysical Journal*, 96(11):4598–4609, 2009.

[GL17] H. Garcke and K.F. Lam. Well-posedness of a Cahn–Hilliard system modelling tumour growth with chemotaxis and active transport. *European J. Appl. Math.*, 28:284–316, 2017.

[GW05] H. Garcke and U. Weikard. Numerical approximation of the Cahn–Larché equation. *Numerische Mathematik*, 100(4):639–662, 2005.

[Hal97] H. Haller. *Verbundwerkstoffe mit Formgedächtnislegierung – Mikromechanische Modellierung und Homogenisierung*. PhD thesis, Technische Universität München, 1997.

[Hor97] U. Hornung, editor. *Homogenization and Porous Media*. Springer, 1997.

[Kha67] A.G. Khachaturyan. Some questions concerning the theory of phase transformations in solids. *Soviet Phys. Solid State*, 8(9):2163–2168, 1967.

[KL00] P. Krüger and M. Lösche. Molecular chirality and domain shapes in lipid monolayers on aqueous surfaces. *Phys. Rev. E*, 62:7031–7043, 2000.

[KM94] T. Küpper and N. Masbaum. Simulations of particle growth and Ostwald ripening via Cahn–Hilliard equation. *Acta Metallugica et Materialia*, 42:1847–1858, 1994.

[KV96] K.J. Klopfer and T.K. Vanderlick. Isotherms of dipalmitoylphosphatidylcholine (dppc) monolayers: Features revealed and features obscured. *Journal of Colloid and Interface Science*, 182:220–229, 1996.

[LC82] F.C. Larché and J.W. Cahn. The effect of self–stress on diffusion in solids. *Acta Metall.*, 30:1835–1845, 1982.

[Lei08] C.T. Leirer. *Dynamik und Struktur in der Phasenkoexistenz von Lipidmembranen.* PhD thesis, Universität Augsburg, 2008.

[LNW02] D. Lukkassen, G. Nguetseng, and P. Wall. Two-scale convergence. *Int. J. Pure Appl. Math.*, 2(1):35–86, 2002.

[Mär02] Roswitha März. The index of linear differential algebraic equations with properly stated leading terms. *Results in Mathematics*, 42(3):308–338, 2002.

[Mei08] S.A. Meier. *Two-scale models for reactive transport and evolving microstructure.* PhD thesis, Universität Bremen, 2008.

[Mer05] T. Merkle. *The Cahn–Larché system: A model for spinodal decomposition in eutectic solder – Modelling, analysis and simulation.* PhD thesis, Universität Stuttgart, 2005.

[MM87] A. Miller and H. Möhwald. Diffusion limited growth of crystalline domains in phospholipid monolayers. *The Journal of Chemical Physics*, 86(7):4258–4265, 1987.

[Möh95] H. Möhwald. Phospholipid monolayers. In R. Lipowsky and E. Sackmann, editors, *Structure and Dynamics of Membranes*, volume 1 of *Handbook of Biological Physics*, pages 161–211. North-Holland, 1995.

[MT97] F. Murat and L. Tartar. H-convergence. In A. Cherkaev and R. Kohn, editors, *Topics in the Mathematical Modelling of Composite Materials*, pages 21–43. Birkhäuser, 1997.

[Mur87] T. Mura. *General theory of eigenstrains.* Springer, 1987.

[MV97] C.W. McConlogue and T.K. Vanderlick. A close look at domain formation in dppc monolayers. *Langmuir*, 13:7158–7164, 1997.

[NBRK91] K. Nag, C. Boland, N. Rich, and K.M.W. Keough. Epifluorescence microscopic observation of monolayers of dipalmitoylphosphatidylcholine: dependence of domain size on compression rates. *Biochemica et Biophysica Acta.*, 1068:157–160, 1991.

[Ngu89] G. Nguetseng. A general convergence result for a functional related to the theory of homogenization. *SIAM J. Math. Anal.*, 20:608–623, 1989.

[Pan13] A.A. Pankov. *G-Convergence and Homogenization of Nonlinear Partial Differential Operators*. Mathematics and Its Applications. Springer, 2013.

[PB05] M.A. Peter and M. Böhm. Scalings in homogenisation of reaction, diffusion and interfacial exchange in a two-phase medium. In M. Fila, A. Handlovicova, K. Mikula, M. Medved, P. Quittner, and D. Sevcovic, editors, *Proceedings of Equadiff 11 International Conference on Differential Equations*, pages 369–376. 2005.

[PB09] M.A. Peter and M. Böhm. Multiscale modelling of chemical degradation mechanisms in porous media with evolving microstructure. *Multiscale Modeling & Simulation*, 7:1643–1668, 2009.

[Pes92] M. Peszyńska. *Flow through fissured media. Mathematical analysis and numerical approach*. PhD thesis, Universität Augsburg, 1992.

[PS08] G.A. Pavliotis and A.M. Stuart. *Multiscale Methods: Averaging and Homogenization*. Springer, 2008.

[SA19] Sigma-Aldrich. Data of DPPC, 2019. `https://www.sigmaaldrich.com/catalog/product/avanti/850355c` Accessed: 2019-09-10.

[Sch13] B. Schweizer. *Partielle Differentialgleichungen*. Springer-Verlag, Berlin, 2013. Eine anwendungsorientierte Einführung.

[Sho91] R. E. Showalter. Diffusion models with microstructure. *Transport in Porous Media*, 6(5):567–580, 1991.

[Sho93] R.E. Showalter. Distributed microstructure models of porous media. In Jim Douglas Jr. and U. Hornung, editors, *Flow in Porous Media: Proceedings of the Oberwolfach Conference, June 21–27, 1992*, chapter 14, pages 155–163. Birkhäuser, 1993.

[Ste05] D. Steppich. *Kopplung von mechanischen und thermodynamischen Eigenschaften von Phospholipidmembranen in der Nähe von Phasenumwandlungen – Bedeutung für Anwendungen und Biologie*. Diploma thesis, Universität Augsburg, 2005.

[Tar78] L. Tartar. Quelques remarques sur l'homogénéisation; Proc. of the Japan–France Seminar 1976 functional analysis and numerical analysis. *Japan Society for the Promotion of Sciences*, pages 469–482, 1978.

[Tis03] C. Tischendorf. *Coupled Systems of Differential Algebraic and Partial Differential Equations in Circuit and Device Simulation*. Habilitation thesis, Humboldt-Universität zu Berlin, 2003.

[TPMS10] P. Toimil, X. Prieto, J. Miones, and F. Sarmiento. A comparative study of f-dppc/dppc mixed monolayers. influence of subphase temperature on f-dppc and dppc monolayers. *Physical chemistry chemical physics : PCCP*, 12:13323–13332, 10 2010.

[Wei02] U. Weikard. *Numerische Lösungen der Cahn–Hilliard-Gleichung und der Cahn–Larché-Gleichung.* PhD thesis, Rheinische Friedrich-Wilhelms-Universität Bonn, 2002.

[ZKO94] V.V. Zhikov, S.M. Kozlov, and O.A. Oleĭnik. *Homogenization of differential operators and integral functionals.* Springer, 1994.